Processing of Composites Group

Master's Thesis

Influence of the Textile Architecture on its Transversal Compaction Behaviour

Markus Hollitsch, BSc

February 2023

MONTANUNIVERSITÄT LEOBEN
www.unileoben.ac.at

AFFIDAVIT

I declare on oath that I wrote this thesis independently, did not use other than the specified sources and aids, and did not otherwise use any unauthorized aids.

I declare that I have read, understood, and complied with the guidelines of the senate of the Montanuniversität Leoben for "Good Scientific Practice".

Furthermore, I declare that the electronic and printed version of the submitted thesis are identical, both, formally and with regard to content.

Date 28.02.2023

Markus Hollitsch

Signature Author
Markus Hollitsch

Acknowledgements

I am grateful for the family I come from, my father and my mother who fostered me throughout my entire life. Thank you for all your love, support and encouragement. Thanks also to all my friends who have accompanied and supported me on my way. I would also like to thank my wonderful fellow students at the Department for Polymer Engineering and Science and especially my student team members of the VLK. Moreover, thanks to all the professors and lecturers at the University of Leoben who enabled me to broaden my horizon and learn and develop numerous skills as well as my understanding and knowledge of technology, science and plastics in particular.

I am particularly grateful for the guidance, support and assistance provided by Assoz. Prof. Dipl.-Ing. Dr. mont. Ewald Fauster and Dipl.-Ing. (FH) Marcel Bender. Thank you for all your efforts and advice, which have helped me to keep my progress on schedule. Many thanks to Univ-Prof. Dr.-Ing. Ralf Schledjewski for the opportunity to work at the Processing of Composites Group since 2020. In addition, I would like to thank all the other members of this chair for their support and team spirit.

Further, I acknowledge the financial support through project Nawaro-Flex (project no. 871403) provided by the Austrian Ministry for Climate Action, Environment, Energy, Mobility, Innovation and Technology within the frame of the FTI initiative “Produktion der Zukunft”, which is administered by the Austria Research Promotion Agency (FFG).

Abstract

To characterize the compaction and relaxation behaviour of different textile reinforcement architectures, a specially developed experimental setup is used in which the specimens are compacted between two rigid steel plates by a defined movement of the crosshead of a universal testing machine. Currently established measurement standards do not yet specify the exact test specimen and geometries. Compaction measurements on different material structures and measurement specifications will help to provide a basis for a specification of the methodology. In this thesis, the relaxation behaviour of different textile architectures is investigated in the context of a novel in-situ impregnation measurement methodology and differences are attributed to the material structure.

For this purpose, two series of compaction measurements are carried out on a total of four structurally different reinforcing materials while changing various process parameters. In particular, the investigations show the influence of fibre volume fraction as well as the number of layers on the course of stress relaxation in the dry and saturated textile state. Especially during the injection phase of the test fluid, the difference between the material responses of the individual textile architectures is shown by three different preselected pressure levels. During the injection phase of a test liquid, the combination of the already existing compaction pressure and the applied fluid injection pressure results in a defined total pressure.

The differences between the compaction pressure levels at the end of the dry and saturated relaxation phases show a significant difference in the strength of the lubrication effect, due to the presence of a fluid, within the investigated textile architectures. A comparison with an International Benchmark Exercise shows that with doubled specimen dimensions, no discernible change in compaction behaviour can be detected. The influence between the pre-impregnation of the specimen with test fluid and in-situ impregnation in a single experiment is also expected to be minor. In addition, influences regarding the measurement results, especially through the handling before testing of the specimens, but also through the test rig itself, have been identified.

Table of contents

1 Introduction

During the processing of fibre-reinforced composites, compaction can occur in various forms and knowledge about the textiles response is necessary when it comes to designing and optimizing different process steps. To achieve a high fibre content in the final composite, which has a beneficial effect on the mechanical properties of the final structure, the fibrous preforms must be compacted before impregnation. In this context, the fibre network is subjected to penetrating compressive forces through the thickness, which are applied at different stages of impregnation with a liquid matrix system, depending on the processing method. This further determines the fibre volume fraction (FVF) in the finished component. However, in some processes, the reinforcement is compacted after impregnation and before the matrix system is cured, to obtain the desired FVF and minimize the volume of voids in the polymer matrix. However, at very high levels of FVF, it may become very difficult to achieve good permeability of the textile reinforcement and consequently a sufficient infiltration of the resin into the preform. As a result, the behaviour of a reinforcement subjected to transversal compaction plays an important role, especially in terms of mould design and equipment specifications for all steps of the manufacturing process. [1]–[3]

Resin Transfer Molding (RTM) and RTM-like processes are process variants for the industrial production of fibre-reinforced composites. In particular, the high level of automation, the low degree of post-processing and the short cycle times in the range of minutes are important advantages. This enables the economical production of highly rigid composites with sometimes complex geometries. Therefore, a comprehensive understanding of these processes and further optimization of all processing parameters along the process chain to achieve a balance between the processability of the preform and the mechanical performance of the final product is essential. [4]–[7]

Transversal compaction tests are particularly useful before RTM processes to determine the initial force required to completely close the mould and subsequently achieve the desired FVF. In addition, such measurements provide

information on the resistance of a textile reinforcement architecture to the applied compaction force and its time-dependent behaviour. This information is particularly useful for RTM applications, as it results in a change in compaction pressure while the height of the cavity between two rigid surfaces remains constant. To be able to describe the transversal compaction behaviour of a textile reinforcement architecture in an application-oriented manner, processing-parameters such as the compaction velocity and rate, holding and relaxation times, the required pressure to reach the desired volume of fibres in the composite as well as the stacking order or the degree of fibre alignment must be taken into account. [8]–[11]

The work at hand is intended to investigate these effects and differences between the present architectures and subsequently improve the understanding of the transversal compaction behaviour of a textile reinforcement. Particularly relevant for this thesis is the influence of textile saturation, especially through in-situ impregnation carried out during the compaction phase. To determine the influence of the textile architecture, compression-relaxation tests are carried out on four different materials. For this purpose, the test series are divided into a pretest and the main test series. In the former, the pressure level of the fluid injection, which can be considered ideal, is determined individually for each textile architecture. For this purpose, with a constant number of layers and a constant FVF and thus a constant compaction height, the fluid injection pressure levels are varied in three stages. In the following main test series, the number of layers is varied in at least two stages and the FVF in three stages to be able to draw conclusions about the behaviour during transversal compaction and to highlight differences between the textile architectures. Thereby, the fluid injection pressure level for each configuration, previously determined in the pretest series, is used during the in-situ impregnation phase.

In the following, the state of the art in transversal compaction measurements of textile reinforcement materials will be elaborated. After the explanation of the experimental setup and procedure, the results of the two series of experiments are presented and described. At the end of this thesis, there is a detailed conclusion highlighting the differences that occur between the textile reinforcement architectures under transversal compaction and especially during fluid injection.

2 State of the art

For the manufacturing of fibre-reinforced polymer composites, textile reinforcement structures are compacted one or multiple times before impregnation, especially when closed moulds are used. Thereby, the thickness of the fabric decreases and the FVF increases, accompanied by other typical compaction effects that are likely to occur, such as nesting, yarn flattening and bending as well as yarn cross-section deformation, to name a few. The use of universal testing machines (UTM), which can measure the force-displacement relation, in a setup with two rigid and parallel surfaces, allows the gathering of information on the load response of fabric reinforcement structures to transversal compaction. Empirical or semi-empirical models derived from such tests are usually expressed as a power-law relation. Depending on the type of textile structure used, the specific material properties, the test setup and the test parameters, the attainable FVF is determined and consequently affects the permeability of the porous fibrous preform as well as the mechanical properties of the final product. [1], [8]–[10]

2.1 Processing and testing

During the processing of fibre-reinforced composites, the fibre network is subject to transversal compressive load. Depending on the processing method, these compressive forces are applied at various stages both before and during impregnation with a liquid matrix system and determine the FVF of the finished component. The manufacturing process of fibre-reinforced composites can generally be divided into two variants. One is a process in which dry fibres are impregnated step by step during manufacture, and the other is one in which pre-impregnated fibre reinforcements are used. Only in some processes is the reinforcement compacted after impregnation to minimize the volume of voids in the polymer matrix and obtain the desired FVF. On the one hand, in filament winding, for example, the individual fibre yarns are compressed by the tension created

when the fibres are placed on a mandrel. In pultrusion, on the other hand, the impregnated fibre yarns are compressed as they are pulled through a die. When prepregs are processed in or outside an autoclave, the impregnated fibre bed reacts to the pressure in the autoclave or the atmospheric pressure applied to a vacuum bag that encloses the layer.

In Liquid Composite Moulding (LCM), among them RTM, rigid moulds are typically used to compress a dry reinforcement before impregnation with the matrix, the compaction behaviour of the preform at a predefined height determines the reaction force on the mould surfaces, which indicates whether a certain FVF can be achieved. After the mould is closed, the resin fills the mould cavity and cures. Here, the injection of the resin can take place in the plane or perpendicular. The RTM process is primarily used to produce high-fibre volume composites for structural applications but can be used for components with lower FVF as well. A higher FVF may be achieved either by applying successive load cycles to an initial target pressure or if time permits, through pre-compaction of the textiles in the mould, by closing the mould to a certain position and corresponding force, allowing relaxation to occur, before injection. [1], [12], [13]

To achieve the desired mechanical properties of the finished composite, the characterization of the relation between compaction pressure and FVF is critical. Thereby, high values of FVF are sought in the manufacture of composites for high-performance parts with a resilient property profile. Changes in this value during compression of the preform also lead to a reduction in permeability, which affects the resin flow during subsequent impregnation. [1]

Transverse impregnation is becoming increasingly important among LCM processes. Compared to in-plane impregnation, it has the potential to strongly reduce flow path lengths. However, the transverse impregnation behaviour is the result of a complex interaction of permeability and compaction behaviour. Especially if the level of pre-compaction is low, the textile will be deformed during impregnation. This deformation can strongly affect the impregnation speed, which is why textile behaviour is crucial for the efficiency and stability of the process. To exploit the full potential of transverse impregnation, the relationship between the

impregnation behaviour of the textiles as well as the process parameters, such as the injection pressure, must be known. [14]

Especially in RTM processes, the compaction response of the fabric has consequences on mould design and equipment specifications. Therefore, the evaluation of the behaviour of the fibre reinforcement structure during the load stages, namely compression, holding and decompression, is of great importance. Such typical compaction tests resemble the majority of the LCM processes, not only RTM but also Vacuum-Assisted Resin Infusion (VARI) as well as Vacuum-Assisted Resin Transfer Moulding (VARTM). Typical load-relaxation tests, in which the component thickness is held constant for a specified time while the force or pressure is measured, allowing the material to relax in the gap between the two rigid surfaces. This relaxation stage provides information on the load variation with time. [15]

Another important effect of transverse compaction of fibre reinforcement fabrics is that the induced pressure squeezes air and resin out of the textile inside the mould cavity, to suppress the formation of voids and gaps as well as to increase and uniform the FVF. In addition, the applied load in conjunction with the surfaces of the tool determines the dimensions and finish of the part. This process is defined as consolidation [16].

A mathematical model presented by Gutowski et al. [16] proposes that the consolidation process involves two important phenomena. One is the viscous flow of the resin in the fibre network, which can be described by Darcy’s law, and the other is the elastic deformation of the fibre network itself. Thereby, the fibre network behaves as a nonlinear elastic medium and the permeability of the rovings is both strongly anisotropic and strongly dependent on the FVF. Both phenomena must be included to allow a complete description of the process. When the consolidation load is first applied at a low FVF, the fibres do not carry a load and the pressure in the resin is equal to the applied pressure. As more and more resin squeezes out, the FVF increases and multiple fibre-fibre contacts are established and now support a fraction of the applied load.

Here, the behaviour of the composite is determined by viscous flow and the deformation behaviour of the fibre network. In addition, the deformation behaviour of the fibres has a controlling effect on the distribution of the FVF across the part thickness.

In compaction experiments on carbon fibre beds impregnated with silicone oil, Gutowski et al. [16], [17] found that at a high FVF above 0.50, the fibres carry a gradually increasing fraction of the applied load, defined as effective stress. This behaviour results from fibre waviness and causes multiple fibre-fibre contacts. Assuming the fibres to be curved beams in bending, the following equation expresses the effective stress $\bar{\sigma}$ in a fibre bed as a function of the FVF V_f [1], [16], [17]:

$$\bar{\sigma} = A_s \cdot \frac{1 - \sqrt{\frac{V_f}{V_{f0}}}}{\left(\sqrt{\frac{V_{fa}}{V_{f0}}} - 1\right)^4} \tag{1}$$

V_{fa} available FVF (i.e. maximum achievable)

V_{f0} initial FVF in the uncompressed preform

In this expression, A_s is a constant that, when associated with crimp, can be converted to the following [1], [16], [17]:

$$A_s = \frac{3\pi E_f}{\beta^4} \tag{2}$$

E_f flexural modulus of the fibre

β ratio of arc length and arc height in woven fibres

It is of significant importance to optimise the processing parameters to achieve an appropriate balance between the processing of the material and the mechanical performance of the final part. Processing parameters such as the number of layers, the level of pressure, the applied compaction rate as well as the number of compaction cycles, or the structure and architecture of the textile influence the stiffness and compaction behaviour of the reinforcement. Therefore, the evaluation

of the behaviour of the preform during transverse compaction is of great interest. In particular, compaction tests are important to know before RTM processing to determine the initial load necessary to completely close the mould and subsequently achieve the desired FVF. Such measurements provide information on the resistance of a textile reinforcement material to the action of the compression force and its time-dependent behaviour. In general, stress can be considered a function of strain, strain rate and time. As a result of the applied loads during transverse compaction, the stress-strain behaviour of the material exhibits classic viscoelastic characteristics, including stress relaxation, strain rate dependency and hysteresis. [18]

Concerning the load cases, a distinction can be made between the following test configurations, as schematically visualized in Figure 1:

a) Compression-decompression
b) Compression-relaxation
c) Compression-creep

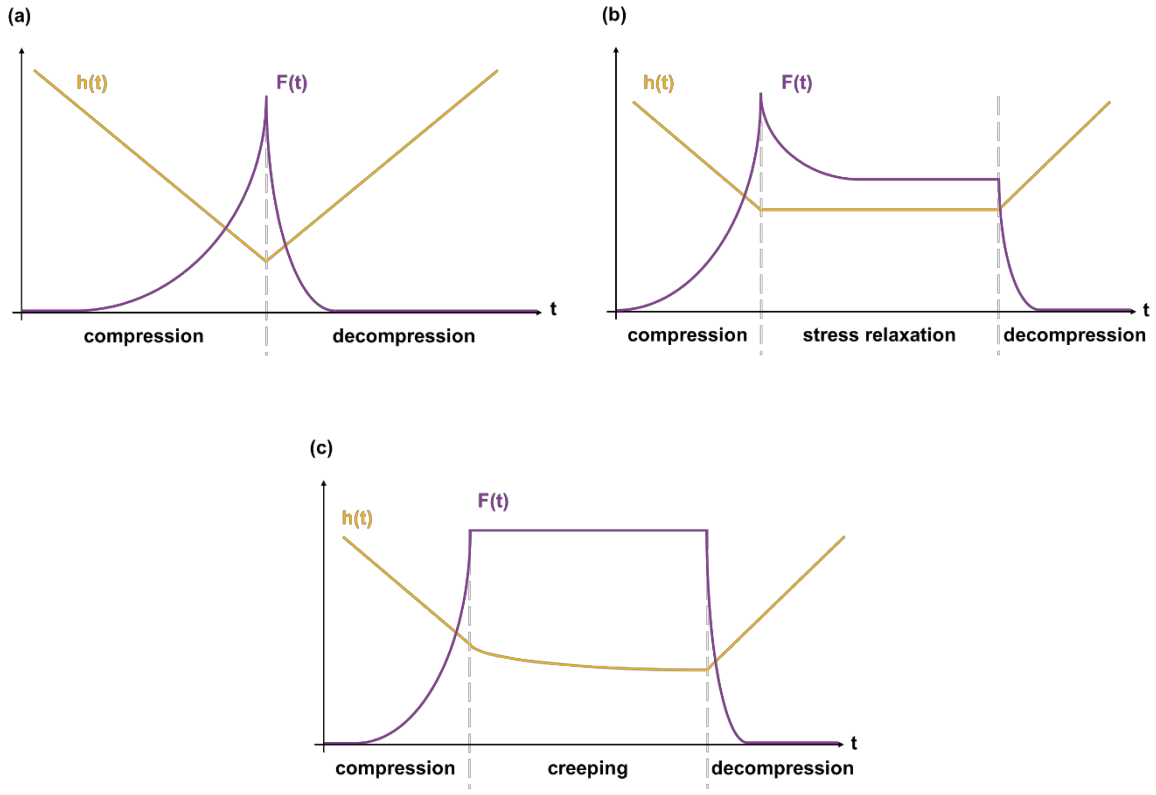

Figure 1: Test configurations for compaction measurements with (a) compression-decompression, (b) compression-relaxation and (c) compression-creep

The first test configuration, the compression-decompression test arrangement, exhibits hysteresis behaviour that includes both stages and can be performed either as a single compression/decompression stage or with cyclical repetitions. Either the force can be applied in the direction of a target value or the specimen can be compressed to a certain height [15]. It is important to mention that repetitive compaction cycles as well as pre-compaction cycles lead to a decreasing compaction resistance of textile reinforcement materials and thereby can enormously reduce the required compaction forces [19]. Although cyclic compaction permits the continuous increase of energy dissipated, it may weaken the stiffness of the fabric and further lead to insignificant relaxation [20].

In a compression-relaxation test, the specimen is compressed to a predetermined cavity thickness and held at that level while the resulting force is monitored. The relaxation phase itself is characterised by a reduction in the load over time, typically leading to a steady-state load level [15]. In a compression-creep test, the specimen is compressed to a predetermined force value and held at that level while the resulting thickness reduction is monitored [15].

Figure 2 shows schematically the aforementioned strain rate dependency for the compression-relaxation test configuration. Three different tests with varying compaction rates are shown together with the resulting compressive load. [18]

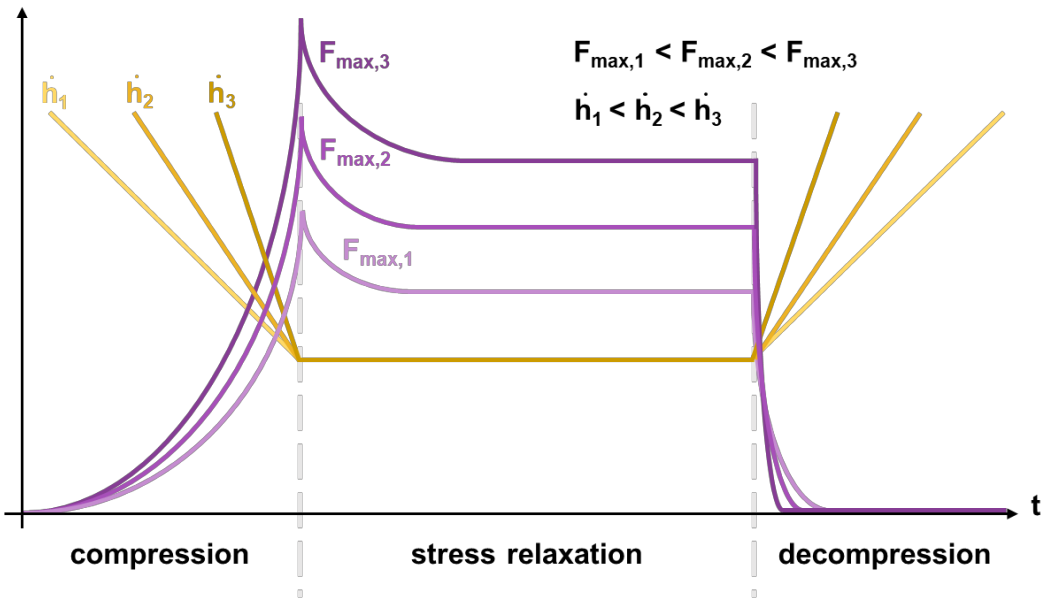

Figure 2: Strain rate dependency of a compression-relaxation test configuration

In this case, higher test speeds lead to increased compaction resistance, whereby the speed dependence is related to the viscoelasticity of the textile materials [19]. A low compaction speed can provide much more time for the fibres to move and realign, resulting in higher energy dissipation and increasing the probability of relaxation [20]. The relaxation factor R, used to quantify the degree of relaxation, is determined by the following equation [21]:

$$R = \frac{h - t}{h} \tag{3}$$

h initial thickness of the specimen

t final thickness in compaction

In general, the higher the relaxation factor, the more relaxation occurs. This factor increases with an increasing number of layers as well as with lubrication. [21]

2.2 Textile reinforcement fibres

2.2.1 Glass fibres

Glass fibres are the most important technical reinforcing fibres due to their economical price-to-performance ratio. Glass-fibre-reinforced polymers are among the most important construction materials today, as they are suitable for high-strength components. Depending on the type of composition and characteristics, they have different designations for the respective field of application, such as E-glass (electrical – low electrical conductivity), C-glass (chemical – high chemical resistance) and S-glass (strength – high tensile strength). In general, they are non-flammable, show excellent mechanical as well as dielectric properties and are temperature resistant up to 400 °C. [2]

There are several manufacturing processes for glass fibres. In general, they are formed from a melt of various oxides as network formers, such as SiO_2, and network converters, such as alkali oxides, which get cooled rapidly to prevent crystallisation. The main component of this complex aqueous mixture is the polymeric film-forming agent. It ensures the cohesion of the fibres and helps to

prevent breakage caused by abrasion. In the composite, the applied finish provides the required compatibility within the matrix-fibre-interface and influences its property profile. Other important components are a lubricant, as the glass shows a high coefficient of friction, as well as the coupling agent to decisively improve the fibre-matrix adhesion. [2]

Textile glass fibres are manufactured by the nozzle drawing process. However, to be drawn, the glass compositions must meet certain conditions during the viscosity change as a function of temperature. In this process, the molten glass gets formed into fibres through a perforated brushing plate, consisting of up to 4000 nozzles with a diameter of 1 to 2 mm, then cooled, coated with sizing and subsequently coiled at high speed. Thereby, the nominal diameter of the glass fibres, usually in the range of 5 to 25 µm, is controlled by the pull-off speed. [2], [3]

2.2.2 Carbon fibres

Carbon fibres are technical fibres that are converted into graphite-like carbon by chemical reactions adapted to the raw material and have a carbon content of 92 to 99.9 per cent by weight. The fibres show a two-dimensional graphite structure and only in exceptional cases have a three-dimensional, crystalline structure. A distinction is made between isotropic and anisotropic types. Isotropic fibres have only low strength and less technical significance, anisotropic fibres show high strength and stiffness with simultaneously low elongation at break in the axial direction. The temperature level in the final treatment is decisive for the properties of the finished fibre. The distinction is based on the fibre strength and stiffness and includes the following types [3]:

- high-tenacity fibres (HT)
- super-tenacity fibres (ST)
- intermediate modulus fibres (IM)
- high modulus fibres (HM)
- ultra-high modulus fibres (UHM)

The most important property of carbon fibres as a stiffening component for carbon fibre-reinforced plastics (CFRP) is the modulus of elasticity. This ranges from 230 GPa, as with HT types, up to 450 GPa, as is the case with UHM types. Carbon fibres are characterized by their high strength-to-weight ratio, which makes this type of fibre a widely used construction material in aerospace applications, numerous high-tech sports articles such as tennis rackets, racing and mountain bikes or boats, but also high-performance components such as monocoques and other parts in motor sports. In direct comparison to glass fibres, they are even lighter in weight, but significantly more expensive. [2], [3], [22]

2.2.3 Viscose fibres

Viscose or rayon fibres are semi-synthetic products, made from natural sources of regenerated cellulose, such as wood and other related materials. It has the same molecular structure as cellulose but shows a different elementary grating in the sorted structural areas [23]. The standard type of viscose fibres shows properties that may not be ideal for all applications. However, the manufacture with a wet-spinning process offers good possibilities in terms of modification. To better adapt the properties of the fibres to the intended use, not only the pull-off speed can be varied, but also solid as well as liquid additives can be mixed into the solution and the precipitation baths (regeneration baths) [24].

In general, the manufacturing process with wet-spinning technology can be divided into three main stages. First, the viscose solution is produced, followed by the spinning process of the threads. The last stage is characterized by the post-treatment of the spun threads. By modifying the manufacturing parameters and the post-treatment, viscose fibres can be very well adapted to the intended processing and use. The use of viscose fibres is similar to that of cotton fibres because of the common basis of cellulose and the associated clothing physiological properties. However, due to the much greater variation possible in fibre geometry (length, crimp, fineness, cross-sectional shape), it surpasses cotton fibres in many application properties. It is also important for processing and thus for use that

viscose is not only available as staple fibres as cotton, but that endless-filaments can be produced. [2], [25]

The properties of viscose fibres vary over a wide range due to structural changes, such as modification additives or changes in the cross-section. The fineness-related tensile strength in the dry state is between 16 and 70 cN/tex and the wet expansion is between 45 % and 300 %. The moisture absorption of viscose fibre is between 11 % and 14 % in a normal climate and thus exceeds that of cotton. This subsequently leads to a reduced wet tear strength, which only reaches 45 % to 65 % of the dry tear strength. This is a significant difference compared to cotton, whose wet tear strength is higher than the dry tear strength. [25]

2.3 Textile preforms

2.3.1 Woven fabric

Continuous reinforcement fibres can be processed into flat preforms using conventional weaving technology. Various weaving types are used, whereby the weaving type must be selected depending on the requirements of the application and the type of fibre to be processed. Woven fabrics (WF) are characterised by bundles of fibre filaments, so-called rovings, which interweave in the warp (0 degrees) and weft (90 degrees) direction to form a particular pattern or weave style. The arrangement of these weaving points decisively determines the behaviour of these fibre architectures during their further processing, especially the draping behaviour, the permeability characteristics as well as the mechanical properties of the later component. Figure 3 shows the three most common weaves (atlas weave, twill weave and plain weave). Due to the only slightly undulated fibres, the atlas weave provides better mechanical properties, but the textile properties regarding drapability and handling are negatively affected. The plain weave shows the highest number of weaving points, thereby very good handling properties are achieved. The mechanical property profile is lowered compared to an atlas or twill weave due to the high fibre ondulation. At the twill weave, the weaving points are arranged next to each other, which somewhat limits the

draping ability. Thus, the twill weave represents a compromise between the good mechanical properties of the atlas weave and the good handling behaviour of the plain weave. [2], [3]

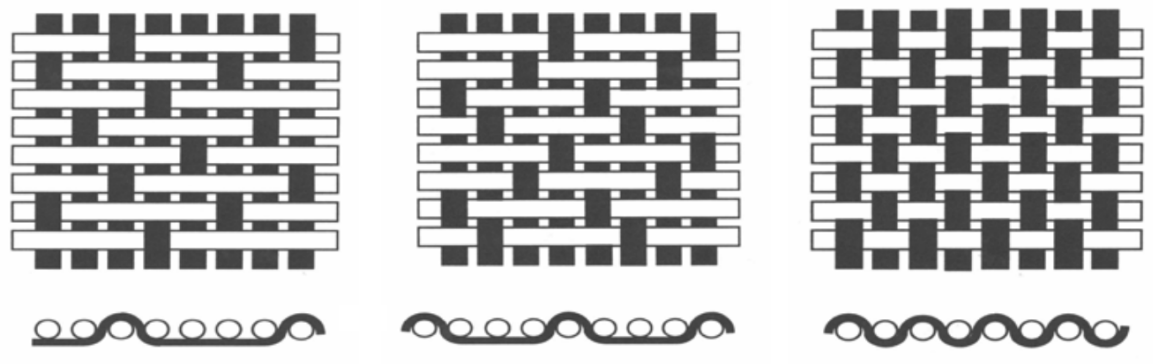

Figure 3: The three most common types of weaves (from left to right: atlas, twill and plain weave) [2]

2.3.2 Non-crimp fabric

Non-crimp fabrics (NCF) are commonly used as semi-finished products for fibre-reinforced polymer applications. NCFs are characterised by their excellent mechanical properties, especially improved strength, stiffness and fatigue life, due to the very low crimp along the fibre direction. Compared to woven fabrics, this type of textile preform is formed by unidirectional, endless and uncurved rovings that are fixed next to each other in the plane to form a layer. Multilayer NCFs, as illustrated in Figure 4, typically consist of several stacked plies with varying fibre orientations that are stacked and stitched together. A polyester yarn in different arrangements can provide fixation between the layers, but thermal treatment is also possible. Different mesh or knit structures are used according to their specific advantages. For example, the tricot weave with a zig-zag arrangement of the stitches offers better draping behaviour, which is essentially due to the larger volume of binding yarns. However, due to the endless fibres and the fixation, in particular, the draping behaviour can be considered disadvantageous. [2], [3]

Despite varying fibre orientations, the individual layers in the NCF may deviate in fibre density or yarn fineness. Thereby, the architecture of the structure and, above all, the fibre orientation of the plies can be defined specifically for the

respective application. The range of applications for NCFs is very broad and includes rotor blades for wind turbines, moulded parts for vehicle and aircraft manufacturing, shipbuilding as well as various sports and leisure articles. [2], [3]

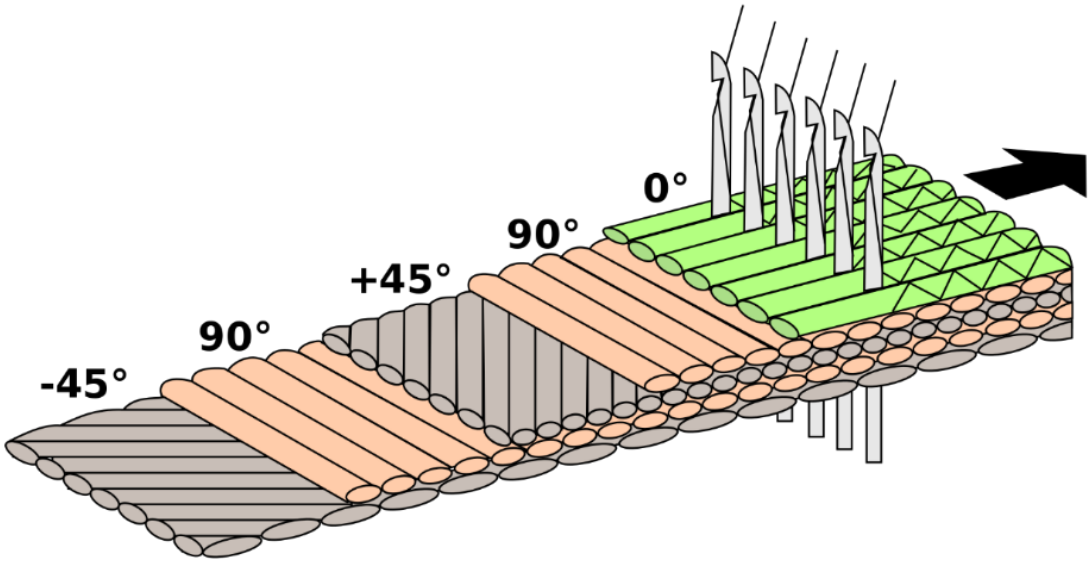

Figure 4: Multiaxial non-crimp fabric with a tricot weave in a zig-zag arrangement [26]

2.3.3 Knitted fabric

In a knitted fabric, the fibres are arranged in a mesh system, which, however, leads to very low utilisation of the mechanical fibre properties. Advantageous properties are the extremely high drapability and the high flexibility concerning the semi-finished product geometry. This means that even complex geometries can be produced net-shape, i.e. in the final contour and without significant waste. On the one hand, the handling of these structures is easy due to the compact geometries. On the other hand, the processing of carbon fibres is very difficult due to the strong fibre ondulations. Further processing or subsequent cutting of meshed fibre structures is also hardly possible. The knitting process is one of the most economical processes in textile technology. However, this must be evaluated concerning the achievable mechanical properties of the field of composites processing. [2]

2.3.4 Veil

Veils are the most widely used semi-finished textile products where typical FVFs of 0.30 and 0.40 can be achieved. They are used extensively, especially in sheet moulding compounds (SMC), but also in resin injection processes, as random fibre mats are easy to impregnate and can serve as flow aids. Furthermore, they are used as cover layers in the production of components to increase the surface quality. [2]

The three most important configurations are shown in Figure 5. A basic distinction must be made between mat systems where the fibres are essentially in the plane and those where the fibres are oriented in all three spatial directions. Depending on the manufacturing process, the fibres can be endless or cut. Another group within the fibre mats are the needle-punched non-wovens, made from various fibrous webs (usually carded webs). Here the fibres are mechanically bonded together through fibre entanglement and frictions after fine needle barbs repeatedly penetrated through the fibrous web. Alternatively, the fibres can be chemically fixed. In this process, the fibres are provided with an appropriate sizing, passed through two rollers and laid in a meandering pattern on a fibre bed aligned in the direction of production. [2], [27]

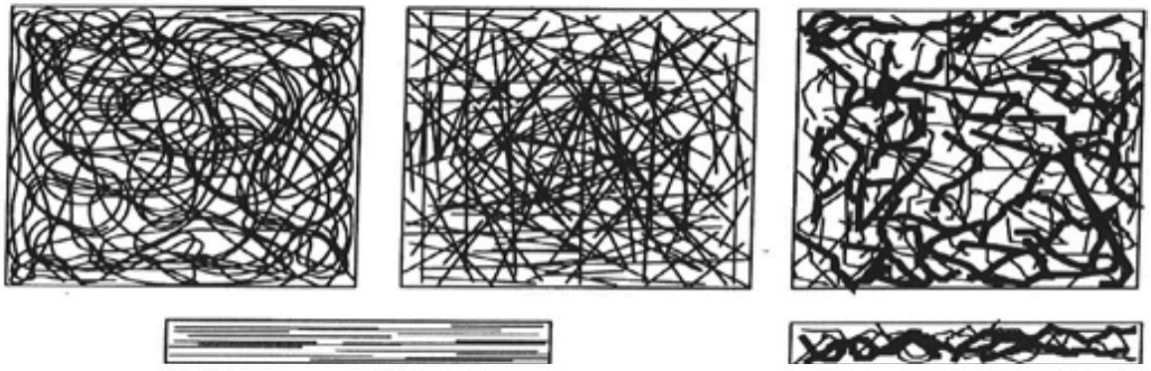

Figure 5: Veil configurations (from left to right: endless, cut and needle-punched fibre mat) [2]

2.4 Compaction behaviour

Robitaille and Gauvin [8]–[10] identified general trends related to the compaction and relaxation of textile reinforcements used for composite manufacturing. Based on the observed parameters, they have determined that in compaction, as the number of layers rises, the representative rigidity, as well as the FVF of the textile structure increases and the stiffening index both for random mats and woven materials, decreases. The authors also demonstrated that the compaction curves move progressively towards higher maximum values with increasing pressure. Moreover, the overall relaxation of the specimen is lower both at higher pressure values and at higher compaction speeds. The opposite is true when the number of layers increases.

Pearce and Summerscales [13] investigated the load-displacement curves for a typical plain-woven glass fibre reinforcement under monotonic load. They mentioned that after repeated loading cycles to a load maximum, relaxation occurs even at the lowest available compression rate. Thereby stored energy is dissipated in a manner that can be represented by an exponential decay relationship and the resulting degree of relaxation is linearly proportional to an increase in FVF. They also concluded that there is a linear increase in the time to reach a target pressure with each additional layer of fabric and further noted that fabric-to-fabric interaction provides a greater constraint than fabric-to-platen interaction.

Worth mentioning is the effect of the thermal history on the transversal compressibility of a textile reinforcement structure, as it shows time-dependent effects. Especially at higher levels of temperature, the fabric packing increases accompanied by a decrease in material relaxation. It shows that a heated specimen follows a parallel tendency, albeit at different levels. [28]

The experimental results can be presented in various forms, such as curves of compaction pressure or compaction force as a function of FVF to porosity or gap height. Empirical or semi-empirical models derived from compaction tests as a result of the response of a textile reinforcement structure, are usually expressed

as a power-law relation, representing the FVF V_f as a function of the applied pressure p during compaction, as follows [1], [8]–[10]:

$$V_f = V_{f0} \cdot p^m \tag{4}$$

V_{f0} initial FVF

m stiffening index

The dependent and independent variables for compaction curves are the FVF as a function of the compaction pressure. For relaxation curves, the dependent variable is the ratio between the current compaction pressure p and the initially applied compaction pressure p_0, while the independent variable is the time t. This relationship is also described as follows [1], [8]–[10]:

$$\frac{p}{p_0} = 1 - c \cdot t^{(1/\alpha)} \tag{5}$$

c pressure decay after 1 s

Here, α forms the relaxation index, which is defined as [29]:

$$\alpha = \frac{p}{p_0} \tag{6}$$

The relaxation process itself can be described by the theories of energy dissipation after a compression-relaxation cycle and on this bases, the relaxation index can be refined according to [20]:

$$\alpha = 1 + \frac{E_d(m+1)}{p_0} \tag{7}$$

E_d volumetric dissipation energy

m stiffening index

The more energy is dissipated, the lower the relaxation index α and the more pronounced the relaxation. Essentially, E_d is the energy dissipated due to friction during yarn movement. Further, it is shown for non-crimp fabrics that the initially applied compaction pressure p_0 increases faster than the volumetric dissipation energy E_d. [20]

A representative thickness-pressure curve of a woven fabric preform under compaction can be divided into three main stages, as illustrated in Figure 6. An initial stage with no applied pressure can be defined as Regime 0, although this is not presented in the shown figure. [30], [31]

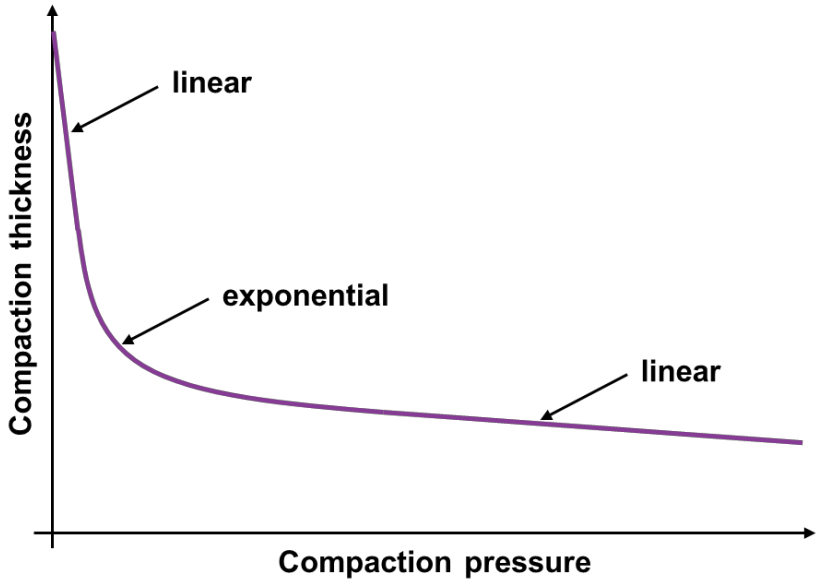

Figure 6: Typical compaction curve with compaction pressure against compaction thickness of a woven fabric

As illustrated by the pressure-thickness curve, the preform gets compacted under increasing levels of pressure. At this stage, the individual fabric layers are only in contact with one another in very few spots. This allows each layer to arch over another without close contact. However, when compaction pressure is applied, the bundles deform, offering almost no resistance due to their low flexural rigidity. The preform quickly enters a state where a single layer is in contact with the adjacent ones, thus entering Regime 1.

At the moment when the woven fabric layers are slightly compacted, Regime 1 initiates which can be considered to be linear. This brings the fibre cross-sections into closer contact compared to those of the initial stage. When compaction rises, the space between the fibres decreases rapidly and the yarn offers little or no resistance to the reduction in thickness. Therefore, the constituent yarns offer little but finite resistance to the compression of the fabric by bending at low pressure. The increased pressure can cause slippage to occur around large pores or gaps where the structure of the stack is not consistent. However, the resistive force of

friction between the points of contact of the individual layers prevents yarns from slipping. During this phase, which is dominated by the bending of the yarns, the deformation of the preform arises almost exclusively from the apparent compressibility of the interstitial space caused by the yarns filling the voids, and not from the compressibility of the fibre material itself.

As the compressive force increases, the contacts between the fibres increase, so that the friction between the fibres offers more and more resistance to the external pressure. Therefore, the transverse pressure resistance of the yarn is no longer negligible, but increases exponentially, as can be seen in the second stage of the compression curve, Regime 2. Here, the larger voids are filled and the remaining interstitial space exists in a more stable structure. The deformation itself is caused by the compression of both, the solid and the deforming voids, which is characterised by the non-linearity of this stage. When further pressure is applied, the solids are strongly deformed and the cross-sectional geometry is considered to have reached self-similarity so that the porosity approaches a constant.

At the last stage, represented by Regime 3, the corresponding fabric pressure curve is directly related to the transverse modulus of the fibre itself and a linear trend. When the voids between the fibres reduce sufficiently and the sliding of the fibres reaches its limit, the fibres themselves start to carry the compression. Here the fibres are in areal contact with each other and the few isolated pores are surrounded by solids. The entire structure forms a network with low porosity, which can be assumed to be a function of the compressibility of a solid.

Polturi and Sagar [31] presented a model for the compaction behaviour of dry fibre assemblies using an energy minimisation scheme. The authors characterised the structural changes for a woven fabric during compression between two parallel plates as follows:

a) The crimp balance is rarely the same for warp and weft yarns, as it is affected by the tension applied during weaving and subsequent finishing processes. This consequently leads to small gaps δ, as shown in Figure 7 a. During the initial compression stage, this gap gradually decreases to

zero, resulting in an increase in curvature in one set of yarns and a corresponding decrease in curvature in the second set of yarns.

b) As soon as the gap δ is zero, as represented in Figure 7 b, further compression results in the flattening of the yarn, accompanied by a reduction in the crimp of the crossing yarns.

c) The flattening of the yarn continues until the individual fibres are in contact, as represented in Figure 7 c.

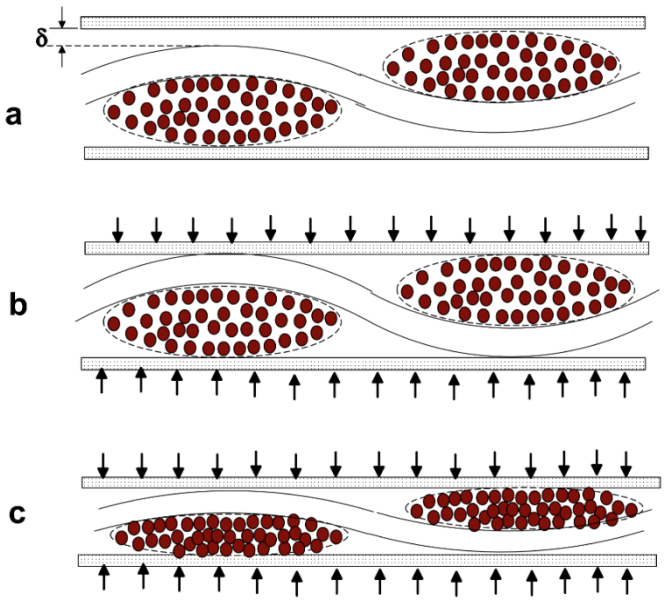

Figure 7: Three stages of compaction of textile reinforcement structure [31]

The illustrated compaction behaviour can significantly influence the permeability as well as the FVF and the geometry of the textile layer, which subsequently affects the elastic properties of the laminate, mode of damage initiation and progression [31]. This inverse relationship between the FVF and preform permeability is represented in Figure 8 [31], [32].

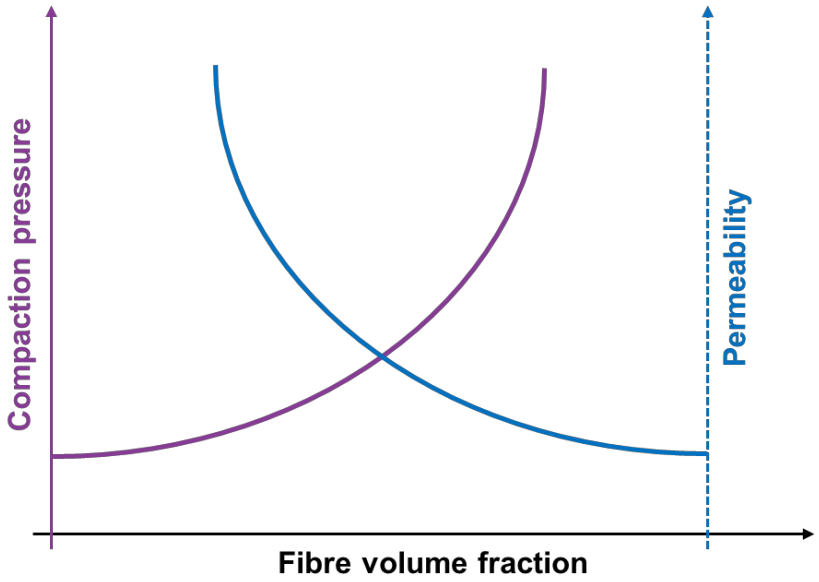

Figure 8: Relationship between FVF and compaction pressure and preform permeability

Somashekar and Bickerton [33] reported that the viscoelastic recovery of a continuous fibre mat and a plain woven fabric remains constant across a range of tests and only varies with the number of layers in a specimen (amount of viscoelastic recovery reduces with an increase in the number of layers). The compaction behaviour of a woven textile is significantly affected by the stacking sequence and also by the nesting characteristics of the rovings as well as their interaction with adjoining layers. The viscoelastic recovery of a continuous fibre mat, on the other hand, depends on the realignment over time of the individual fibres in the yarns, the yarns themselves and the fabric layers. While nesting does take place, there might be no intertwining or embedding of filaments of other layers. Therefore, the individual layers of a plain-woven fabric are more free to realign themselves, as compared to a continuous fibre mat. Furthermore, the resistance of woven fabrics against deformation decreases when the linear or yarn density increases or the number of crossing points is increased [32].

Non-crimp fabrics on the other hand would be expected to have less relaxation than woven fabrics, as the fibres bend less and the fibre network has fewer possibilities to reorganise itself [34]. For non-crimp fabrics, in particular, it is shown that increasing the stitching length, increasing the linear yarn density as well as

the usage of 0/90° fibre orientations instead of ±45° tend to increase the resistance against deformation, while the stitching type has no influence [32].

2.4.1 Single-layer deformation

Chen and Chou [35] described the elastic deformation of a single-layer fabric as follows. Initially, the compressive force acts at the highest points of the top and bottom surfaces of the fabric. As the compressive force increases and the external force distributes over a contacting area, the elastic deformation of the fabric extends, and the FVF increases while the thickness of the fabric preform decreases. In addition, the contact area expands and the shape of the yarn cross-section changes as the external force increases. Finally, when the force reaches a certain value, the fabric cannot be compressed any further.

2.4.2 Multi-layer deformation

For multi-layer reinforcement structures, Robitaille and Gauvin [8]–[10] identified that, as the number of layers increases, the representative rigidity as well as the initial FVF increase, while the stiffening index decreases. In conclusion, with a rise in the number of layers at the same applied level of compaction pressure, the specific stiffness of a textile reinforcement structure reduces. This behaviour can be represented by means of mechanical springs for the individual layers and inter-layer-interfaces, as illustrated schematically in Figure 9.

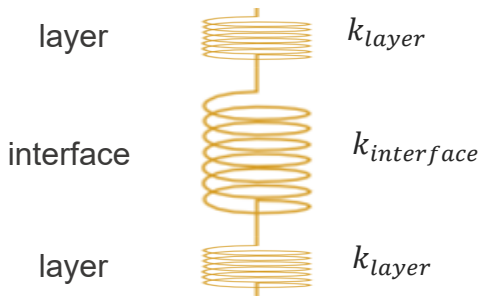

Figure 9: Mechanical spring model with an inter-layer-interface [36]

The inter-layer interface is expected to show a higher level of elasticity than a fabric layer due to nesting effects, so the spring constant of a single layer must also be higher. To represent a serial connection of several layers, the equivalent spring constant k_{eq} can be calculated as a function of the individual spring constants k_i according to:

$$\frac{1}{k_{eq}} = \sum_{i=1}^{n} \frac{1}{k_i} \tag{8}$$

Furthermore, the following equation represents a replacement model for calculating the overall spring constant for a number of layers n as a function of the spring constant of a single layer k_{layer} as well as that of an inter-layer-interface $k_{interface}$:

$$k_{eq} = \frac{1}{n \cdot \frac{1}{k_{layer}} + (n-1) \cdot \frac{1}{k_{interface}}} = \frac{1}{n \cdot \left(\frac{1}{k_{layer}} + \frac{1}{k_{interface}}\right) - \frac{1}{k_{interface}}} \tag{9}$$

Since the spring constant represents the quotient of expansion and force, the overall stiffness and thus the equivalent spring constant of the structure decreases as the number of layers increases and less force is required to compress the specimen to a desired level of height.

Following Chen and Chou [37], the compaction of a multi-layer woven-fabric preform not only flattens the yarn bundles, reduces the pores and gaps among the fibres and yarns, which can also be observed with a single-layer, but also results in more elastic deformation, shows nesting and inter-layer packing with the adjacent layers. Obviously, on the one hand, nesting does not need to be considered for a single-layer preform. For a multi-layer preform, on the other hand, one of the most important contributions to preform compaction is the nesting of layers. The significant reduction in thickness and increase in FVF due to nesting is only caused by geometrical shifts between adjacent yarns. The compressive force acts at the outermost points of the outer sides of the lowest and uppermost fabric layers as well as at the points of contact in the intermediate layers. As the externally applied compressive force increases, the contacting area expands and the force distributes homogeneously. As a result, the elastic deformation of the

fabric extends and the thickness decreases, while the shape of the yarn cross-section changes to a flat oval form and the FVF increases. When the applied force reaches a limit, the fabric cannot be compressed any further and the shape of the yarn cross-section approaches a rectangle.

To describe the maximum nesting cases in multi-layer fabric preforms, it is helpful to make the distinction between two-layer preforms and those consisting of three or more layers. Since there is only one interface between the layers, the nesting case of a two-layer preform represents the simplest problem. Here, the upper and the bottom layer have the same configuration under elastic deformation and the resulting thickness reductions are identical. With the use of the beam theory and simplifying by assuming that the stiffness of the preforms in the thickness direction for non-nesting fabrics is only half as high as for maximum nesting. [37]

Nesting decreases the initial thickness, with the lowest initial thickness occurring at the maximum nesting case [38]. The relationship between initial thickness h and final thickness in compression t, can be expressed by the following relation:

$$t(p) = h - \Delta(p) \tag{10}$$

Δ thickness deformation

Here, t changes in relation to h and Δ at a given pressure p. In conclusion, at a given pressure, $\Delta(p)$ is constant and $h(p)$ significantly affected by h, which is determined by the amount of nesting and keeps constant once the layers are established [38].

With regard to multi-layer preforms with three or more layers, Grieser and Mitschang [19] investigated the differences in compaction behaviour between a 3-ply and a 6-ply carbon fibre non-crimp fabric. They showed that at an equal superficial density, 6-ply preforms require 75–88 % higher compaction forces than 3-ply preforms and further noted, that this relationship remains constant with decreasing or increasing total superficial density which is directly affected by the ply number. Because of lower standard deviations, textiles with higher superficial density are easier to compact and more suitable to achieve robust processes.

Polturi and Sagar [31], as well as Chen et al. [39], defined yarn cross-section deformation, yarn flattening, yarn bending deformation, void/gap condensation and nesting as the basic effects that affect the compaction behaviour of textile reinforcement structures. Figure 10 schematically shows an uncompressed and compressed state of the effects on the left and a typical compaction curve with the FVF against the compaction force on the right to indicate when the effects occur.

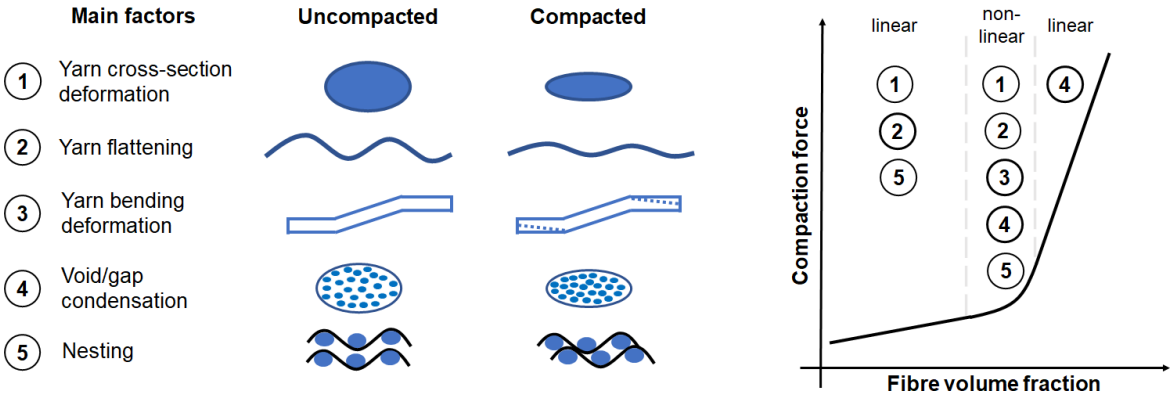

Figure 10: Basic compaction effects when compacting a textile reinforcement structure (left) as well as typical force progression with the occurring effects over the FVF including a relaxation stage (right) [19], [31]

Depending on the material itself as well as the current stage of the compaction curve, different effects are dominant. The flattening of the yarns has almost no influence on the compression of non-woven fabrics, whereas it influences the compaction behaviour of woven fabrics and random mats. The factor of void/gap condensation is more important to describe the compaction behaviour of random mats and woven fabrics than it is for non-woven fabrics. The resulting compaction behaviour of a textile reinforcement structure is a complex mixture of these basic effects, with nesting being a dominant factor, especially in woven fabrics. [19], [31], [39]

Therefore, Figure 11 shows a schematic illustration of the nesting effects between (a) woven and (b) non-crimp fabrics. The crimped weave structure on the left provides space for the adjacent plies to nest in, resulting in an apparent nesting effect. In comparison, with non-crimped fabrics, as shown on the right, it is more difficult for the layers to nest into each other due to the restricted movement caused by the stitching yarn. Instead, some threads sink into the gaps between the plies, resulting in a reduction in thickness.

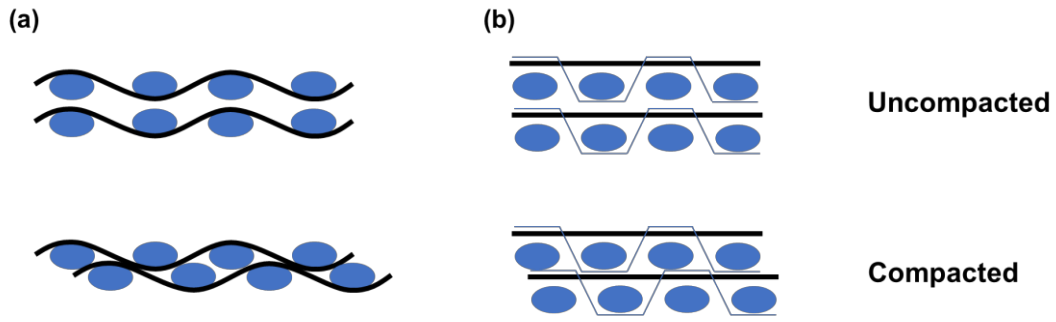

Figure 11: Schematic of nesting effects for (a) woven and (b) non-crimp fabrics [1], [29]

Furthermore, it is reported by Yousaf et al. [40] that the degree of ply compaction, as well as the degree of nesting between the individual plies, are influenced by yarn architectures. In the case of plain, twill and sateen fabrics, the thickness reduction during transverse compaction is highest for twill and sateen and lowest for the plain weave fabrics, which can be attributed to the fact that the latter shows the highest number of interlacements per unit area. Therefore, the larger float length of twill and sateen fabrics results in a loose structure, allowing for more bending deformation during compression. In general, better nesting is present for plain weave fabrics, but during compaction of multi-layer stacks of the aforementioned types of weaves, the bending deformation contributes more towards thickness reduction than the nesting of the layers. As a result, the average thickness of a ply in a two-ply nested pack of twill is about 5–8 % smaller than in a single-ply preform [41]. Lomov et al. [42] showed that the effect increases proportionally to (n-1)/n for n-ply preforms, increasing the effect between 10 to 15 % for plain weave fabrics. For non-crimp fabrics, the inter-tow spacing and stitching yarn thickness influence the degree of nesting. In addition, the reduction in thickness is greatest in 0/90° fabrics compared to ±45° fabrics, which can be attributed to differences in the mesh architecture of the stitching yarn on the fabric surface and different yarn spacing, which allows for better inter-tow nesting [40]. However, the experimental position of the layers is not regular, which means that when the orientations of the layers are different, which represents the standard case, the nesting is much smaller [43].

The nesting coefficient γ is a useful way to quantify the extent of nesting and can be calculated as follows [29]:

$$\gamma = \frac{t_n}{t_1} \tag{11}$$

t_1 thickness of a single layer

t_n thickness per layer when the number of layers is n

A lower nesting coefficient means a more pronounced nesting effect. The nesting coefficient decreases as the number of layers or the pressure increases. At maximum pressure, the nesting coefficient tends to be stable as the number of layers increases, indicating that the deformation of the nesting may be very strong when the gaps are completely filled. [29]

2.4.3 Dry and wet compaction

Comparing the relaxation of preforms in dry and wet states, it can be seen that lubrication influences the relaxation process, but has no significant effect on the compression curves themselves. This can be explained by the squeezing of the fluid and the lubrication effect. The fluid squeezed from the preform dissipates the stored energy and, at the same time, more fibre movement leads to more frequent friction within the preform. Although lubrication can reduce the coefficient of friction, the contribution of fluid extrusion and fibre movements to increasing energy dissipation is generally more remarkable. Considering the low friction of textile fibre reinforcements, especially non-crimp fabrics, lubrication has no significant influence on the compaction behaviour. However, relaxation tests on carbon non-crimp fabrics show that the relaxation phase is influenced by parameters such as lubrication and initial pressure, on account of the energy dissipation during the process. [29]

Further, it is reported that the compaction behaviour of dry woven fabrics is not significantly affected by the compaction speed [44]–[46]. Similarly, the compaction speed has only a limited influence on dry carbon non-crimp fabrics. The results of wet compaction tests with different compaction speeds show analogous curves, which also indicates a limited influence of the compaction speed for wet non-crimp fabrics [29]. Kruckenberg et al. [21] reported that lubrication reduces the frictional forces during nesting and yarn deformation and allows the fabric to approach a

maximum packing fraction. Thereby, the FVF in relaxation increases not only with the number of layers but also with lubrication. In general, thicker stacks are easier to compact, as are lubricated stacks [34].

Another consideration must be the degree of compaction and the type of preform, as both influence the infiltration time [39]. Glass fibre-mat preforms show, an increase in fibre and yarn realignment and reorientation due to the lubrication effect as well as interactions between consecutive layers during the compaction stage [47]. Plain-woven fabrics and unidirectionally knitted materials show similar infiltration behaviour for the same degree of compaction. Thereby, the infiltration time increases with the FVF, as the permeability of the preform decreases [39].

2.5 Injection of fluids

2.5.1 Basics of flow processes

When injecting a low-viscosity matrix system into a fibre reinforcement structure, a fundamental distinction must be made concerning the propagation of the flow front. This must be differentiated into one-dimensional, in-plane or two-dimensional and three-dimensional flow. [2]

One-dimensional flow (1D)

A one-dimensional form of Darcy's law can be obtained, which is particularly important for permeability measurement methods, as follows [2]:

$$v = -\frac{k_x \, \Delta \mathrm{p}}{\eta \, \Delta \mathrm{x}} \tag{12}$$

v average velocity of the fluid in the direction of the coordinate x

k_x permeability tensor in one-dimensional form

η viscosity of the fluid

Δp pressure difference

Δx flow length

Two-dimensional flow (2D)

In the case of in-plane flow, due to the different material structures, two different forms of flow front geometry can be distinguished. In the two dimensions considered, a circular propagation of the flow front of the injected fluid occurs in the case of an isotropic material and elliptical propagation in the case of an anisotropic material. For example, veils show a circular propagation and non-crimp fabrics an elliptical one, since there is a clearly defined preferred flow direction. [2], [48]–[50]

For the incompressible flow of viscous fluids in porous media, the continuity equation and Darcy's law form the fundamentals [51]. In isotropic materials, the partial differential equation for the pressure field is found as the Laplace equation, which can be solved analytically. In anisotropic materials, however, the resulting pressure field cannot be solved directly [52]. Alternatively, with the use of coordinate transformation, the real elliptical flow front propagation can be reduced to a model with cylindrical flow front geometry and the mathematical problem can be solved one-dimensionally. Through a transformation, the main axis permeabilities of the real system are obtained [48], [53].

Three-dimensional flow (3D)

Injection of a viscous fluid into a stack of flat reinforcement textiles via a vertically placed sprue hole leads to a three-dimensional radial spreading of the liquid within the fibres, as shown in Figure 12 for an anisotropic material on the left as well as for an isotropic material on the right. In principle, this arrangement allows the acquisition of all data required for a determination of the three main axis permeabilities in one test. Here, the derivation of a permeability model is analogous to the two-dimensional case. [2]

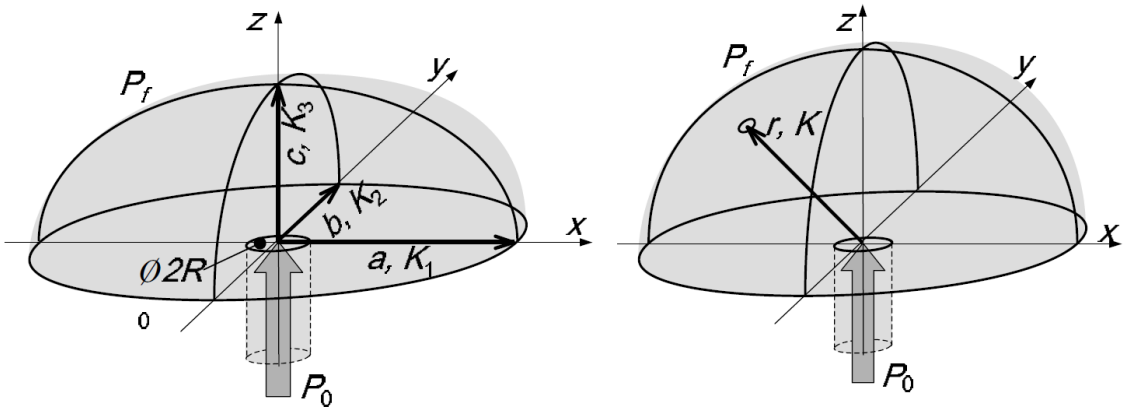

Figure 12: Point injection for left anisotropic and right isotropic material [2]

2.5.2 Influencing factors on preform permeability

As already described, permeability is a parameter of the textile reinforcement structure and therefore independent of the process itself. However, this also means that the permeability must be recorded independently and individually for each textile structure. For example, a plain weave fabric shows a higher permeability than a comparable twill weave fabric at the same level of FVF. In addition to the architecture of the textiles, the handling and processing of semi-finished products play a decisive role. Shearing occurs during draping, which has a significant influence on permeability. Furthermore, the homogeneity of permeability is significantly reduced by handling and draping [2]. In addition, the transversal permeability of a textile reinforcement fabric depends on the mobility of the fibres [16].

A further permeability-reducing effect was found to be a heterogenization of the FVF distribution, which also occurs when no overall compaction takes place. The permeability in the transverse direction thus depends not only on the FVF but also on the pressure drop or respective flow rate. Concerning the flow rate, stagnation or even a decrease can occur when the pressure drop increases. Fluid flow strongly increases the resistance to deformation when the FVF is low, but this influence can be reversed at higher fibre contents. [14], [31], [32], [54]

2.5.3 Wetting of compressed reinforcing materials

Hautefeuille et al. [12] identified and localized the driving forces inducing the deformation of an impregnated fibre reinforcement specimen subjected to consolidation. Among the forces acting on the fibre network, the drag force is greater than the form resistance. The authors further highlighted the capability of fluid flow to cause a displacement in the fibrous reinforcement, the so-called washout phenomenon, which leads to significant changes in fibre architecture. An early observation of the washout phenomenon was made by Han et al. [55], who pointed out the ability of the fluid to cause segregation in the thickness between a fibre-free region and the fibre-bed during fluid injection orthogonal to the plane. Typical injection curves are shown in Figure 13 [18]:

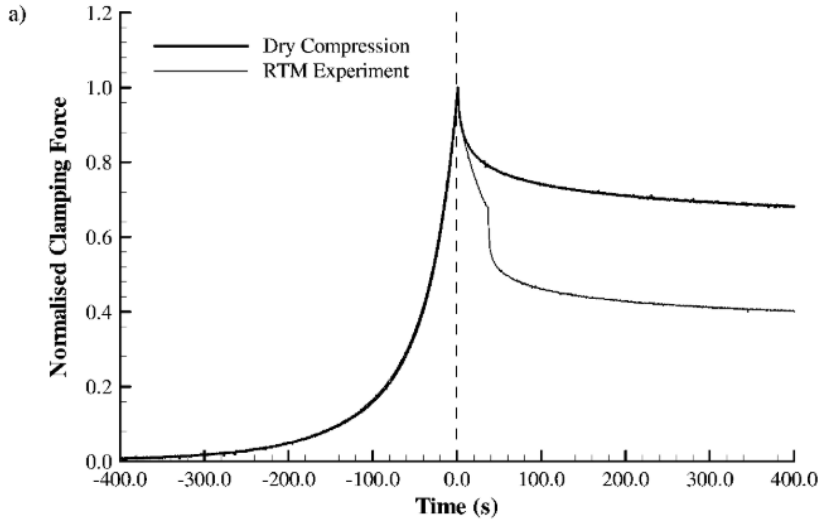

Figure 13: Compaction curves for dry experiments as well as with injection [18]

The dry compression curve shows a rapid increase as the cavity thickness reduces. After reaching a force maximum, the phase of relaxation begins and the fibres in the fabric layers reorganize. Before injection, the RTM curve is identical but drops significantly below the dry curve at the beginning of the injection phase, which starts immediately after the mould is completely closed in its final position. The behaviour shows a balance between the force due to the pressure of the fluid and the accelerated stress relaxation within the reinforcement. The presence of a fluid serves to lubricate the fibre-to-fibre connections, allowing the reinforcement to transition to a state that requires lower compressive stress. After the injection is

complete, the curve suddenly drops as the force generated by the internal fluid pressure is dissipated. Shortly after, the RTM curve exhibits an identical relaxation rate as the dry curve but settles at a much lower level. [18]

3 Experimental

The objective of the experimental part of this study is to analyze the transverse compaction behaviour using four structurally different textile reinforcement materials, particularly during in-situ impregnation during the stress relaxation phase. Specifically, the influence of FVF and the number of layers at different fluid injection pressure levels on the stress relaxation profile will be examined.

3.1 Reinforcing materials

The reinforcement materials used on the course of this thesis are listed in Table 1. These are a total of four different material architectures, three of which are glass fibre materials and one is made of viscose.

Table 1: Overview of the properties of the textile reinforcement materials used

	EBX 600	**Hexcel 1202**	**MA 111-300**	**Viscose V4**
Textile architecture	NCF	WF (Twill 2/2)	Veil	Knit
Fibre material	Glass	Glass	Glass	Viscose
Nominal areal weight	620 g/m^2	300 g/m^2	300 g/m^2	450 g/m^2
Fibre density	2.6 g/cm^3	2.6 g/cm^3	2.6 g/cm^3	1.49 g/cm^3
Thermoset binder	No	Yes	No	No
Stitching yarn	Polyester	-	-	-

Figure 14 presents the aforementioned materials.

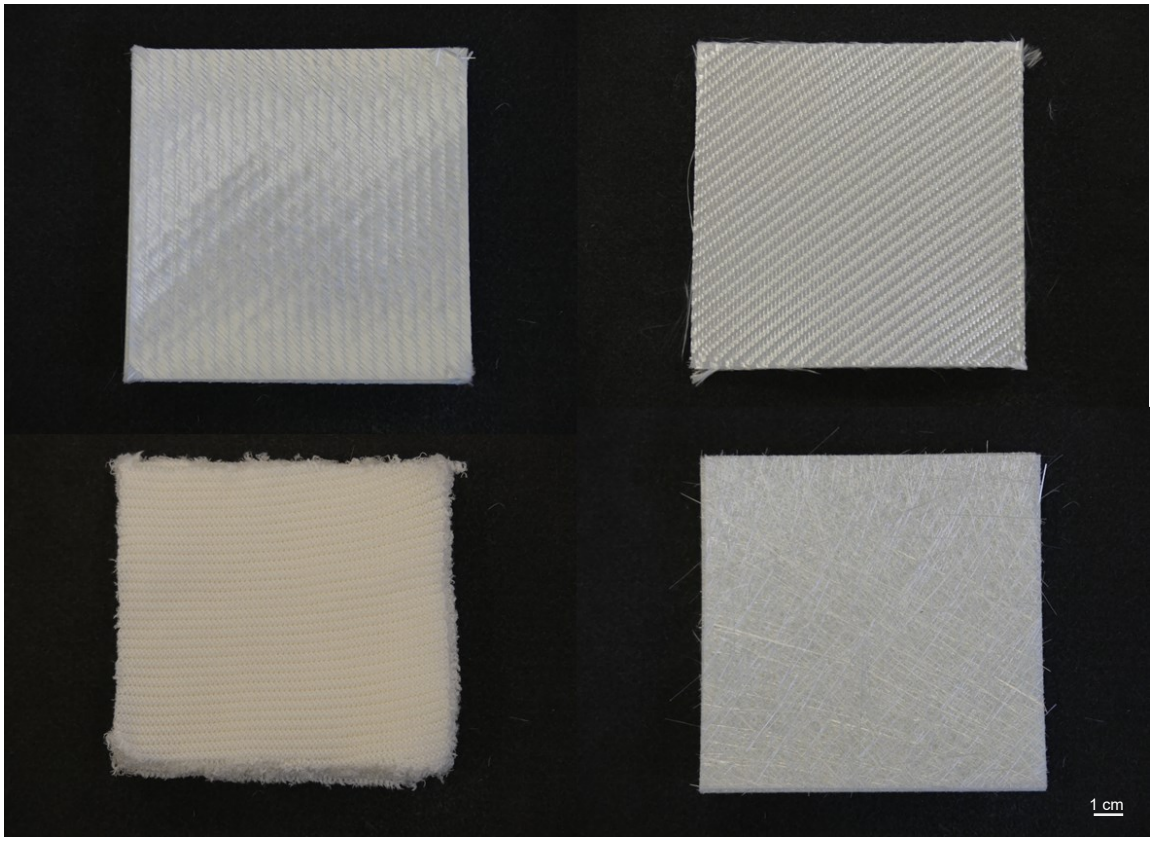

Figure 14: Test samples of the four reinforcing fabrics: NCF (top left), WF (top right), Knit (bottom left), Veil (bottom right)

3.2 Test fluid

The test fluid is a silicone fluid of the type Xiameter PMX-200 with a viscosity of 100 cSt from the manufacturer Dow Corning. It is a polydimethylsiloxane polymer that is processed to form essentially linear polymers in a wide range of average kinematic viscosity. It is characterized by its crystal clear appearance and high solubility in organic solvents such as aliphatic and aromatic hydrocarbons as well as the halocarbon propellants used in aerosols. In water, it is easily emulsified with standard emulsifiers and common emulsification techniques. The fluid's specific gravity is 0.964 at 25 °C with a refractive index of 1.403. The open cup flash point is above 326 °C, the melting point is at -28 °C and the pour point is at -65 °C. The viscosity-temperature coefficient is 0.59 and the surface tension is 20.8 dynes/cm at 25 °C.

3.3 Test setup

In order to characterise the transversal compaction behaviour of textile architectures, a specifically developed test rig is used. The setup shown in Figure 15, mounted to an universal testing machine (UTM) from Hegewald & Peschke, is used for this purpose.

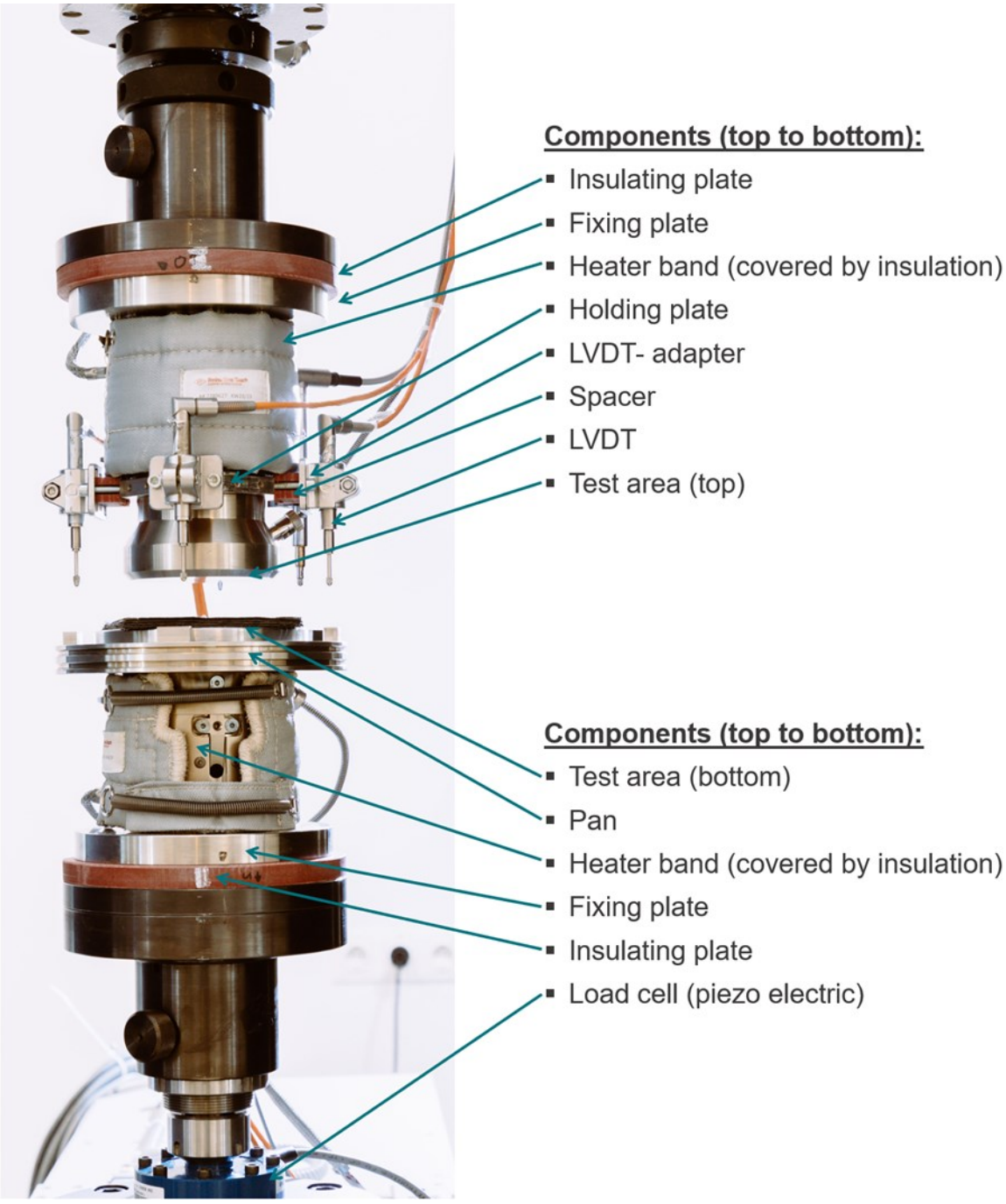

Figure 15: The test setup used in this thesis, mounted on a UTM from Hegewald & Peschke

The corresponding test specimen is located between two round and flat metal plates, whereby the upper side is rigidly attached to the UTM. The stamp with a diameter of 100 mm forms the upper test surface. The lower part of the setup is mounted on a movable crosshead that can attain variable test speeds. Both sides are mounted via a fixing plate and thermally decoupled utilizing an insulating plate. In addition, the test surfaces can be heated via the insulated heating bands fixed around the metal connection structures.

Located around the upper test surface, Linear Variable Differential Transformers (LVDT) are mounted via the corresponding adapters and spacers. During the measurement, all of the five LVDTs are in use and record the attained positional data. One of them is used for motion control of the UTM. The LVDT data, load cell readings as well as crosshead position is archived by means of the UTM control software LabMaster. The control takes place via specifically stored block programs, which adapt the test speed exactly at the predefined positions, according to the selected settings, and thus regulate the position. The automated control of fluid injection as well as the recording of all the LVDTs generated data is realized with a specifically developed LabView application.

The fluid injection gate with a diameter of 10 mm is centrally positioned at the lower test area. Here, the fluid is injected into the test specimen from below, through the risers connected to it. The test area is surrounded by a semicircular channel to collect excess fluid, which can be drained off directly through another opening in the channel itself. Figure 16 shows the feeding tube reaching into the lower test setup with the attached fluid pressure sensor and the injection opening in the test area itself.

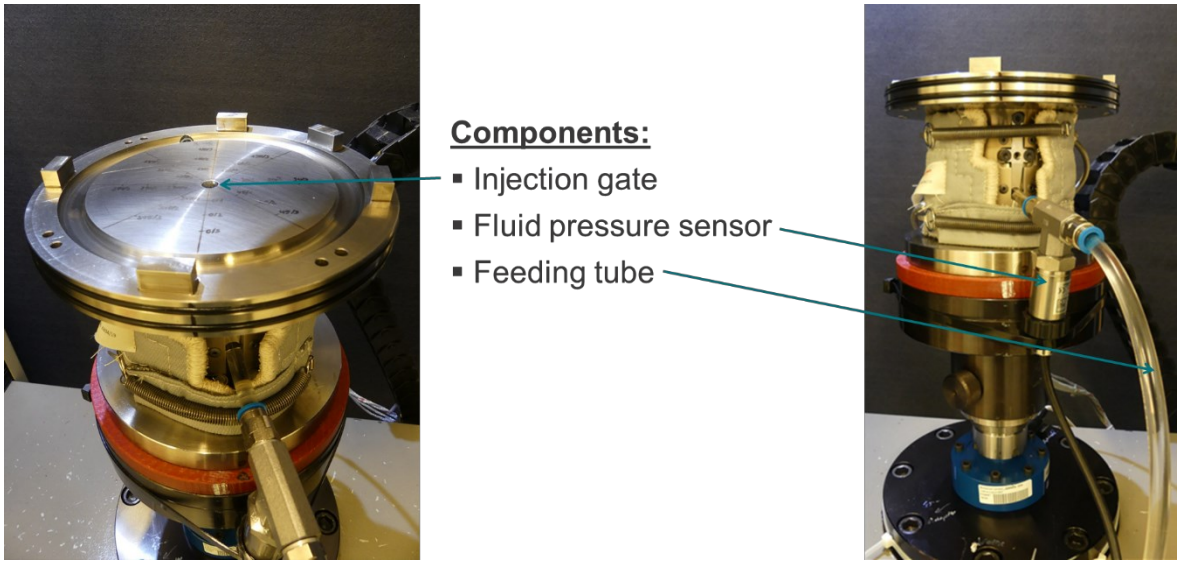

Figure 16: Lower test setup with injection gate, feeding tube and fluid pressure sensor

The feeding tube is mounted to a pressure pot which in turn is coupled to a compressed air supply that is regulated by a corresponding control unit via the LabView application. Inside the pressure pot is the silicone oil supply and between the fluid pressure sensor and the pressure pot a valve to regulate the fluid supply. Before each measurement, it must be ensured that sufficient test fluid is available in the pressure pot. To prevent air in form of bubbles from accumulating inside the feeding tube, it is flushed with fluid beforehand.

The piezo-electric load cell on the very bottom of the test rig records the force-related measurement data inside a measuring range of up to 30 kN, whereby an upper limit of 27 kN is set to protect it from potential damage. This test setup allows an investigation of the compressional and decompressional characteristics of a specimen under compaction as well as its relaxation behaviour. This is of importance, particularly for the RTM process, in ensuring the shape consistency of the textile structure within the mould.

3.4 Test configuration

Figure 17 illustrates how a transversal compaction experiment, in the compression-relaxation configuration with in-situ impregnation, is designed.

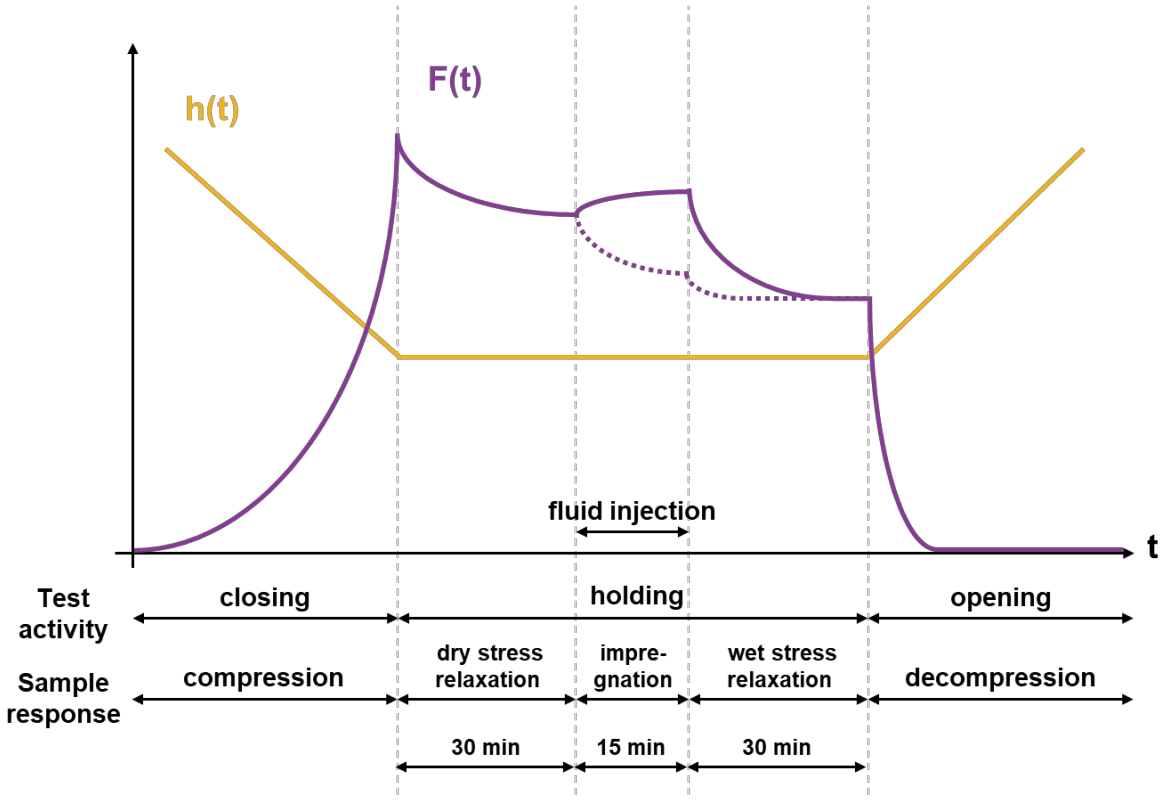

Figure 17: Compression-relaxation test-configuration with in-situ impregnation

A typical relaxation test is characterised by a compression of the textile by moving the test surfaces together to a calculated target height. This is followed by a correspondingly long holding phase to allow the material to relax and finally, a decompression phase in which the gap is opened again to end the test. Depending on the material architecture, this holding phase may vary in time, but the aim is to maintain a relatively stable pressure level at the end of this period. In this thesis, such an experiment is complemented by in-situ impregnation of the fabric sample. The main advantages are the characterization of dry and wet compressibility in a single measurement as well as reduced experimental time, material usage and influence of material variability.

It is expected that the relaxation curves of the individual textile architectures in the dry and impregnated areas largely overlap. During the injection phase, a higher

pressure level, depending on the injection pressure level, can be assumed. Thereby, the total force indicated by the load cell readings is made up of two components, the pressure from fluid injection and the pressure exerted during compaction, which is caused by the resistance of the specimen to the movement of the testing machine. The latter depends primarily on the relaxation capacity of the specimen itself and can vary considerably. Figure 17 shows two different curves, one drawn as a solid and the other as a dashed line. These should give a possible outlook on the potential pressure course or reaction of the material during the in-situ impregnation.

The measurements are carried out on four materials as introduced in Section 3.1. They are cut to square test specimens with an edge length of 120 mm utilizing an automated cutting machine and stacked homogenously in varying layer configurations. This test specimen dimension ensures that the textile is completely compressed by the stamp with a diameter of 100 mm.

3.5 Design of experiments

In the first step, a pretest series is performed, to determine the optimal fluid injection pressure level for each test specimen. Due to the limited supply, the knitted fabric was not tested here. The number of layers was kept constant at five, whereas the FVF was chosen at 0.45. In contrast, the fluid injection pressure was varied between three different levels at 0.8, 1.4 and 2.0 bar. Particularly with highly permeable materials such as the Veil, increased fluid consumption is to be expected, especially at the highest pressure level.

The central question here is how high the injection pressure level can ultimately be selected without causing undesirable effects within the textile structure. Such undesirable effects can be, for example, an occurring fibre washout or significant damage in the architecture, such as a displacement of fibre bundles or deformations in the layer structure. Especially at low compaction levels, this may become critical. These effects are evaluated optically by photographing the individual specimens before and after the measurement and then evaluating them

qualitatively. Finally, the relaxation and injection phase were in terms of the material response of the four tested materials.

To compare the textile architectures under transversal compaction, the number of layers and the FVF are varied several times in the subsequent main test series. The injection pressure remains constant, but takes into account the given material difference and is selected based on the results of the pretest series.

Finally, the material responses are again to be characterized and the textile architectures are compared on this basis. Here, an increasing compaction pressure is to be expected with increasing FVF on the one hand and a decreasing number of layers on the other hand.

In order to compare the material architectures, the FVF and the number of layers are varied. For the NCF and WF, the FVF gradually increased to 0.45, 0.50 and 0.55. Both materials are prepared in test specimens of 3 and 5 layers. An additional series with 14 layers of the WF was realized in order to allow a reference to a benchmark exercise [1] using the same specimen material in this configuration. Further, the Veil is prepared with 3 and 5 layers but only set to a FVF of 0.35, 0.40 and 0.45, as the measurement range of the load cell i did not allow for higher levels. Due to limited material availability, the Knit is measured in only one series with a configuration of 5 layers. In contrast to the Veil, however, a somewhat higher level of compaction can be achieved, which is why the measurements are performed at a FVF of 0.40, 0.45 and 0.50 respectively.

To reach the desired FVF, the compaction height of the specimen is determined by the following equation [8]–[10], [13], [45]:

$$h = \frac{m_A\, n}{\rho_f\, V_f} \tag{13}$$

m_A	areal weight of the fabric
ρ_f	density of the fibre
n	number of layers
V_f	FVF

For the NCF, the stitching yarn must be taken into account and the following equation is used to calculate the compaction height [45]:

$$h = \frac{{m_{A,total}}^2}{\left(m_{A,fabric} \cdot \rho_{f,fabric} + m_{A,yarn} \cdot \rho_{f,yarn}\right)} \cdot \frac{n}{V_f} \quad (14)$$

$m_{A,total}$ areal weight of the fabric and the stitching yarn in total

$m_{A,fabric}$ areal weight of the fabric

$m_{A,yarn}$ areal weight of the stitching yarn

$\rho_{f,fabric}$ density of the fibre in the fabric

$\rho_{f,yarn}$ density of the stitching yarn

The resulting target compaction height for the compression-relaxation experiments are summarized in Table 2, depending on the FVF and number of layers to be set.

Table 2: Target compaction height h [mm] at FVF and number of layers

		FVF [-]				
Material	**Layers [-]**	0.35	0.40	0.45	0.50	0.55
NCF	3	-	-	1.59	1.43	1.30
	5	-	-	2.65	2.38	2.17
WF	3	-	-	0.77	0.69	0.63
	5	-	-	1.28	1.15	1.05
	14	-	-	3.59	3.23	2.94
Veil	3	0.99	0.87	0.77	-	-
	5	1.65	1.44	1.28	-	-
Knit	5	-	3.78	3.36	3.02	-

Of importance for the evaluation is the diagram shown in Figure 18 with the three highlighted measuring points. Thereby, $p_{max,dry}$ represents the maximum pressure achieved in the dry state as a result of the compression to the desired target

height, within the initial phase of the experiment. $p_{end,dry}$ is the point after 30 min of dry relaxation of the material in the constrained position and $p_{end,saturated}$ is the one in the saturated state after the injection phase with the test fluid. The latter two are average values of pressure data acquired in the last 10 s of the corresponding relaxation stage.

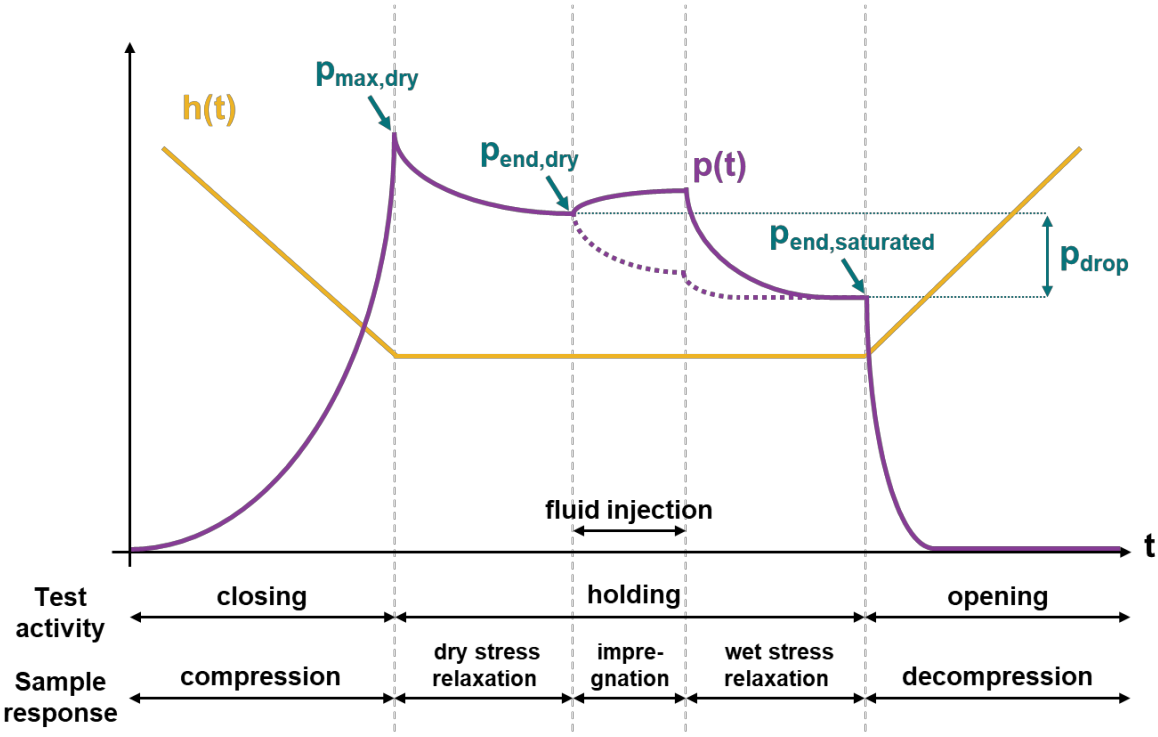

Figure 18: Compression-relaxation test-configuration with in-situ impregnation and measurement points

Another important remark concerns the fluid injection phase. At the beginning of the experiment, the pressure in the feeding line is built up and thereby immediately present as soon as the valve releases the injection. However, as soon as the injection is stopped, this pressure must be released. The resulting pressure curve thus influences the initial range of the saturated relaxation phase. It can be assumed that there is no fluid pressure outside the compressed area below the stamp. Further, isotropic, in-plane permeability prevails, as the compressed area underneath the stamp shows a circular shape. This fluid injection pressure curve, as illustrated in Figure 19, can be described by an exponential decay function. This contribution to the total load measured by the load cell can be analysed in further detail, however, this is beyond the scope of this thesis.

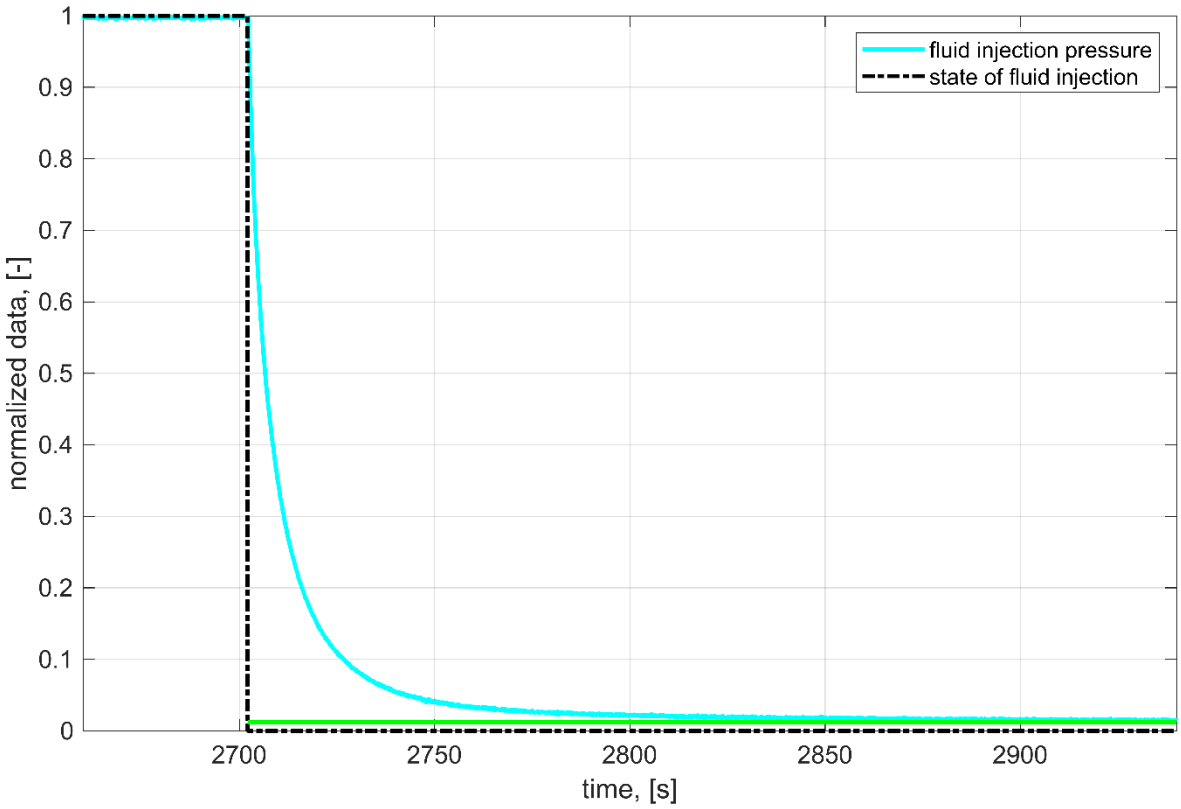

Figure 19: Fluid injection pressure decay

3.6 Test procedure

Prior to a compaction experiment, the test rig must be prepared accordingly. First, all LVDTs as well as the joints of the feeding tube must be checked for proper functioning. To obtain correct measurement data, the LVDT must be set to zero as soon as the test surfaces are in contact with each other. Subsequently, the test rig is used to measure a total of five blind curves at a force of 20 kN each with a movement speed of the crosshead of 1 mm/min. These specimen-less preliminary tests serve to ensure the setup compliance during the phases of compression and decompression, to indicate any force-dependent incorrectness in the crosshead position measurement and to prevent potential errors. This measurement procedure is carried out before and after each test day. If there are any inconsistencies in the results, these blind curves can be used to compare them with each other and, if necessary, to detect any changes in the stiffness of the test rig and evaluate the influence accordingly. Thereby, it is necessary to evaluate the

machine's behaviour once before and after testing, to verify the results and to ensure that the setup of the test rig is not influenced by any means. Subsequently, the test stand is set to a force and path distance of zero once more as well as the LabView software is prepared for the fluid injection.

Each experiment starts with determining the weight of the specimen and the careful positioning of it on the clean lower test surface. Afterwards, the crosshead of the universal testing machine is moved in the direction of the stamp to compact the sample to the calculated compaction height, depending on the FVF to be set. The test speed is set to 1 mm/min, but the closing speed can be increased until the textile is in contact with both test surfaces. As soon as the target height is reached, the first holding phase start and lasts for a total duration of 30 min.

Afterwards, the test liquid is then continuously injected into the textile at a predefined pressure level. To ensure complete impregnation, the injection phase lasts for 15 min, but highly permeable materials, such as the Veil, may require less time. To conserve the fluid, a commercially available coffee filter is used to filter and reuse it.

Following the injection phase, a wet stress relaxation phase of 30 min is carried out. The test is completed by opening the cavity with a downward movement of the crosshead at a speed of 1 mm/min. The specimen is then carefully removed from the test surface, weighed, and the surfaces cleaned for the next measurement. An initial evaluation of the relaxation and injection phases is performed after all measurements are taken.

4 Results

In this section, the results of the pretest and main test series are reported. First, the outlier approach is explained, as all measurement series presented are taking this into account. To keep the recorded measurement data comparable, all subsequent measurements are set to a time of zero seconds at the point of maximum pressure reached.

4.1 Outlier approach

To reduce the scatter within the measurement data, the following outlier approach is introduced for any inconsistent measurement curves. First, the time-pressure curves during compression and relaxation are examined and checked to see if there are strong deviations or irregularities in the trend itself. Outliers are identified as experiments where the maximum load during the initial dry compression phase deviates by more than 20 % from the median value of the corresponding series. The basic assumption here is that, with the same configuration in the dry compaction state, the curves should overlap.

This procedure is illustrated by the example shown in Figure 20, from the pretest series of the WF. Here, complete data sets are available at three different levels of fluid injection pressure, namely 0.8, 1.4 and 2.0 bar. The plotted data shows a rather wide span for all of the three groups.

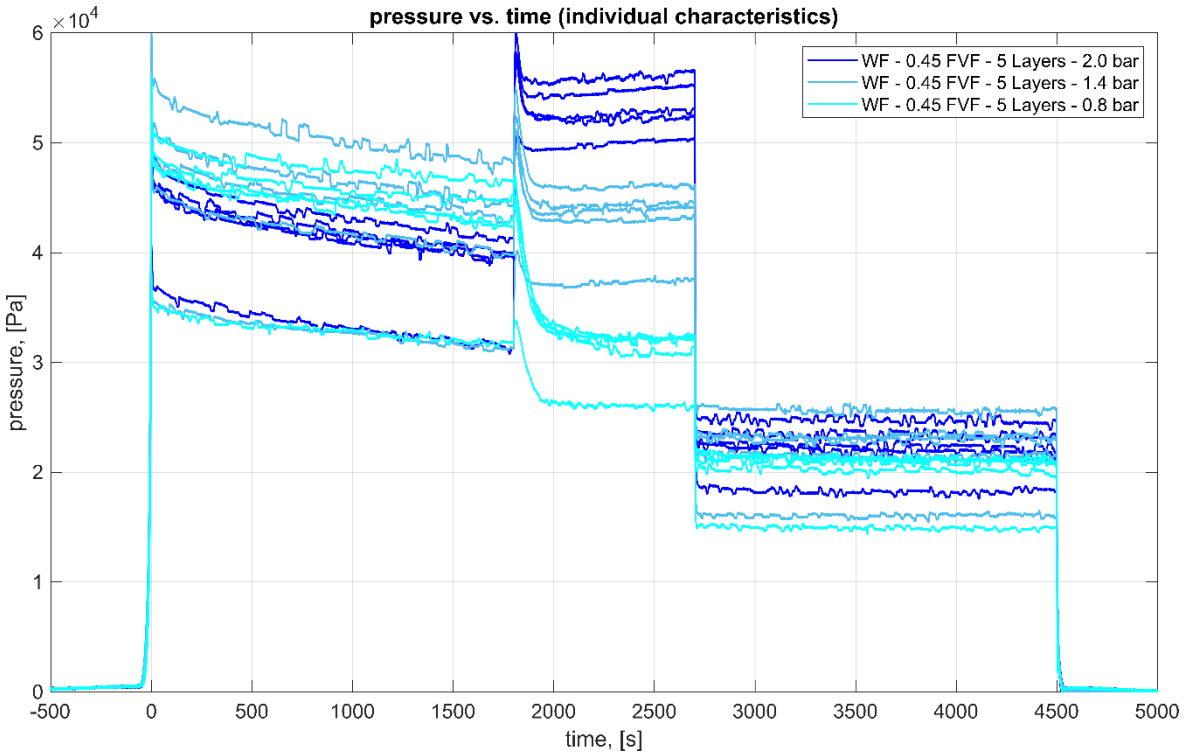

Figure 20: Measurement series including outliers as individual characteristics

Figure 21 shows the data remaining after application of the outlier approach described above.

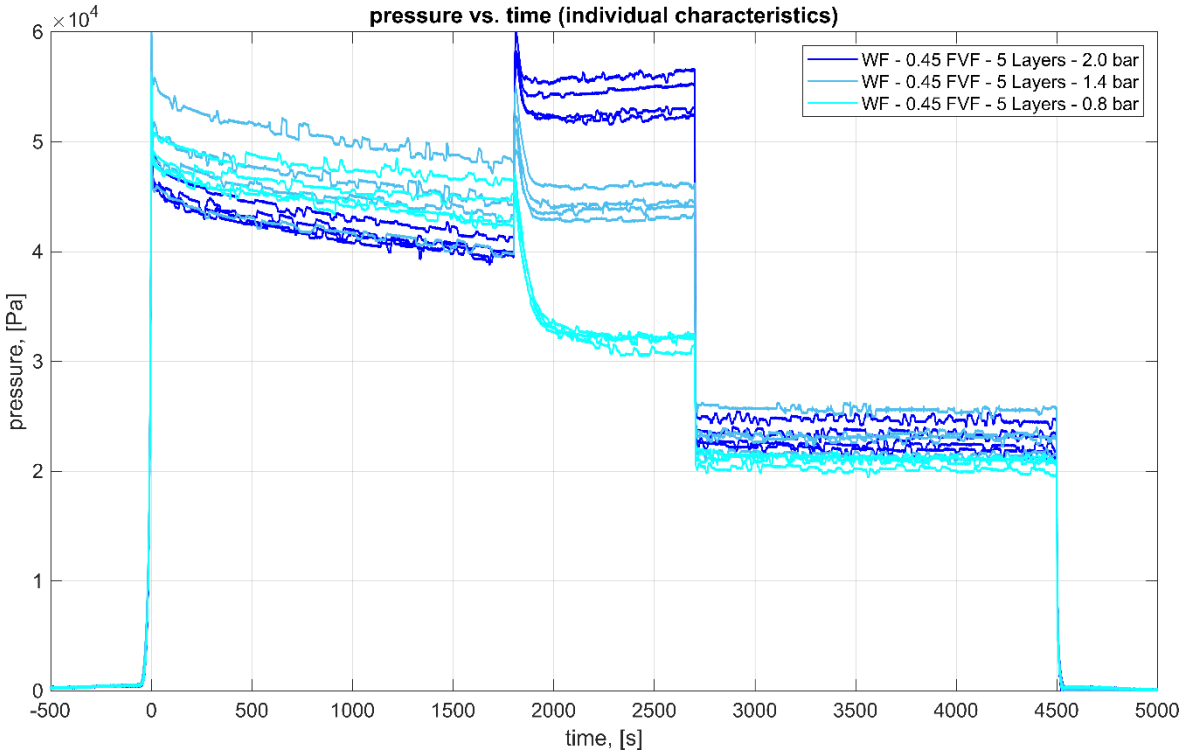

Figure 21: Measurement series excluding outliers as individual characteristics

A direct comparison shows that by using the outlier approach, irregular courses can be excluded. This leads to a significant reduction in the scatter of the measurement data in all areas, namely the dry compaction, the impregnation phase as well as the wet compaction at the end. Table 3 shows the number of outliers identified according to this scheme for the pretest series, sorted by fluid injection pressure and type of specimen.

Table 3: Number of outliers at the pretest series

Material	0.8 bar	1.4 bar	2.0 bar
NCF	1	1	1
WF	1	1	1
Veil	3	2	-

Table 4 shows the same overview of the number of outliers occurring for the main test series, sorted by FVF, number of layers and type of specimen.

Table 4: Number of outliers in the main test series

		FVF [-]				
Material	**Layers [-]**	0.35	0.40	0.45	0.50	0.55
NCF	3	-	-	1	0	0
	5	-	-	1	1	0
WF	3	-	-	0	1	0
	5	-	-	1	0	1
	14	-	-	0	0	0
Veil	3	1	2	-	-	-
	5	3	1	1	-	-
Knit	5	-	0	0	0	-

4.2 Evaluation of the pretest series

In the pretest series, the compaction results of the three reinforcement materials, namely the NCF and WF as well as the Veil, are presented. First, the injection pressure profiles are shown and then the pressure-time diagrams are presented, once as an enveloped representation and on the other hand with individual characteristics.

4.2.1 Injection pressure

As the fluid flows through the feeding line from the pressure pot to the location of the pressure sensor, pressure losses occur due to wall friction in the tubes as well as at instruments along the feeding line such as the temperature sensor and ball valve. Concerning the results of the injection pressure level, the NCF is considered first. Therefore, Figures 22 – 24 compare the fluid injection pressure setpoint with the measured pressure data at the three individual pressure levels 0.8, 1.4 and 2.0 bar.

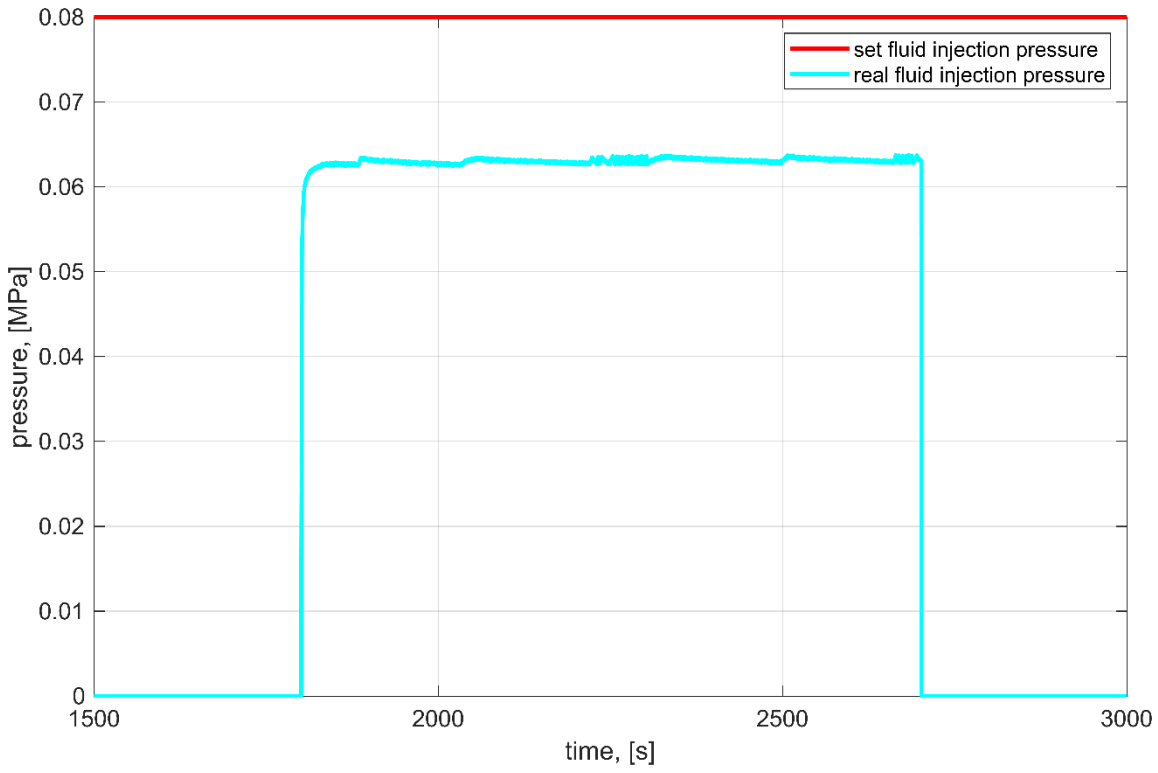

Figure 22: NCF – real against set fluid injection pressure at 0.8 bar

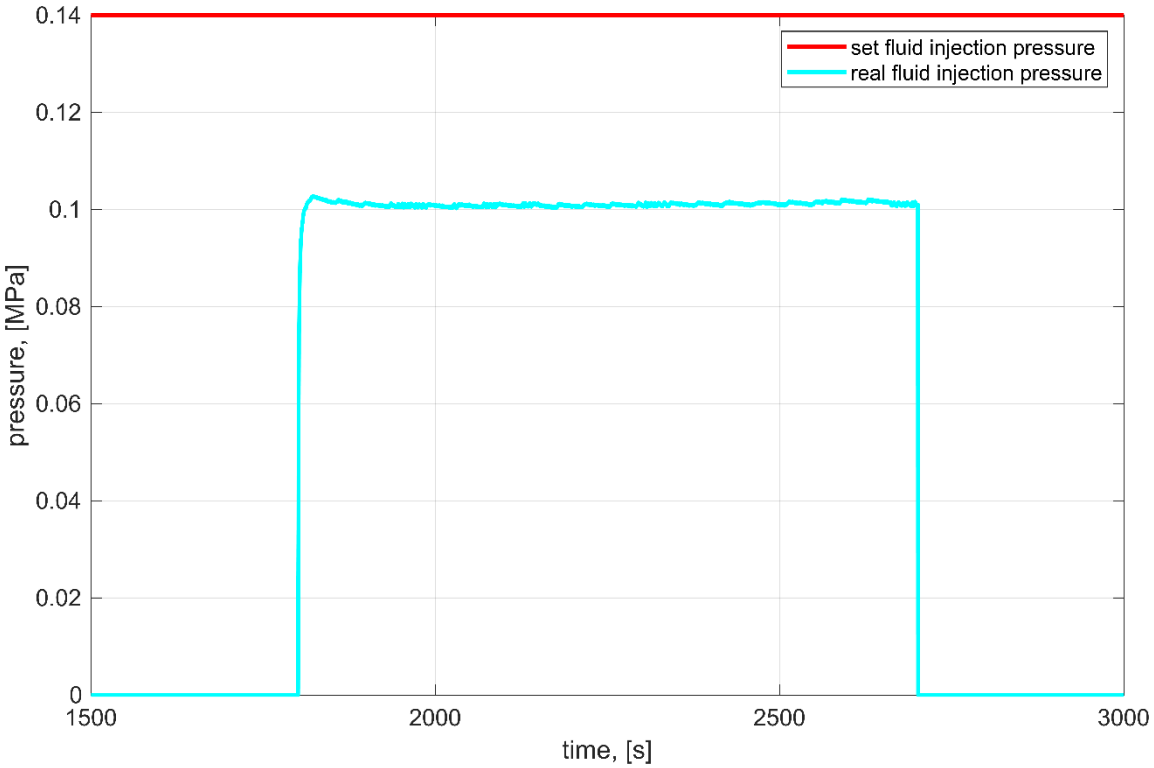

Figure 23: NCF – real against set fluid injection pressure at 1.4 bar

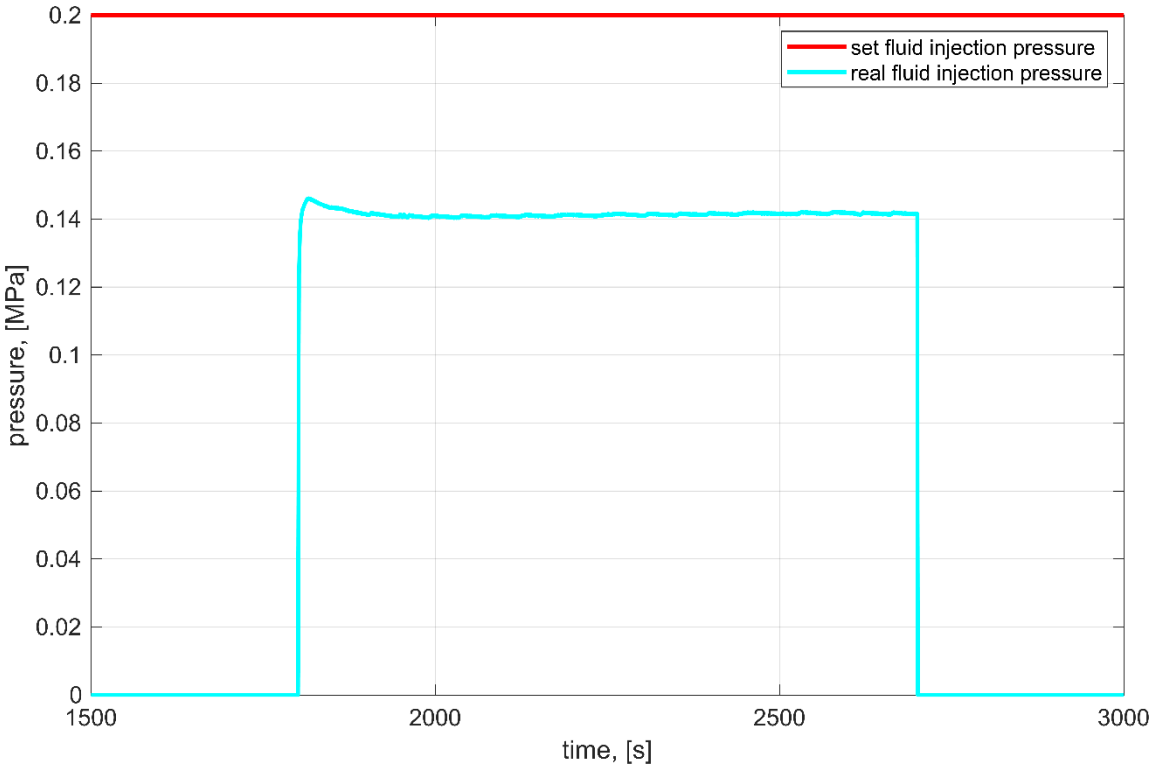

Figure 24: NCF – real against set fluid injection pressure at 2.0 bar

In the following, Figures 25 – 27 show the corresponding comparisons for the WF.

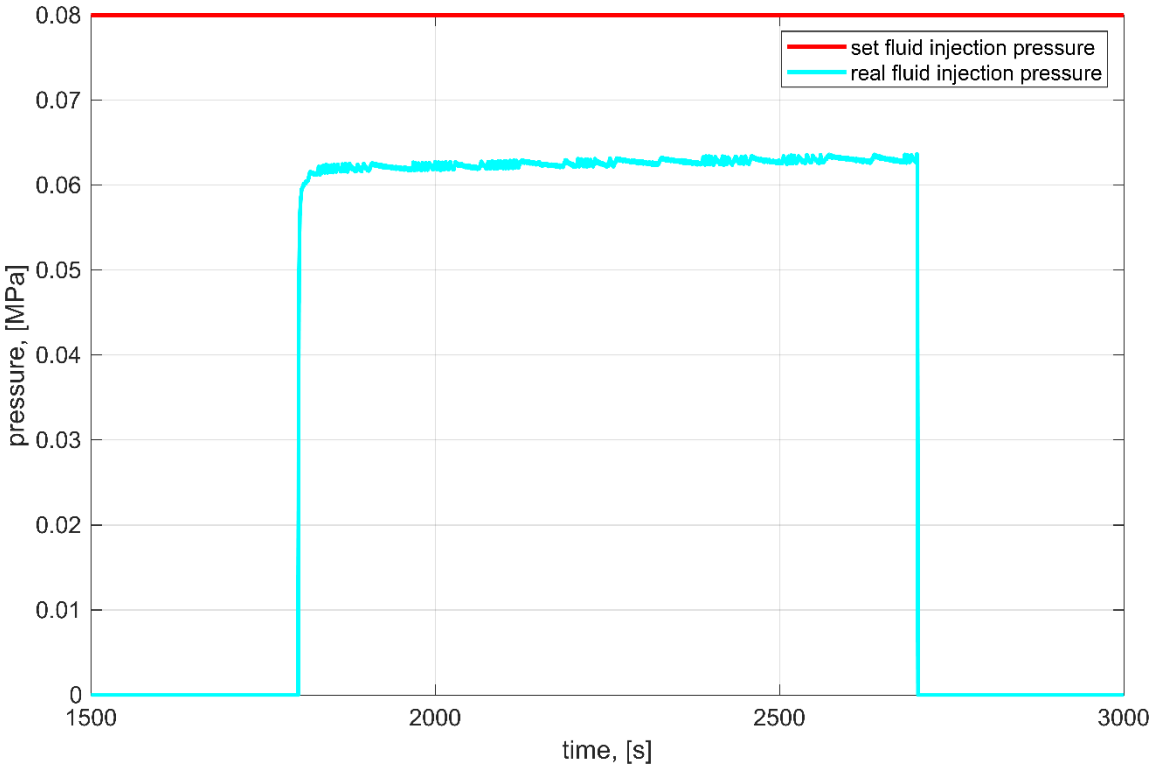

Figure 25: WF – real against set fluid injection pressure at 0.8 bar

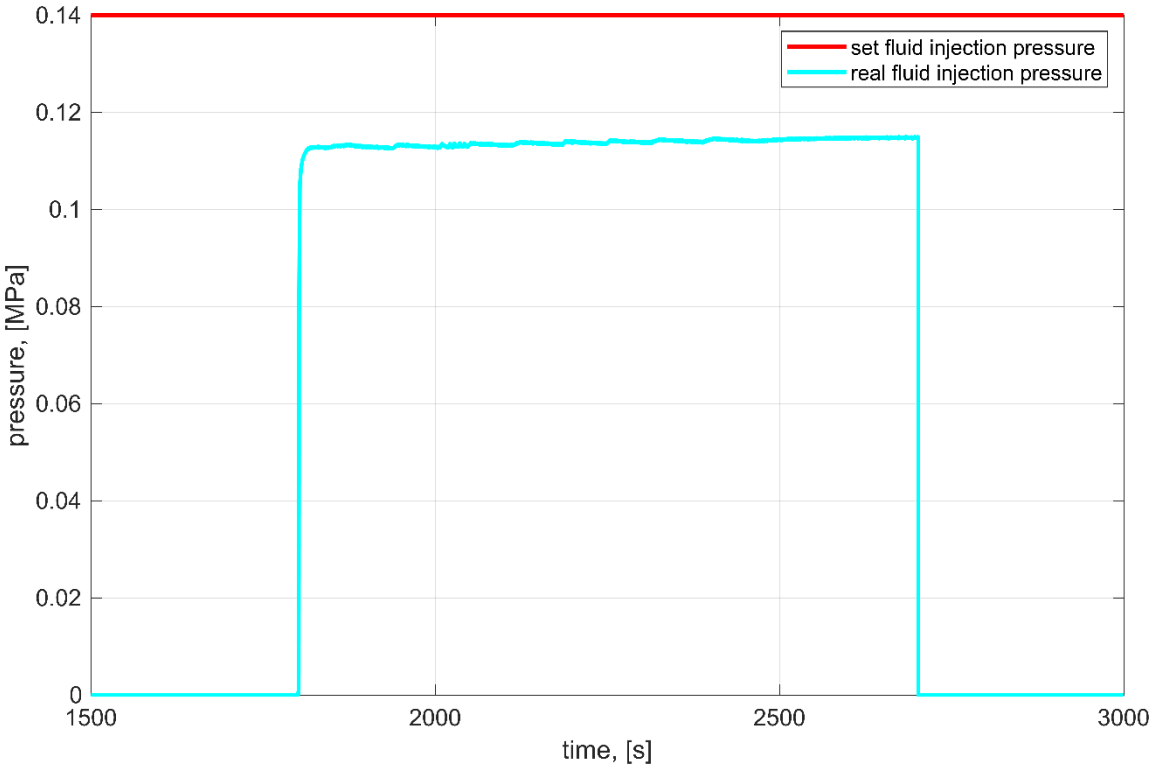

Figure 26: WF – real against set fluid injection pressure at 1.4 bar

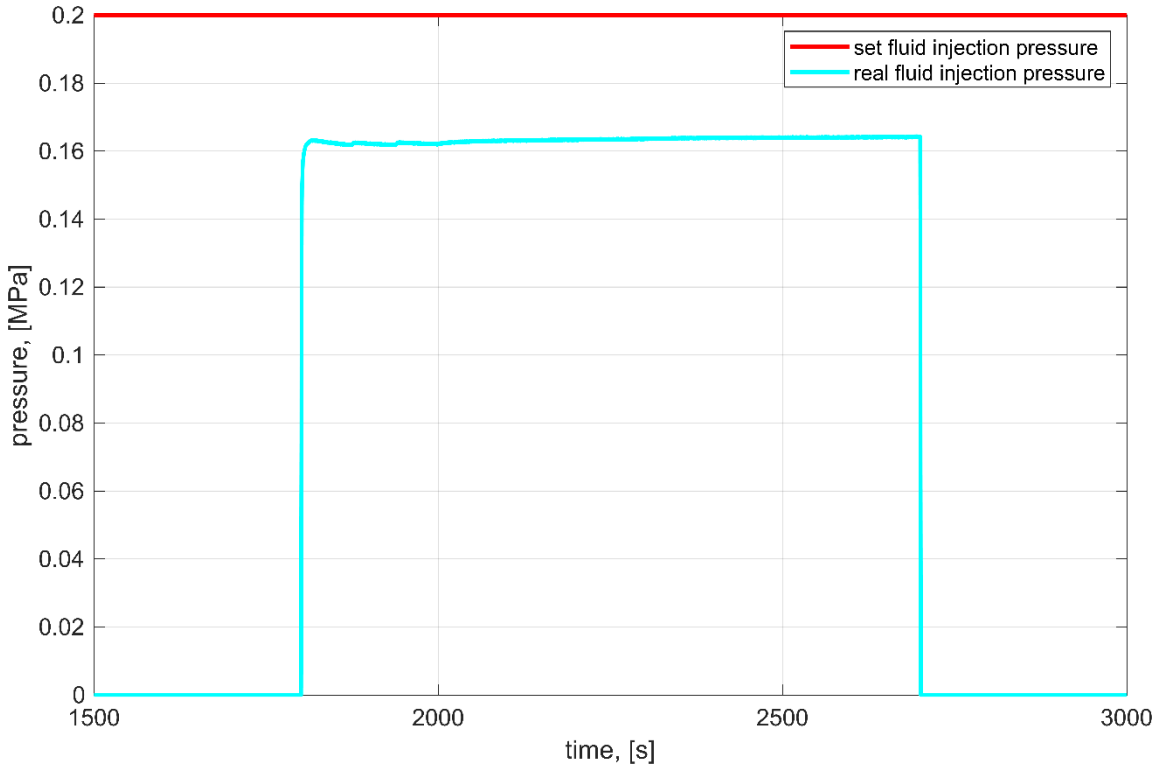

Figure 27: WF – real against set fluid injection pressure at 2.0 bar

Finally, Figures 28 – 30 show these comparisons for the Veil.

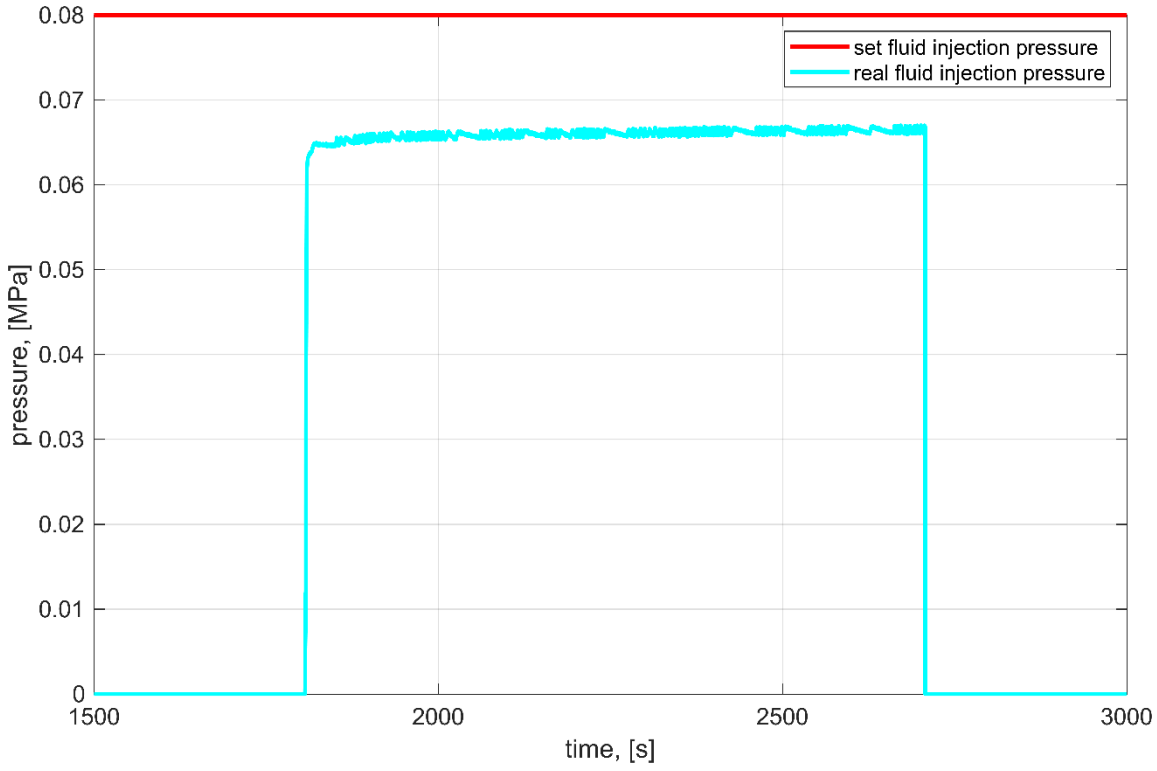

Figure 28: Veil – real against set fluid injection pressure at 0.8 bar

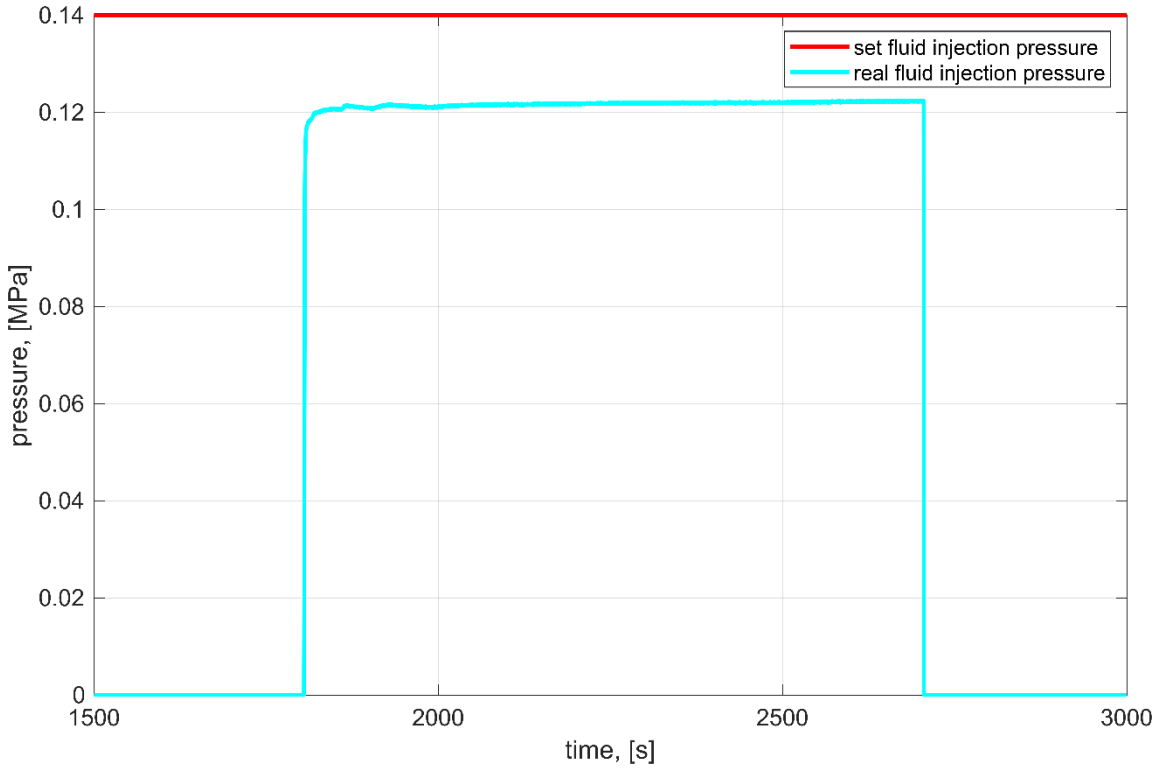

Figure 29: Veil – real against set fluid injection pressure at 1.4 bar

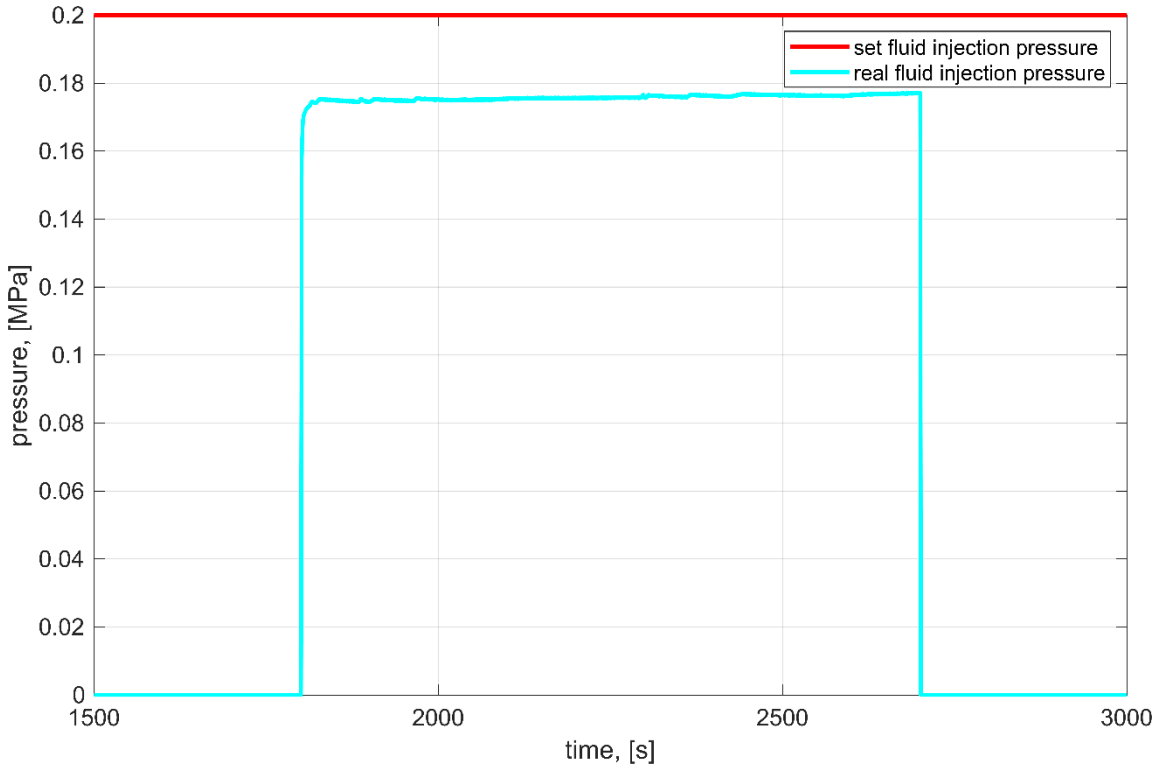

Figure 30: Veil – real against set fluid injection pressure at 2.0 bar

For all measurements, after 30 min of dry-stress relaxation, the fluid injection starts and lasts for a total of 15 min before the pressure drops back to the origin level. Especially at the NCF, the fluid pressure initially rises abruptly and quickly settles to a comparatively stable plateau. This first spike can be explained by the contact of the liquid column with the textile. In general, the fluid level is just below the bottom side of the specimen and not yet in contact until the start of the injection phase therefore cannot saturate the textile in advance. In the case of the WF, at the start of the injection phase, this initial increase in the real fluid injection pressure curve is less pronounced, but still present. However, the curve does not reach a plateau, but rather tends to continuously approach a maximum of the achievable real fluid pressure. The Veil shows a constant fluid injection without fluctuations in the course and a significant spike in the initial part of the injection phase. As with the WF, a slight increase in the real fluid injection pressure level can be observed over time. Table 5 gives an overview of fluid injection pressure setpoints and the measured fluid pressure values. The latter are provided in terms of the range of final fluid pressure data for each series of experiments, which in turn is calculated as the average value of the last 10 seconds of fluid injection. In addition, the deviations with respect to the setpoints are provided in terms of absolute and relative pressure drop, calculated by the following two equations:

$$\Delta p_{abs} = p_{fluid,set} - p_{fluid,real} \tag{15}$$

$$\Delta p_{rel} = 1 - \frac{p_{fluid,real}}{p_{fluid,set}} \tag{16}$$

Table 5: Set against real fluid injection pressure (min./max.)

	$p_{fluid,set}$ [bar]	$p_{fluid,real}$ [bar]	Δp_{abs} [bar]	Δp_{rel} [%]
NCF	0.8	0.58 .. 0.64	0.16 .. 0.22	20.3 .. 27.2
	1.4	1.02 .. 1.08	0.32 .. 0.38	22.6 .. 27.2
	2.0	1.18 .. 1.46	0.54 .. 0.82	26.9 .. 41.1

WF	0.8	0.62 .. 0.64	0.16 .. 0.18	20.4 .. 22.3
	1.4	1.13 .. 1.16	0.24 .. 0.27	17.0 .. 19.2
	2.0	1.62 .. 1.66	0.34 .. 0.38	16.9 .. 18.8
Veil	0.8	0.64 .. 0.67	0.13 .. 0.16	16.3 .. 20.6
	1.4	1.22 .. 1.24	0.16 .. 0.18	11.4 .. 13.1
	2.0	1.77 .. 1.82	0.18 .. 0.23	8.9 .. 11.5

For the NCF, a higher fluid injection pressure leads to an increase in the deviation between the set and real values. A consistent trend is observed in the relative deviations for the Veil and WF, where higher setpoints result in lower relative pressure losses. Furthermore, the NCF exhibits the highest relative pressure losses, the Veil the lowest and the WF falls in between.

The Darcy-Weisbach equation [56]–[58] characterizes the pressure loss Δp due to viscous effects in a fully flowing cylindrical pipe with a uniform diameter D and is proportional to a pipe length L. For this case, it can be written to as follows [58]:

$$\Delta p = \lambda \cdot \frac{\rho}{8} \cdot \frac{\bar{v}^2}{A} \cdot U \cdot L \tag{17}$$

$\bar{v}$ mean flow velocity
ρ density of the fluid
A cross-sectional area of the pipe
U perimeter of the pipe
λ flow coefficient

It should be noted here that the mean flow velocity enters quadratically and thus has a considerable influence on the resulting pressure loss. Based on the results in Table 5, different flow velocities in the feeding tube can be assumed for the three different textiles. These in turn result from different permeability of the tested materials (Darcy's law). Accordingly, different permeability values for the reinforcement materials lead to differences in the flow velocity in the feeding tube and the associated pressure losses. [56]–[58]

4.2.2 Compaction

This section shows the results of the pretest series, separated according to the individual materials tested at the three corresponding pressure levels. Figure 31 shows the enveloped minimum and maximum value compaction results for the NCF and Figure 32 the corresponding individual characteristics.

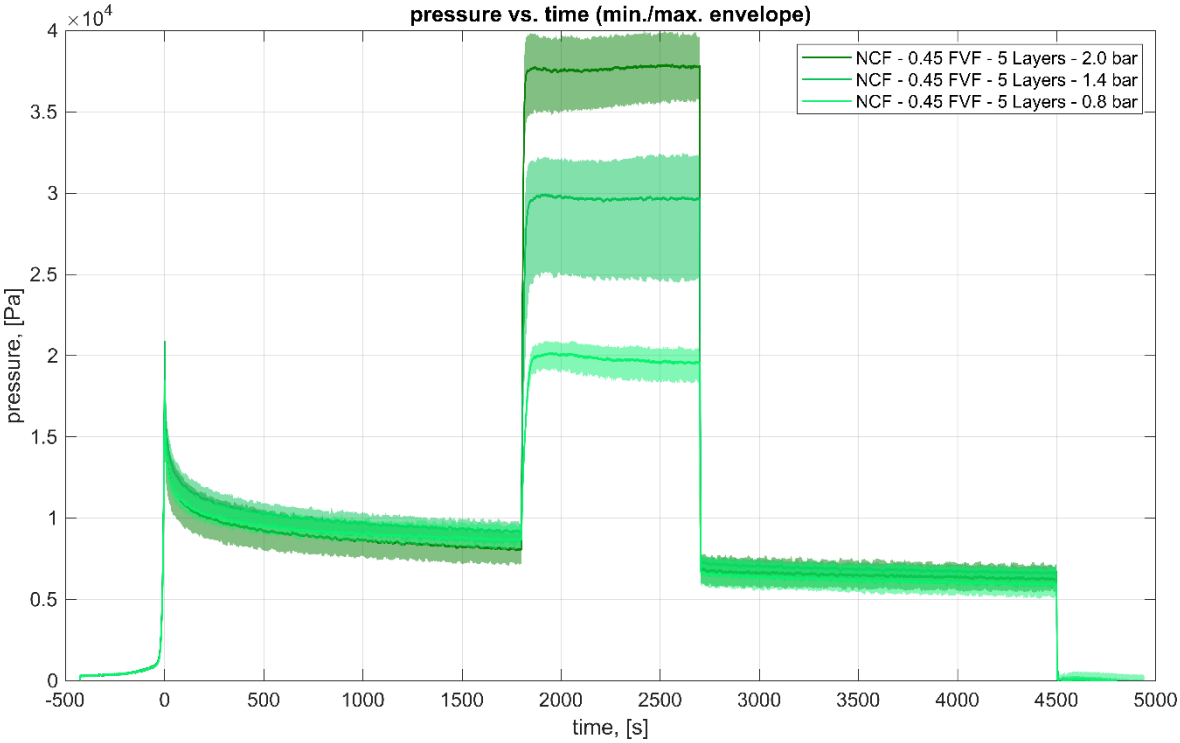

Figure 31: NCF – 0.45 FVF – 5 Layers – pressure vs. time (min./max. envelope)

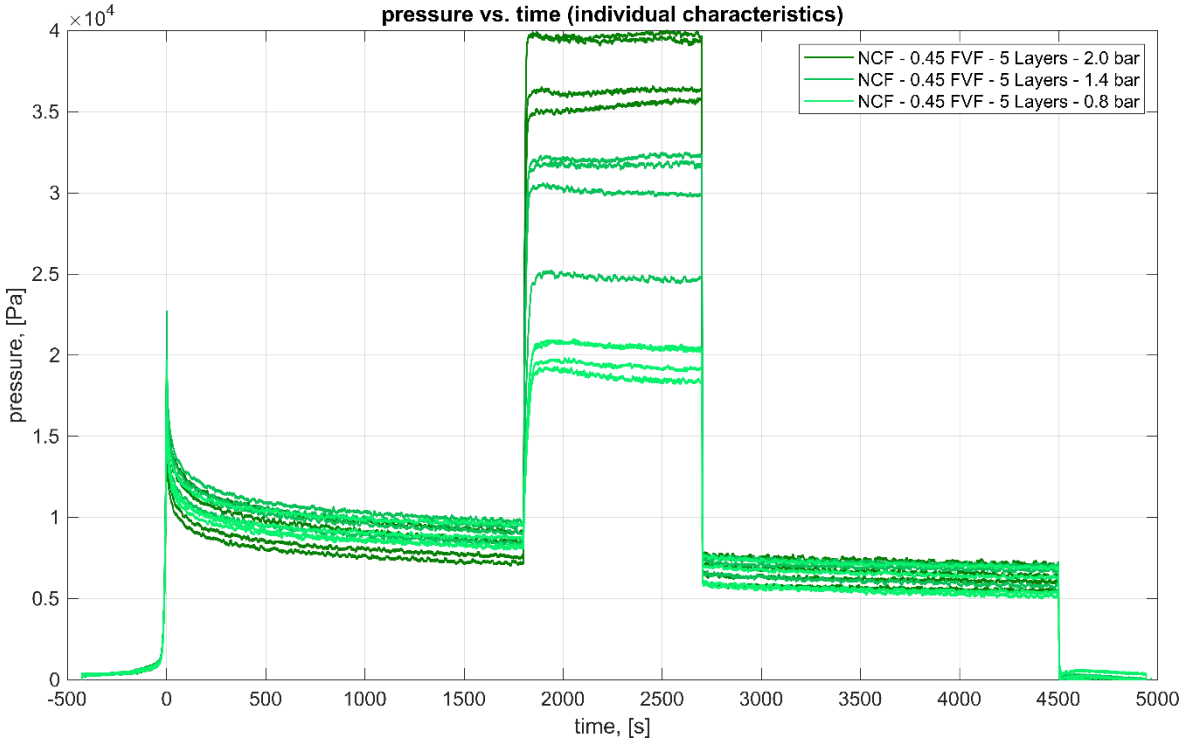

Figure 32: NCF – 0.45 FVF – 5 Layers – pressure vs. time (indiv. characteristics)

The two relaxation curves in the dry and saturated state, before and after the injection phase, show a good agreement. However, there are slight fluctuations in the injection phase itself. Especially in the course at 1.4 bar it can be seen that one line is clearly at a lower level than the remaining trends. At 2.0 bar, respectively two lines are close to each other, but clearly at different levels. As a result, the representation with envelopes in the area of the fluid injection shows a significantly greater width for the two upper-pressure levels. Overall, it can be observed that with increasing fluid pressure levels, the influence of this increases and thus shifts the pressure range significantly to higher levels. In the dry relaxation stage itself, a relatively rapid approach to a more stable pressure level can be observed. The course of saturated relaxation follows on almost seamlessly, but at a noticeably reduced level.

Figures 33 and 34 show the envelope for the maximum and minimum values as well as the associated individual characteristics for the WF.

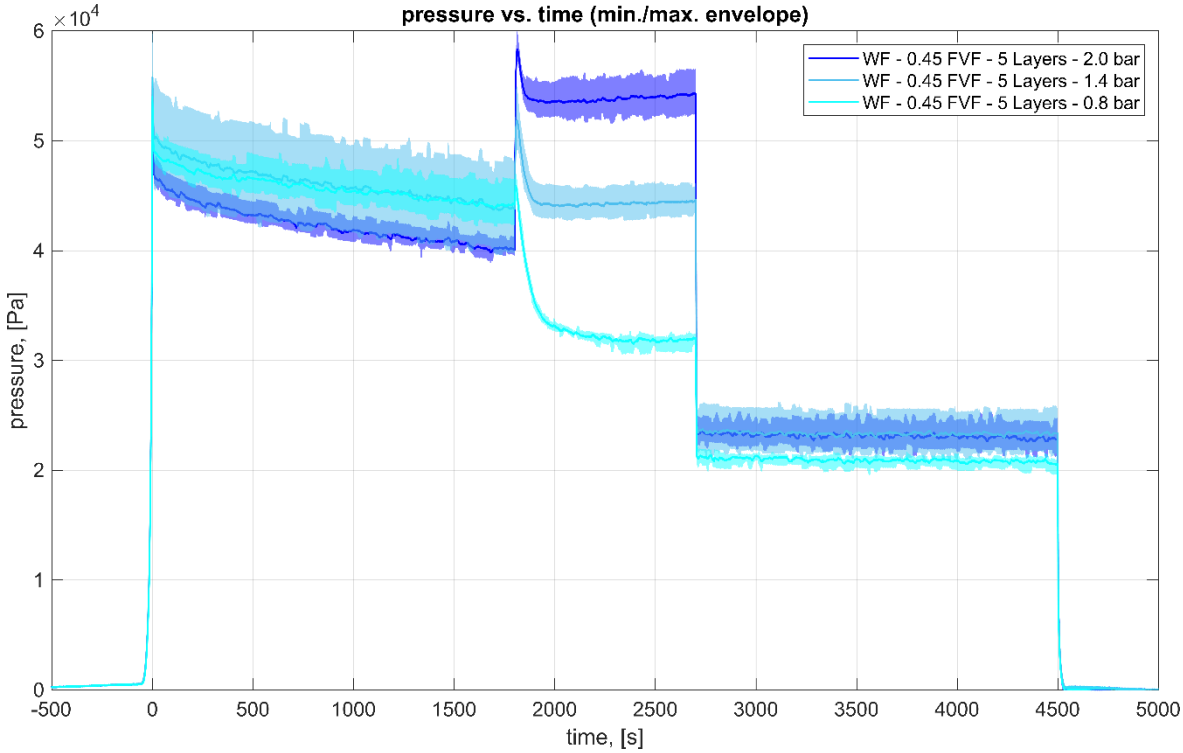

Figure 33: WF – 0.45 FVF – 5 Layers – pressure vs. time (min./max. envelope)

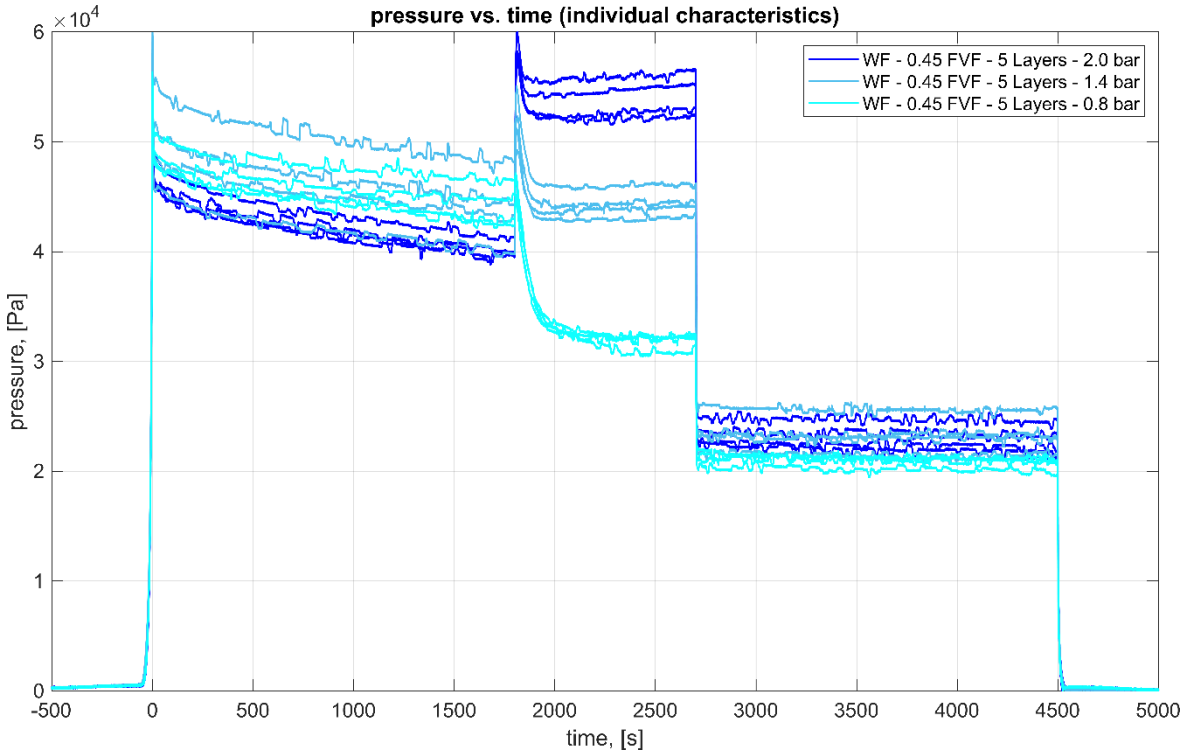

Figure 34: WF – 0.45 FVF – 5 Layers – pressure vs. time (indiv. characteristics)

Here, in the relaxation curves for the WF, the individual trends overlap somewhat better in the saturated region than in the dry one. In direct comparison to the NCF, the data shows more scatter, but this may be explained by the significantly higher overall pressure levels over the course. In addition, it can be observed that the relaxation process approaches a comparatively stable pressure level noticeably slower. In the saturated relaxation region itself, no further significant reduction of the pressure level can be observed. In the phase of the injection, a sudden increase can be seen, at first due to the start of the impregnation, followed by a rapid decrease of the remaining curve. This suggests, among other things, a fast impregnation of the material as well as a comparatively quick attainment of a new energy level of the material in the saturated state. At the end of this phase, the differences between the individual measurement series are recognizable in the respective applied fluid pressure levels.

Finally, in Figures 35 and 36, the pressure-time curves of the Veil are shown, once again as the minimum and maximum values envelope as well as with individual characteristics.

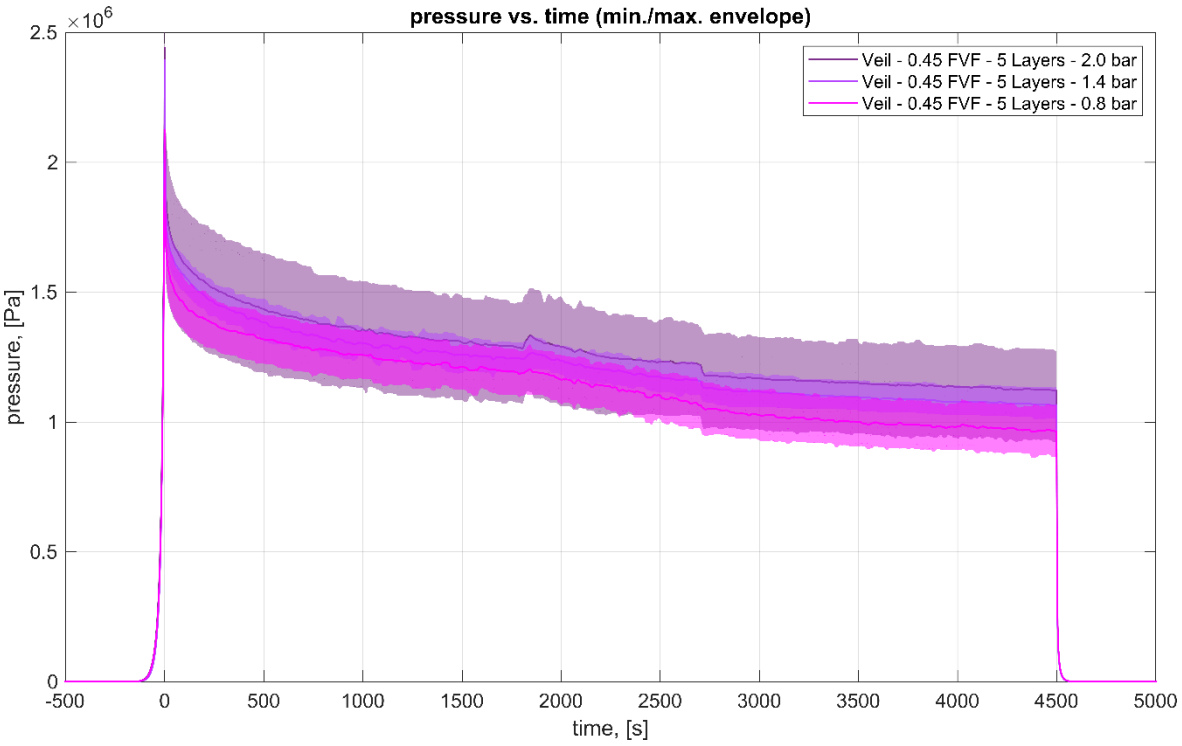

Figure 35: Veil – 0.45 FVF – 5 Layers – pressure vs. time (min./max. envelope)

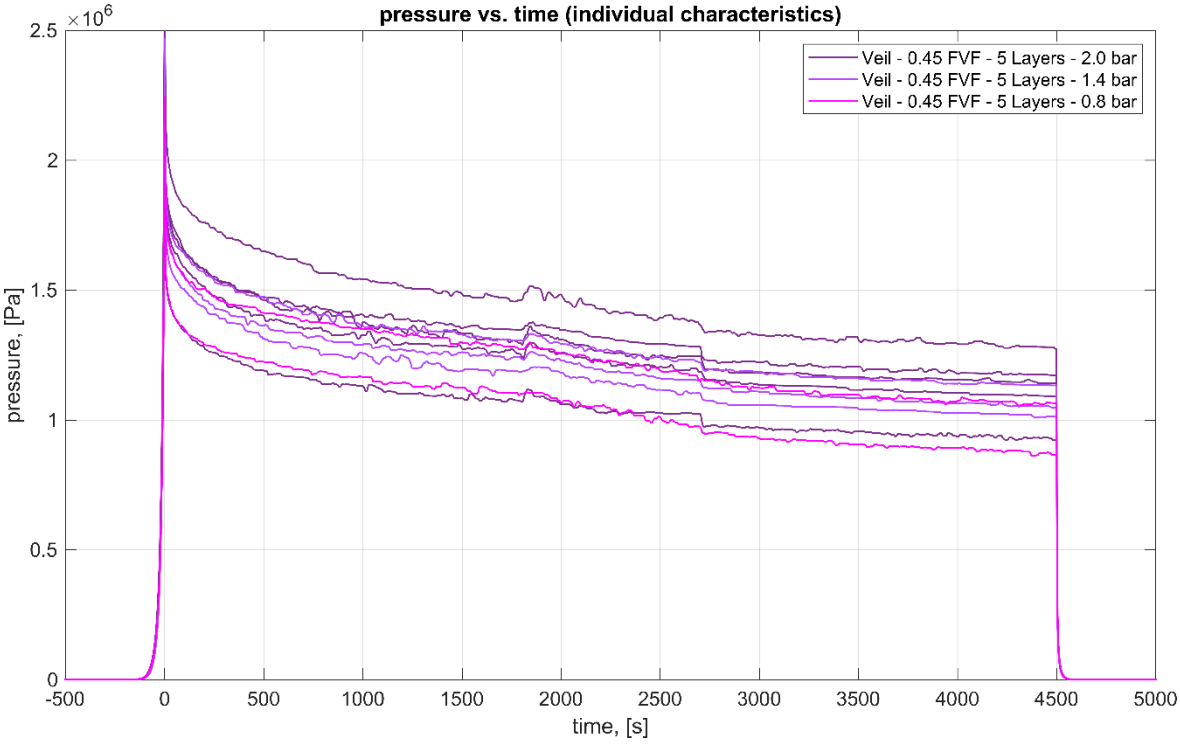

Figure 36: Veil – 0.45 FVF – 5 Layers – pressure vs. time (indiv. characteristics)

In contrast to the previous series of measurements, the clear overlapping of the entire course's overall applied fluid pressure levels is recognizable here. Over the entire course, a relatively stable pressure level is established relatively slowly, but faster than in comparison with the WF. In the phase of injection, there are hardly any distinguishable courses. As the pressure level increases, the time of the start and end of the injection phase becomes slightly more distinguishable. The share of the fluid injection pressure in the total pressure is rather low, due to the significantly higher level of compaction pressure.

Table 6 provides an overview of the median values determined for the individual measurement series using $p_{max,dry}$, $p_{end,dry}$ and $p_{end,saturated}$ as defined in Figure 18. In addition, the pressure drop between the dry and saturated levels at each fluid injection pressure level is provided for each configuration.

Table 6: Overview of the results of the pretest series

	$p_{injection}$ [bar]	$p_{max,dry}$ [kPa]	$p_{end,dry}$ [kPa]	$p_{end,saturated}$ [kPa]	p_{drop} [%]
NCF	0.8	18.3	8.5	5.9	31.5
	1.4	21.0	9.3	6.8	27.9
	2.0	18.8	8.0	6.2	22.5
WF	0.8	53.7	43.9	20.8	53.5
	1.4	55.6	43.6	23.1	46.8
	2.0	52.5	39.9	22.8	43.0
Veil	0.8	2126.5	1188.5	965.8	18.7
	1.4	2357.2	1242.1	1047.8	14.5
	2.0	2466.1	1298.9	1141.1	12.9

4.3 Comparisons of the pretest series

To be able to draw a better comparison between the results obtained for the three tested materials, the pressure values are plotted as normalized data. Here, the pressure-related data are normalized by the maximum pressure in the dry phase that occurs as soon as the target compaction height is reached. Figures 37 – 39 show, the results of the pretest series as normalized pressure against time as enveloped curves in the minimum and maximum range for all three materials, starting with the pressure level of 2.0 bar.

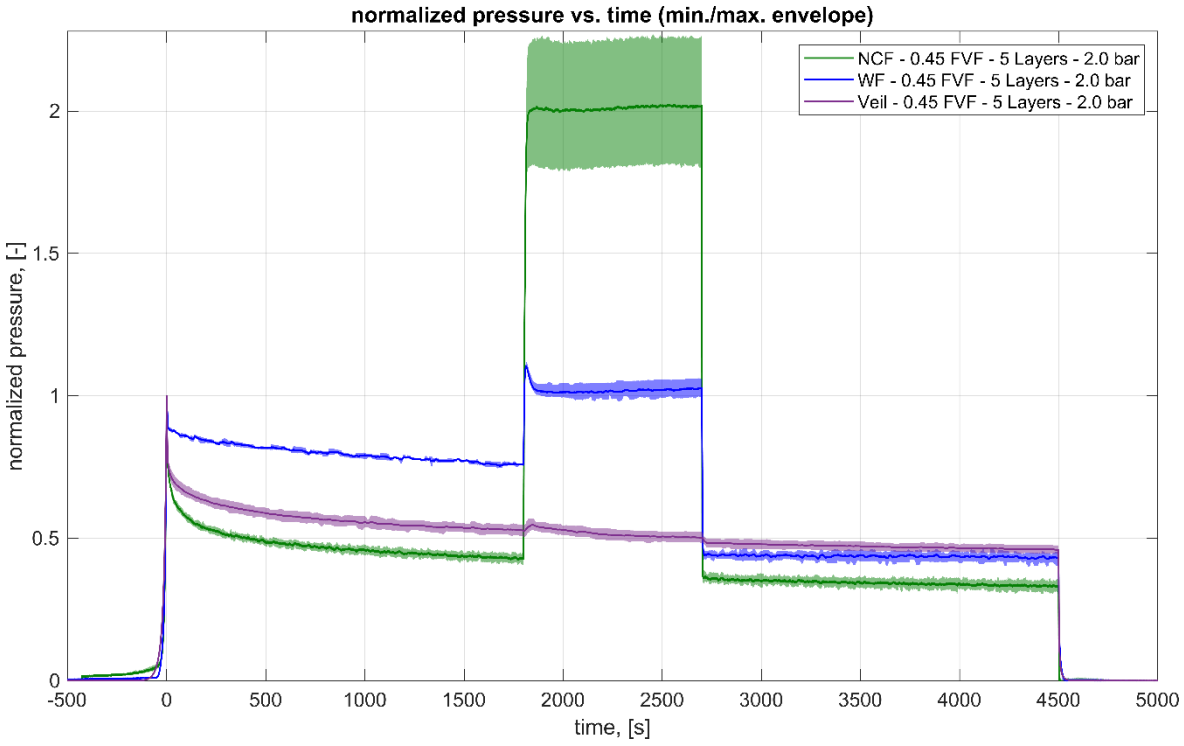

Figure 37: Normalized pressure vs. time (min./max. envelope) – 2.0 bar – 0.45 FVF – 5 Layers

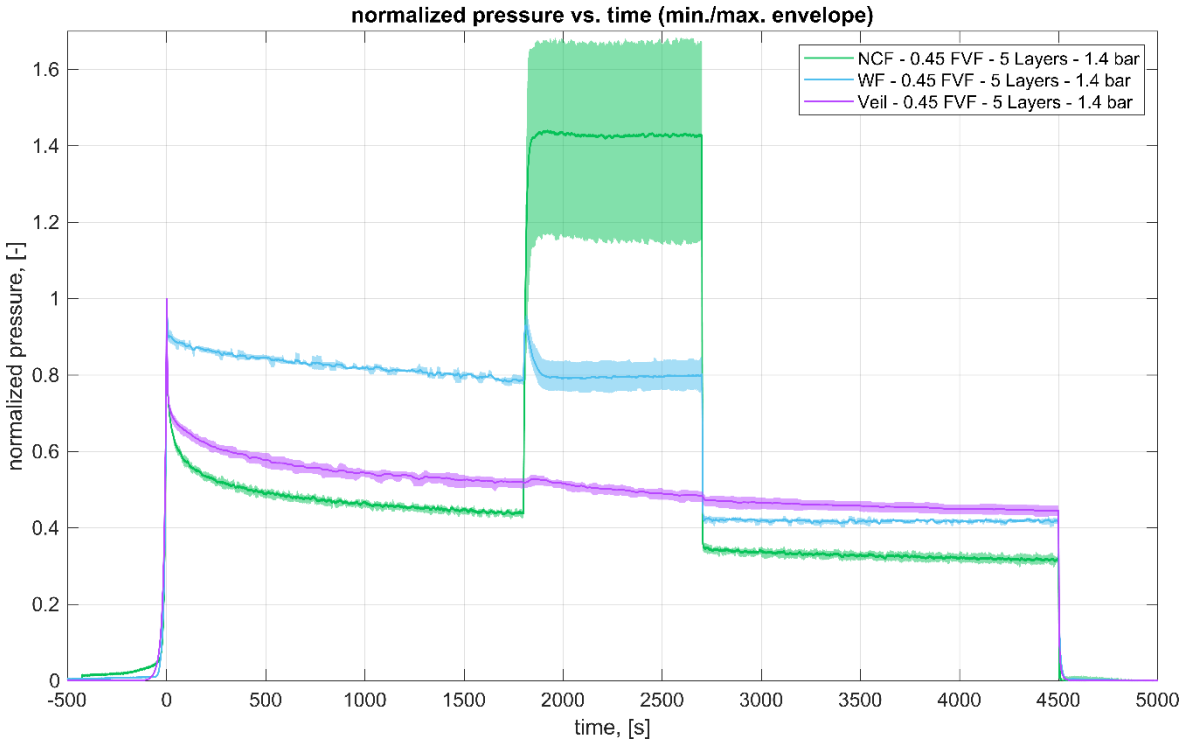

Figure 38: Normalized pressure vs. time (min./max. envelope) – 1.4 bar – 0.45 FVF – 5 Layers

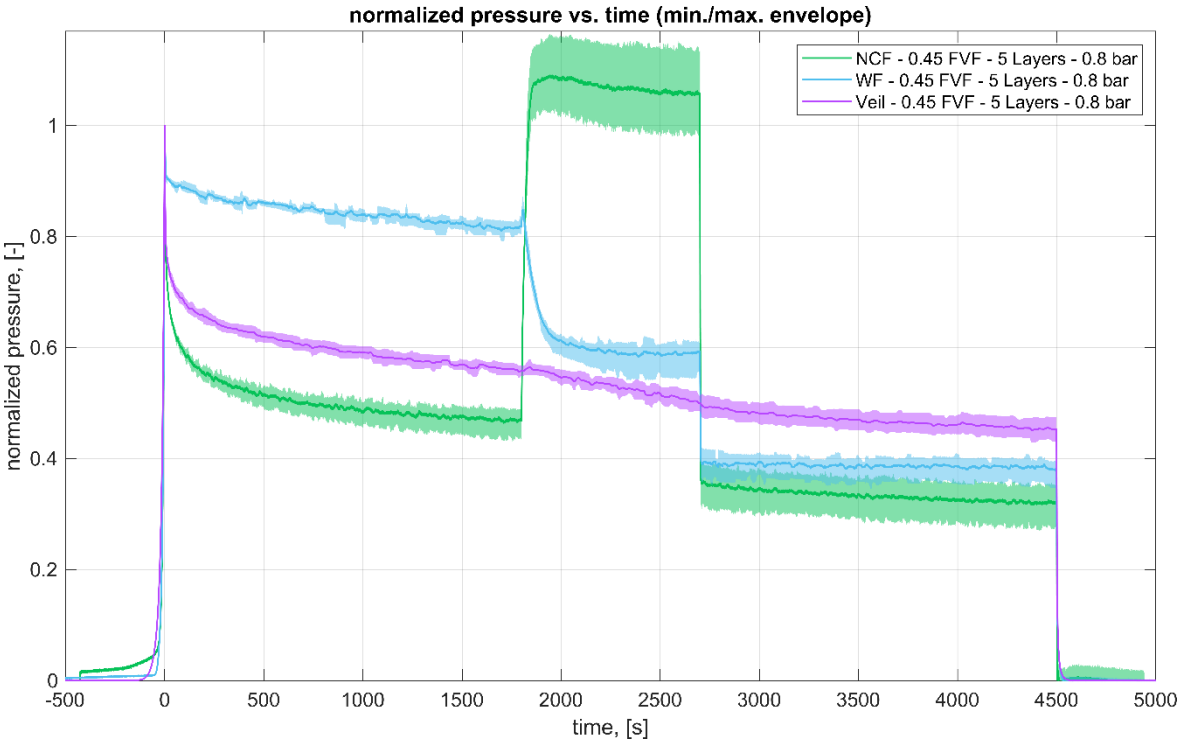

Figure 39: Normalized pressure vs. time (min./max. envelope) – 0.8 bar – 0.45 FVF – 5 Layers

The reaction and behaviour of all three materials was found to vary significantly, depending on the level of fluid pressure applied. Overall, a decrease in pressure level can be observed in each trend, typically occurring at the beginning of the saturated relaxation curve or shortly after the injection has ended. Particularly striking in this representation is the proportion and influence of the fluid injection pressure. With the Veil this is comparatively less recognizable, here, however, the two materials WF and NCF distinguish this phase from the dry and saturated relaxation stage. Here, it is evident that the NCF reacts most pronounced to the in-situ impregnation. This is also where the share of the fluid pressure in the total pressure is most pronounced.

The tested WF yields similar compaction pressure levels than the NCF and also shows a strong response to the injection phase. Here, however, a very rapid and significant decrease in the pressure level with increasing saturation of the specimen is shown. With the Veil, on the other hand, this strong influence of the fluid pressure is not noticeable due to the high measured overall pressure level, but precisely because of the material architecture present, a complete impregnation is guaranteed by far the fastest. Due to this high permeability, it does

not make sense to work with high pressures regarding the consumption of the test fluid, since impregnation already occurs sufficiently quickly at the lowest pressure level setpoint. This is different for the WF and NCF, where it is possible to work with high fluid injection pressures, since the impregnation of the specimen, especially for the WF, takes significantly longer. The selected high-pressure level, however, guarantees a fast and complete impregnation of the specimen. Here, even at the highest applied pressure level, no damage to the textile reinforcement can be observed with any of the configurations.

4.4 Evaluation of the main test series

In the main test series, the different configurations with variations in the number of layers and the FVF are presented. From the results of the pretest series, it can be derived that it is reasonable to choose a fluid pressure level of 2.0 bar for the NCF as well as WF and the lowest level of 0.8 bar for the Veil, among other factors due to the high permeability of this architecture. The results of this test series coincide for all materials at a FVF of 0.45. Since the measuring range of the load cell is already at its maximum with the Veil, the subsequent measurements are performed at lower FVFs.

Starting with the NCF at 3 layers and 3 different FVFs, Figure 40 shows the pressure-time trend as the minimum and maximum envelope and Figure 41 the individual characteristics.

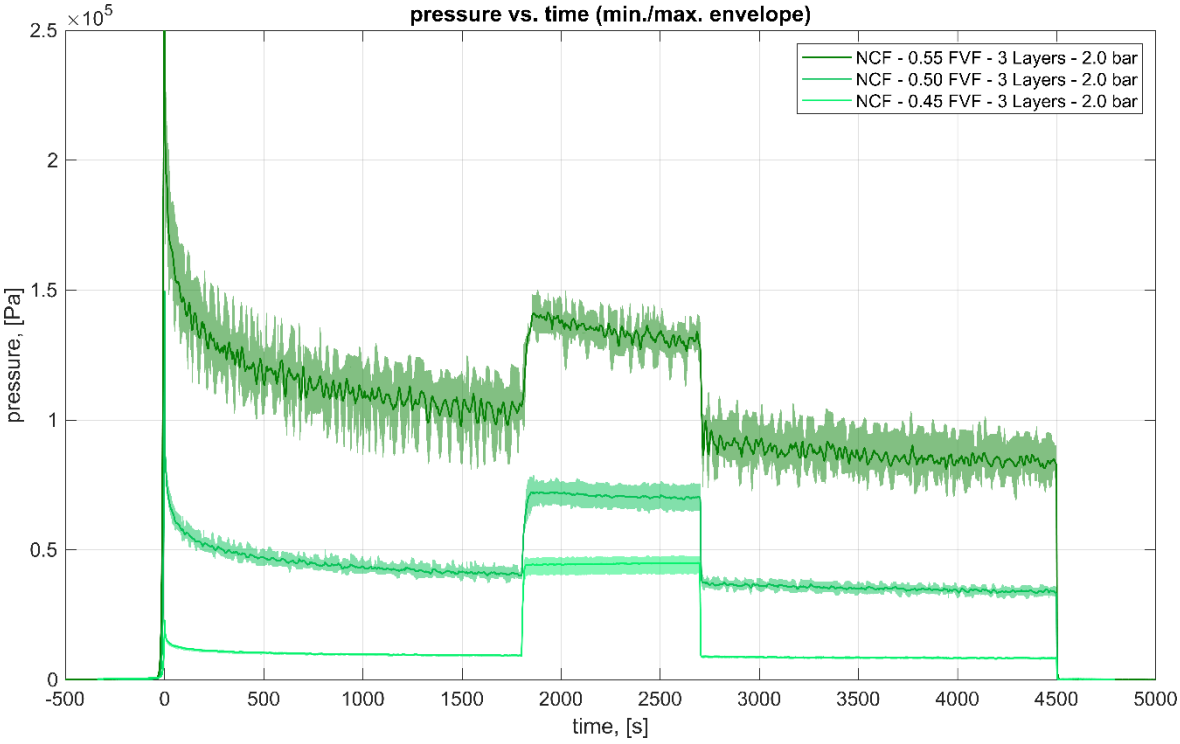

Figure 40: NCF – 3 Layers – pressure vs. time (min./max. envelope)

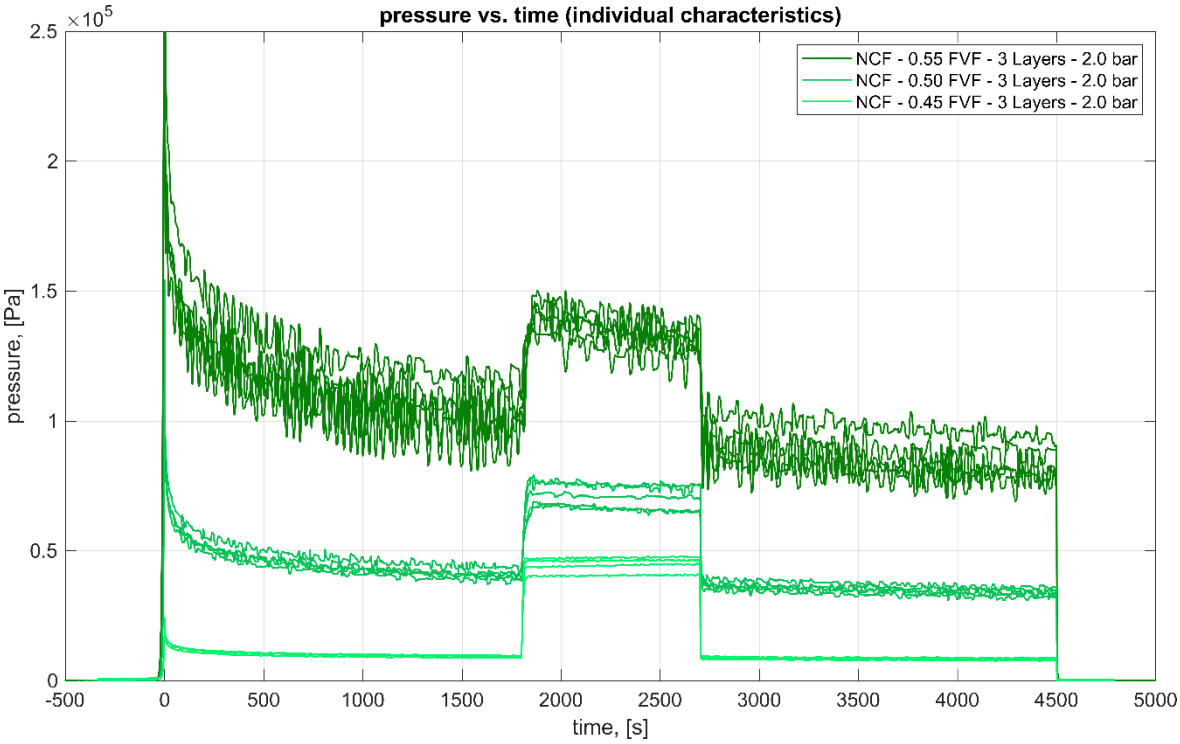

Figure 41: NCF – 3 Layers – pressure vs. time (indiv. characteristics)

Particularly noticeable is the strong oscillation of the measured pressure curve, which increases strongly, especially with higher FVFs. Nevertheless, the curves

match very well in the dry and saturated compaction path, in particular at the lowest pressure level. At higher FVF, the spread, apart from the fluctuations, increases noticeably. In the phase of injection, the trend appears as expected from the pretest series for the NCF. However, the pressure curve decreases slightly during this phase at higher pressure levels.

Figure 42 and 43 show again the enveloped and individual characteristics of the measurements for the NCF, but in a 5-layer configuration.

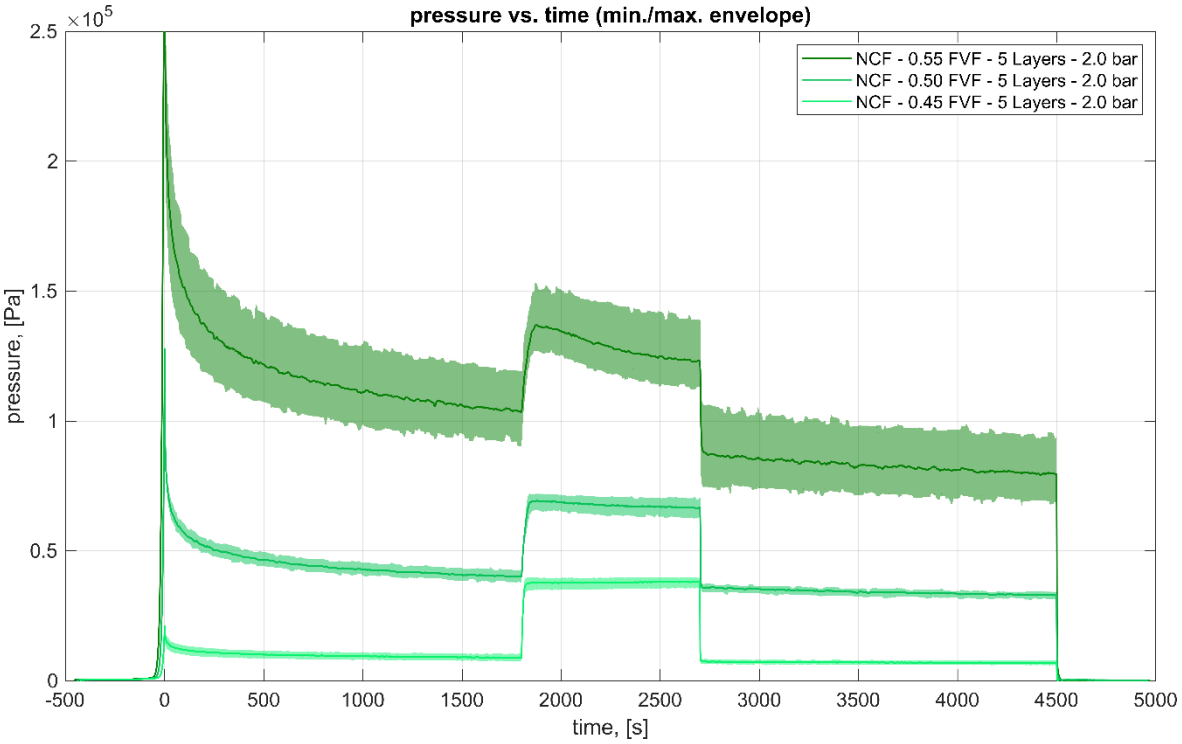

Figure 42: NCF – 5 Layers – pressure vs. time (min./max. envelope)

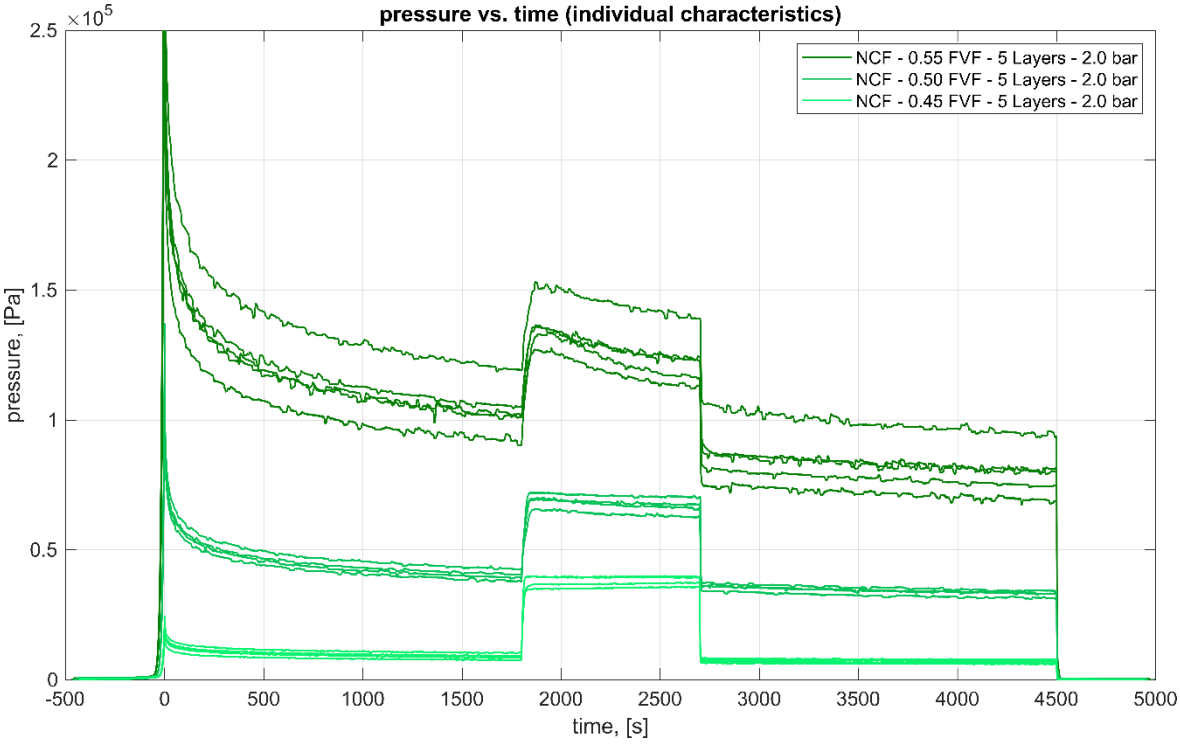

Figure 43: NCF – 5 Layers – pressure vs. time (indiv. characteristics)

Here, an almost identical course emerges as with the 3-layer configuration. Particularly noticeable is the significantly reduced fluctuation in the measurement data itself. However, this scatter is still noticeable, especially in the configuration with the highest FVF. The obtained injection curves show an identical picture, as with 3-layer specimen.

Continuing with the WF in the three-layer configuration, Figure 44 presents the minimum and maximum envelope and Figure 45 the individual characteristics.

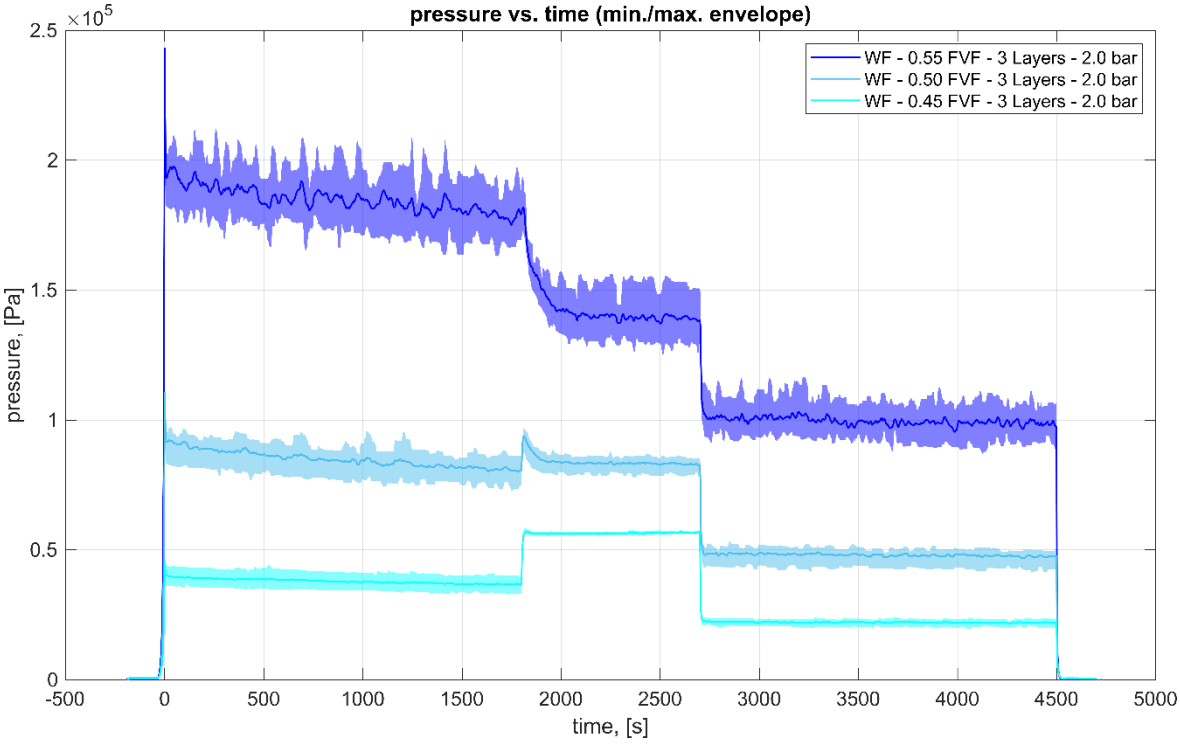

Figure 44: WF – 3 Layers – pressure vs. time (min./max. envelope)

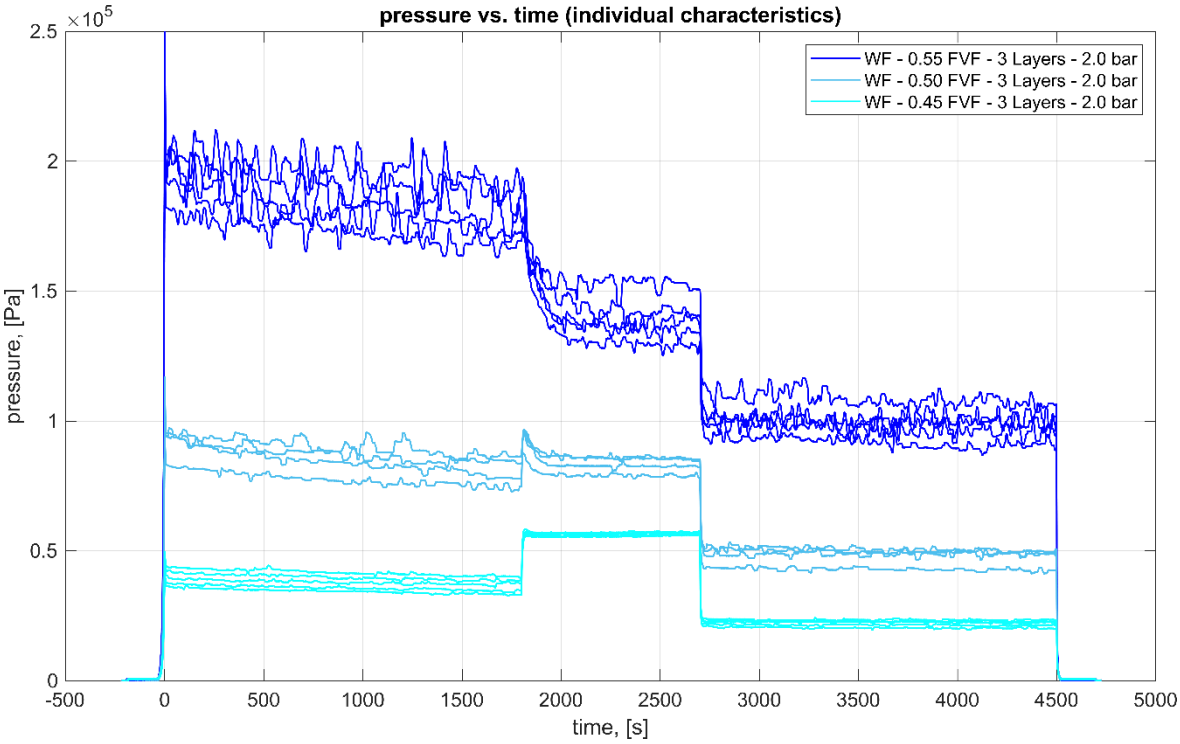

Figure 45: WF – 3 Layers – pressure vs. time (indiv. characteristics)

Here again, strong oscillations in the course of the measurements are noticeable at the higher FVF. Thereby, the individual trends match far better in the lower FVF

range. Overall, the material relaxes quite rapidly at all levels and continuously strives towards a new energy level, characterized by the slowly decreasing trend during the dry relaxation stage. In the phase of the fluid injection, a sharp spike appears, followed by a rapidly decreasing pressure level. In the process, the material relaxes to a new state that requires less energy and the share of the fluid injection pressure together with the compaction pressure, resulting in the total pressure, remains at a near-constant level. As soon as this fluid pressure fraction drops, the compacted specimen in the saturated area remains at a stable pressure level for the remaining measurement period.

Figures 46 and 47 show the corresponding enveloped curve and the individual characteristics of the 5-layer configuration of the WF.

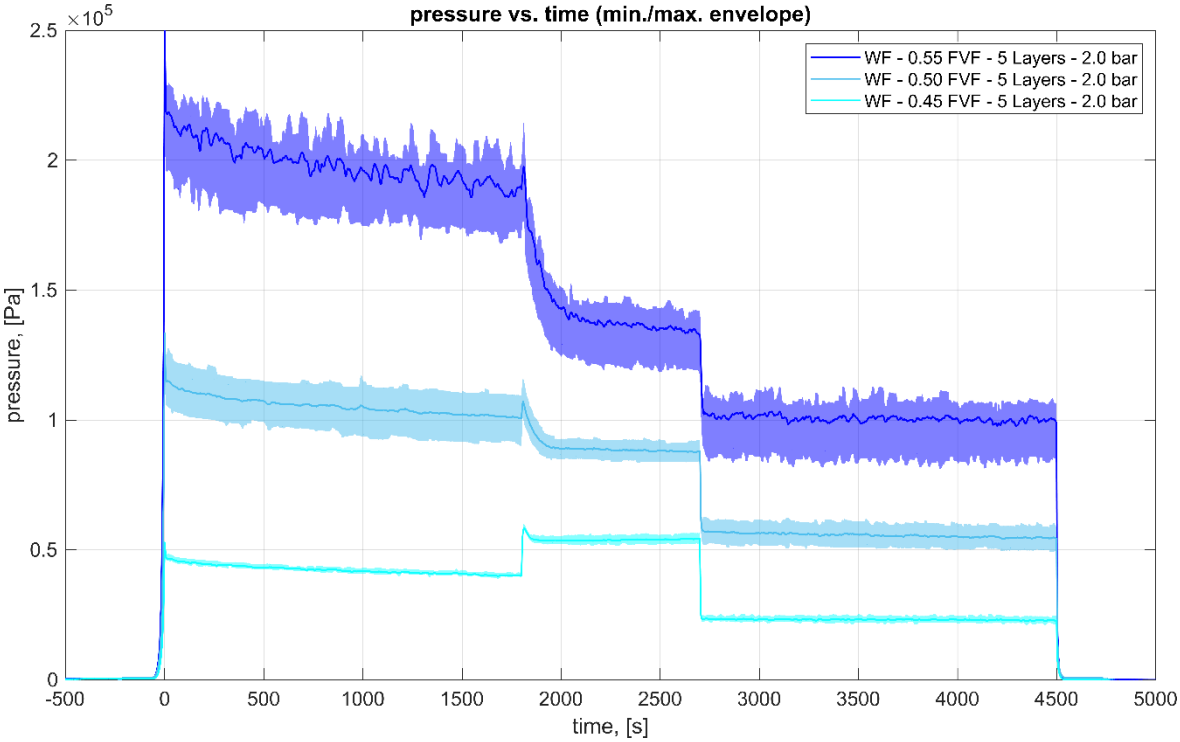

Figure 46: WF – 5 Layers – pressure vs. time (min./max. envelope)

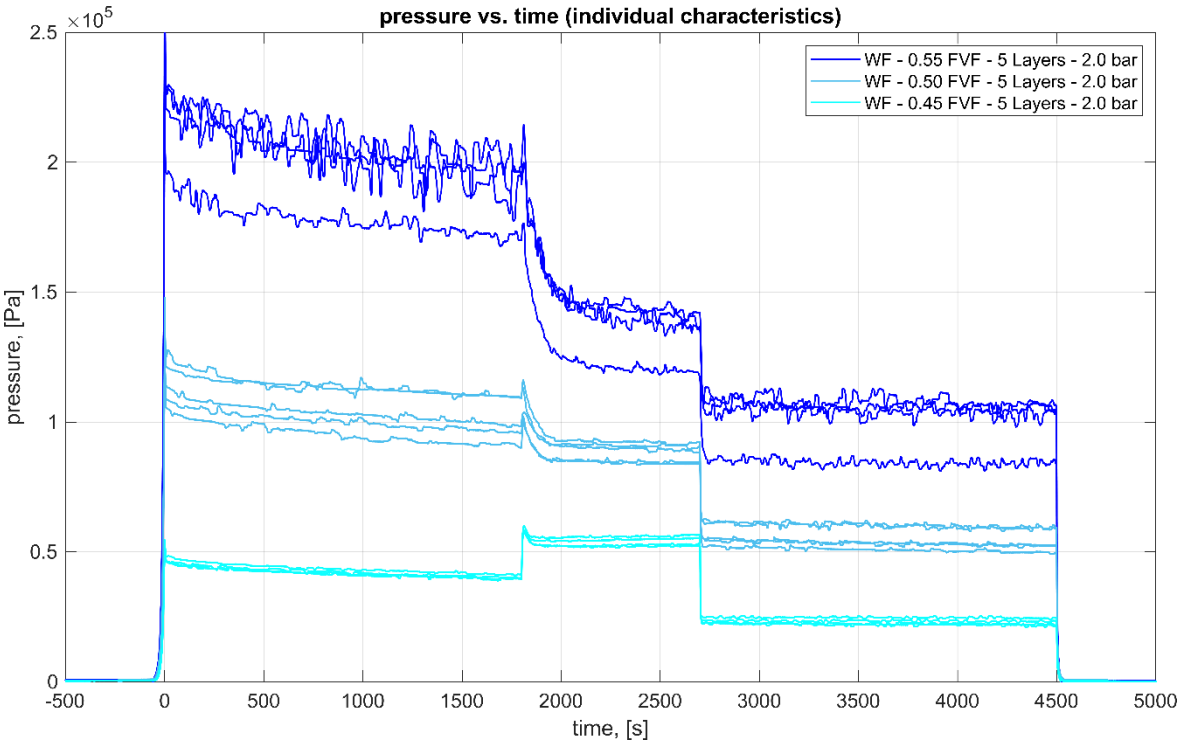

Figure 47: WF – 5 Layers – pressure vs. time (indiv. characteristics)

In these illustrations, the same picture as with the 3-layer configuration can be observed. In addition to the strong oscillations at the higher compaction range, a single measurement of the configuration with a FVF of 0.55 is particularly noticeable. This is slightly below the remaining accumulation of measurement curves, but still within the defined outlier tolerance. The remaining pressure-time trends are similar to that of the 3-layer configuration and otherwise show no peculiarities or deviations.

Finally, for the WF, Figures 48 and 49 show the corresponding enveloped curve and the individual characteristics of the 14-layer configuration.

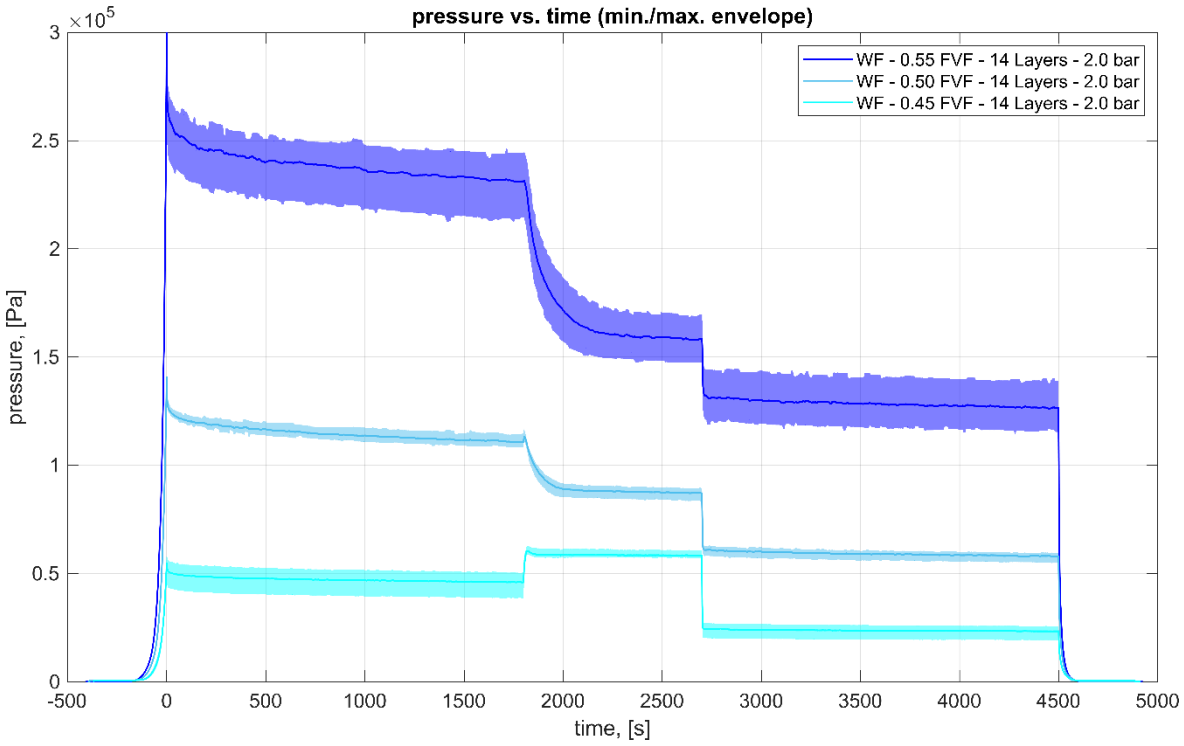

Figure 48: WF – 14 Layers – pressure vs. time (min./max. envelope)

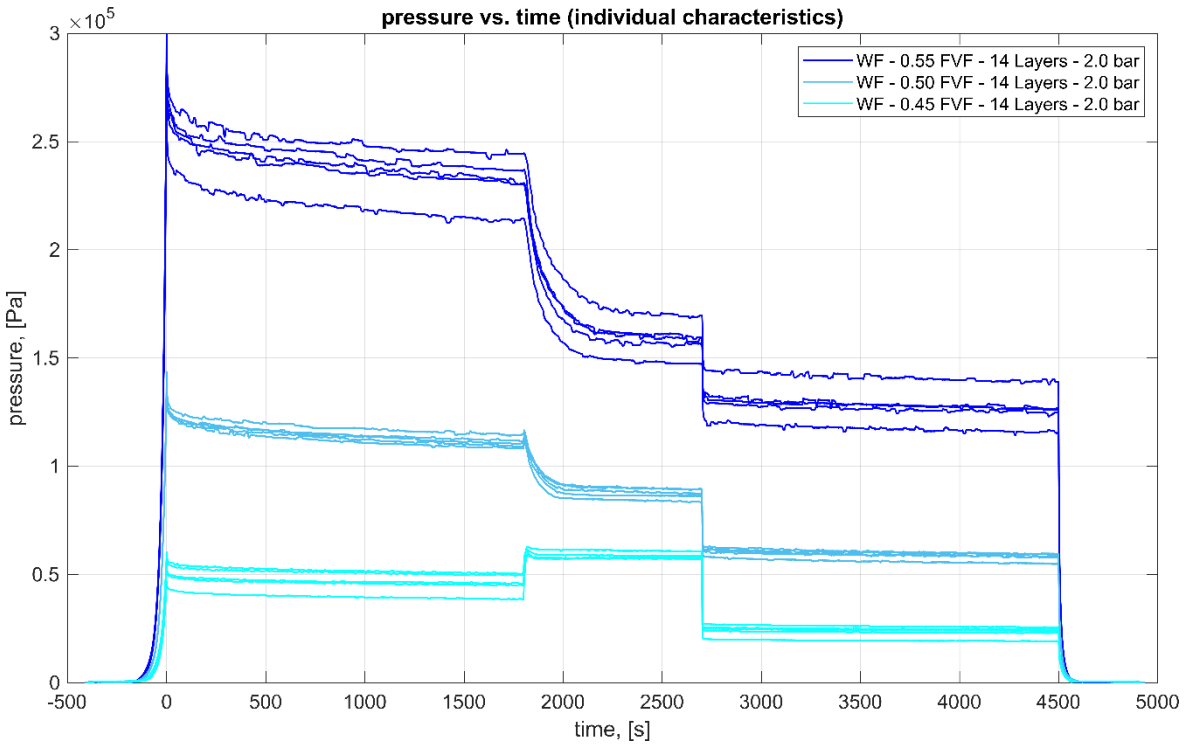

Figure 49: WF – 14 Layers – pressure vs. time (indiv. characteristics)

Here, a very similar representation to the measurement series with 3 and 5-layers can be observed. The degree of oscillation decreases significantly and is thereby

less noticeable. Important to mention, are the higher maximum pressure values reached, compared to the results obtained for the 3- and 5-layer specimen. The measured pressure-time trends follow the same scheme as already expected from the present WF measurement series and do not differ qualitatively from each other.

Furthermore, the experiments with the Veil are presented. Starting with the configurations consisting of 3 layers, Figure 50 shows the envelope for the minimum and maximum value representations and Figure 51 the corresponding individual characteristics. The measuring range of the load cell in this configuration is not sufficient to measure at a FVF of 0.45. As a direct result, this test arrangement is not included.

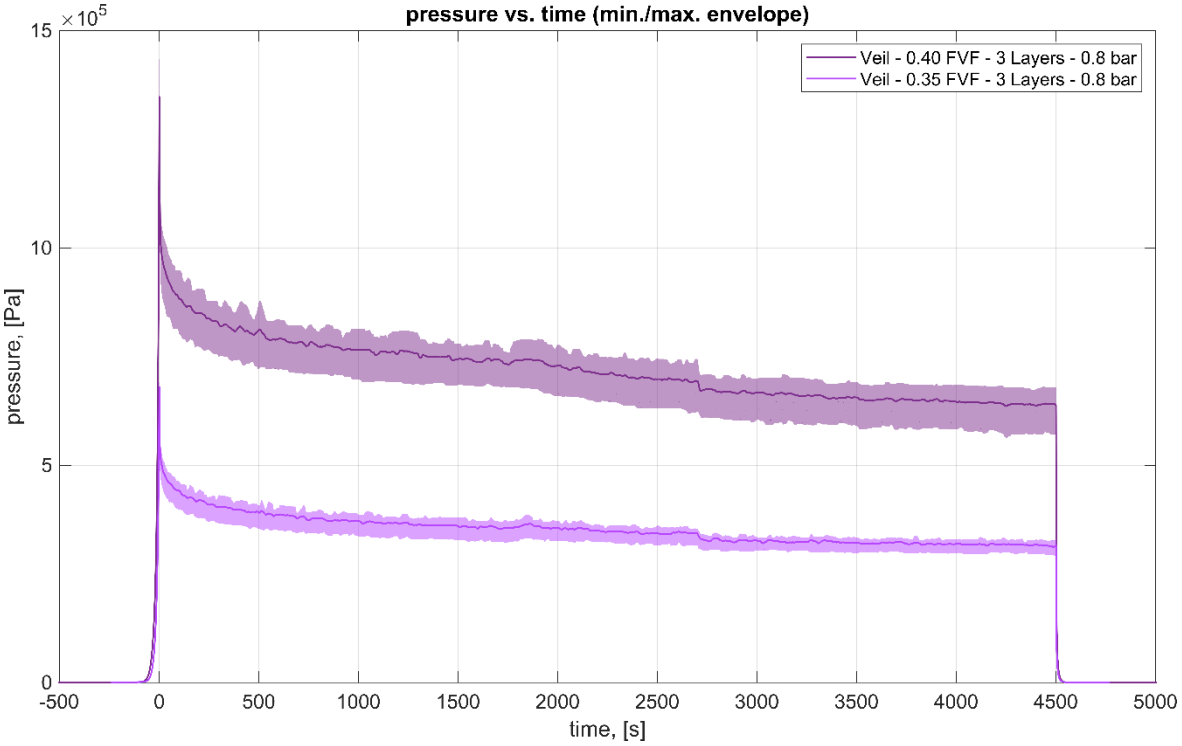

Figure 50: Veil – 3 Layers – pressure vs. time (min./max. envelope)

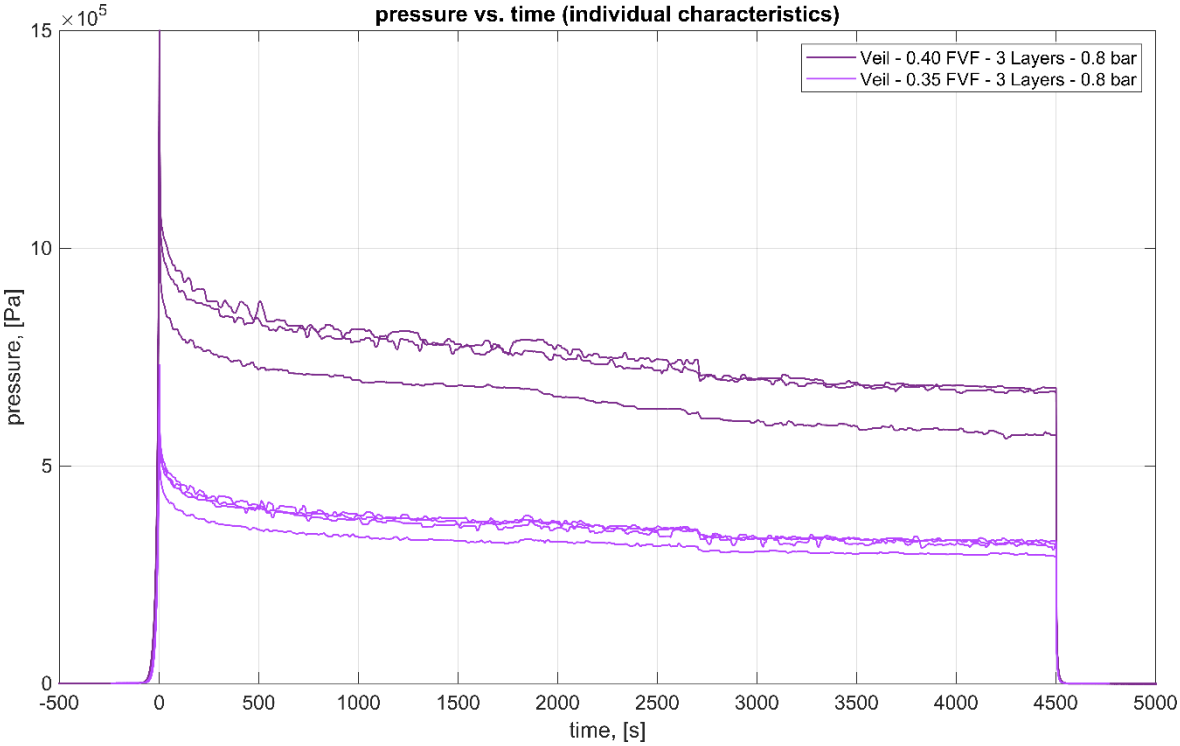

Figure 51: WF – 3 Layers – pressure vs. time (indiv. characteristics)

It is particularly important to mention that comparatively many outliers occur in this series of experiments at the upper tolerated pressure limit of the piezoelectric load cell. For the remaining courses, the scatter range can be considered moderate, relatively speaking it is comparable to the ones presented so far. Once again, a pressure-time trend as already expected from the pretest series can be observed. Here, the injection phase can hardly be distinguished from the dry as well as the saturated relaxation stage. The relaxation itself occurs relatively quickly, especially for 3 layers and the specimen configuration approaches a new state that requires less energy and thus can be considered ideal. This new desired state is influenced by the impregnation with the test fluid in a marginal way, but at least most pronounced at the upper-pressure range.

Further, Figure 52 shows the envelope and Figure 53 the individual characteristics of the 5-layer specimen configurations of the Veil.

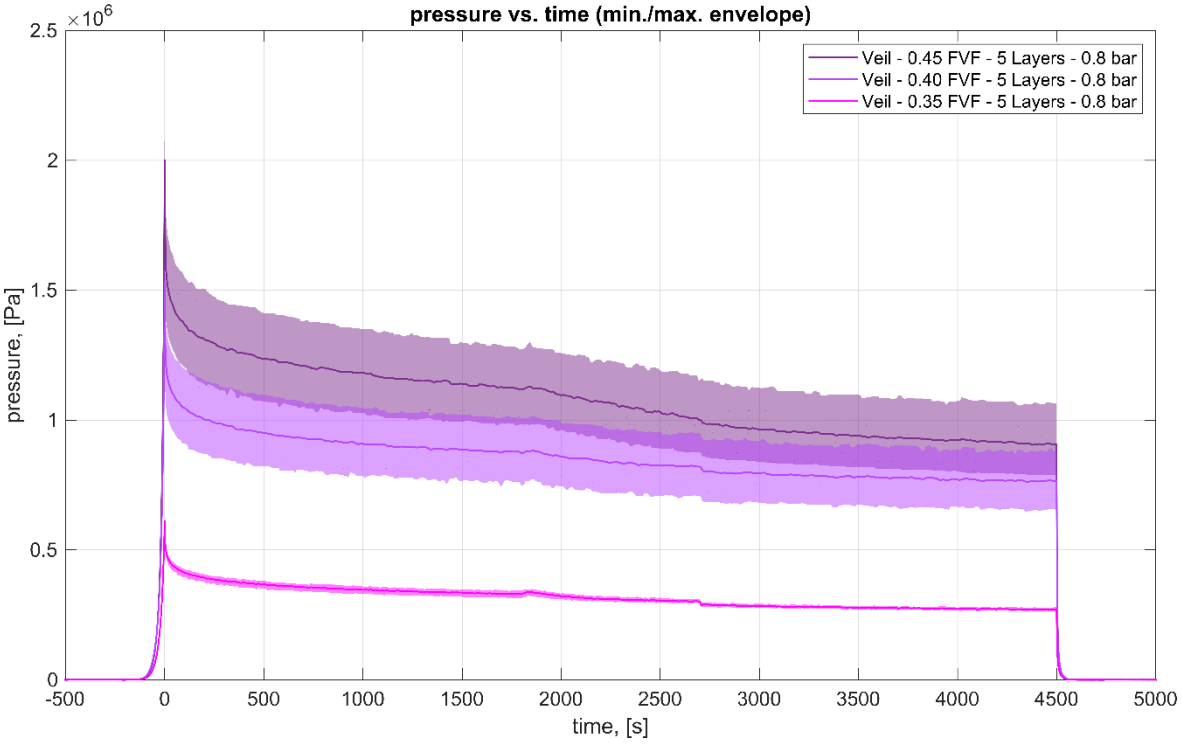

Figure 52: Veil – 5 Layers – pressure vs. time (min./max. envelope)

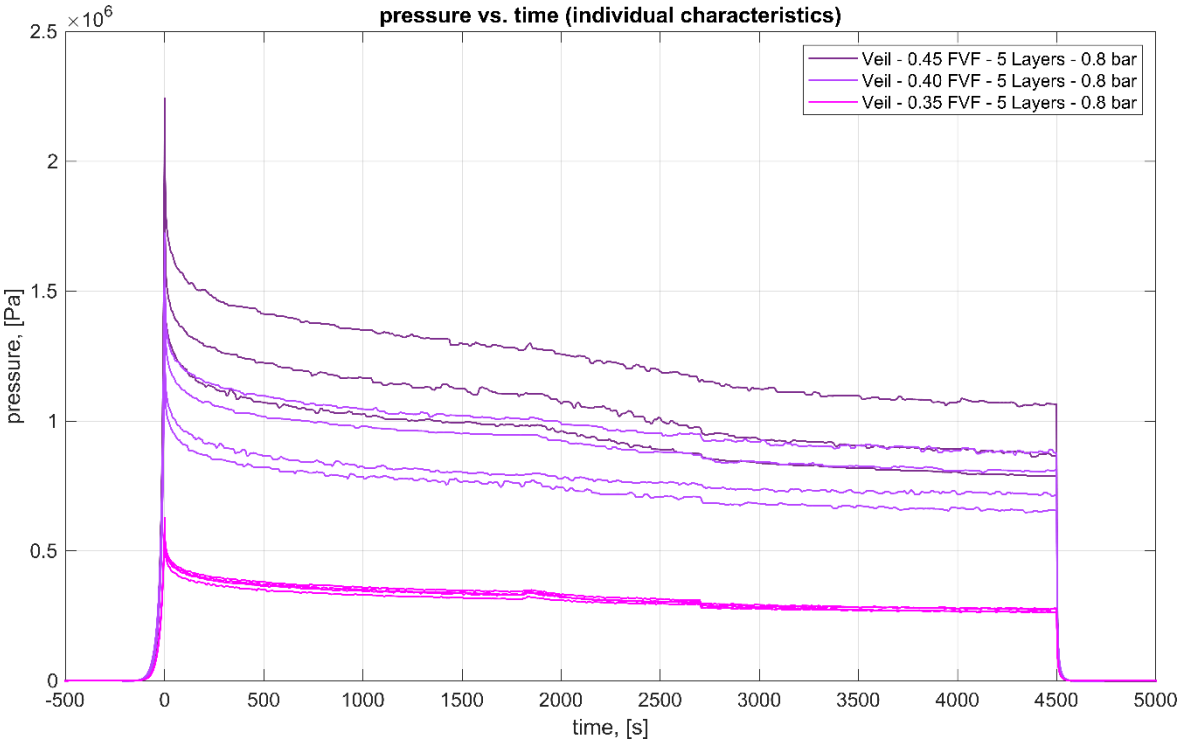

Figure 53: Veil – 5 Layers – pressure vs. time (indiv. characteristics)

In general, the illustrations show the already known trends as to be expected. The measurement configuration at FVF of 0.45, responds most clearly to the injection

phase and is in particular recognizable. The scatter within the measurement data increases again with increasing FVF. Finally, the measurement results of the Knit are presented in Figure 54 as the minimum and maximum envelope and in Figure 55 as individual characteristics.

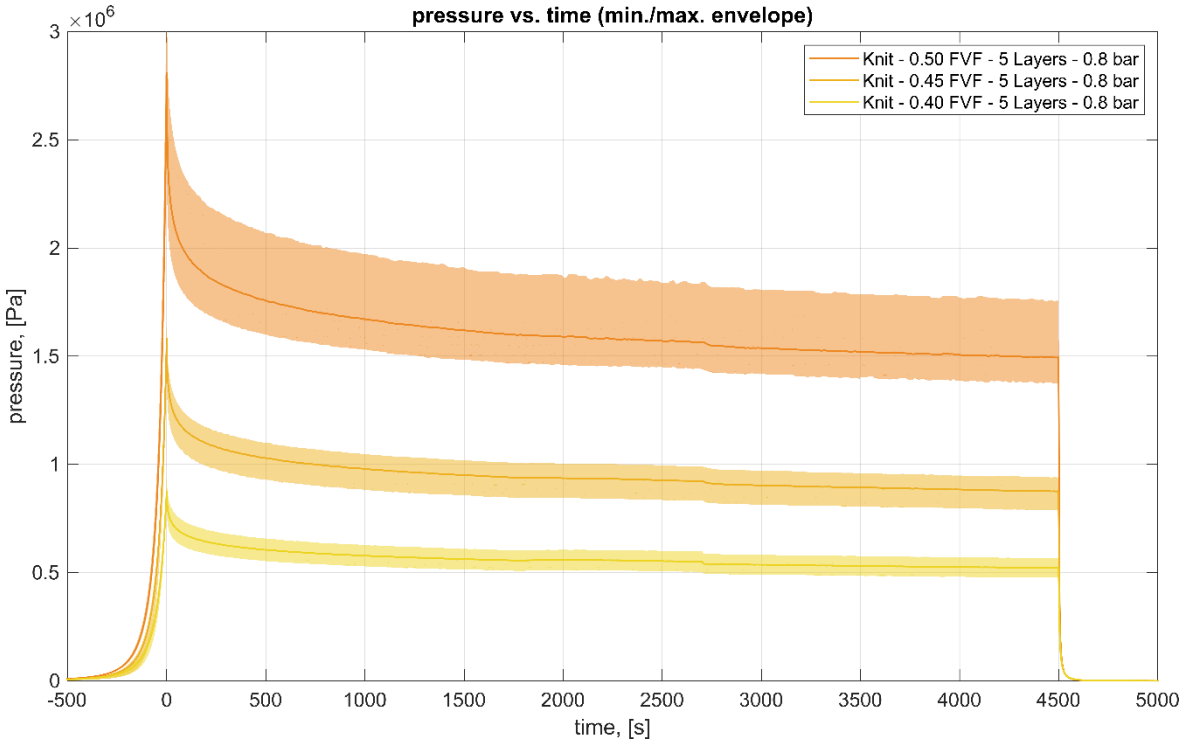

Figure 54: Knit – 5 Layers – pressure vs. time (min./max. envelope)

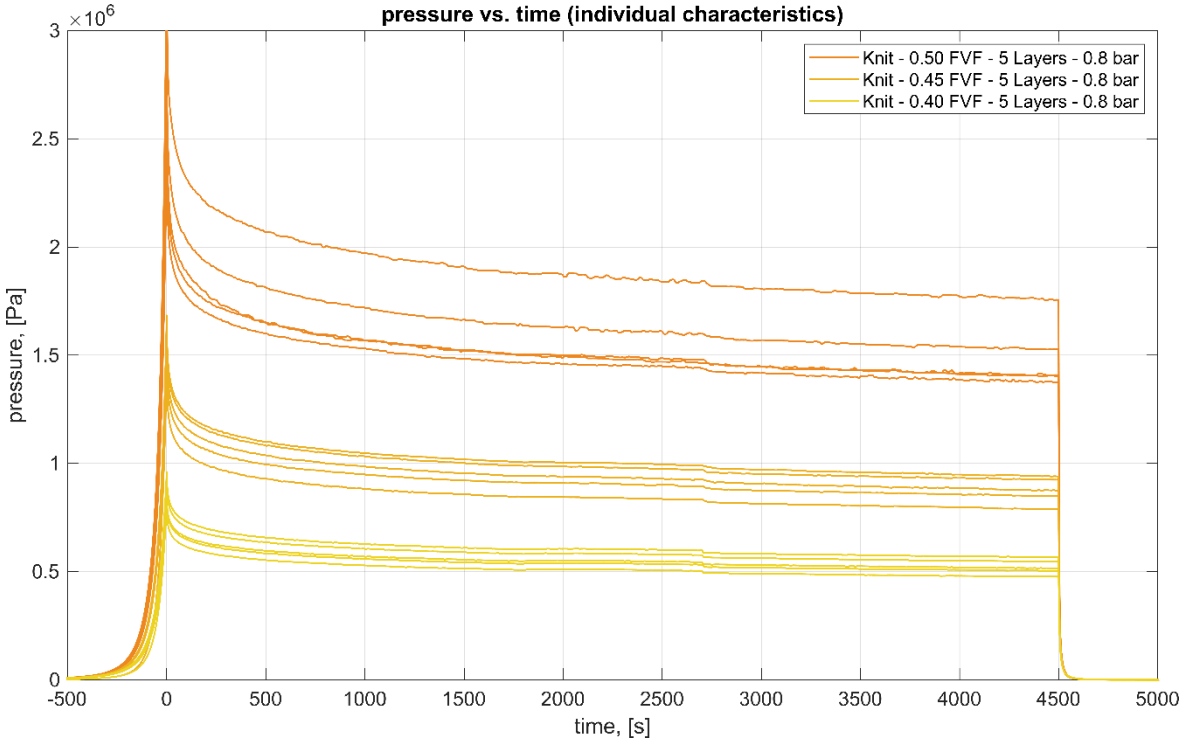

Figure 55: Knit – 5 Layers – pressure vs. time (indiv. characteristics)

The trends presented are very similar to the Veil material, but still, show a slightly different relaxation curve. Again, the pressure data show increasing scatter with increasing FVF. Concerning the comparatively high pressure values achieved, however, these are within an acceptable range. Especially at the lower compaction levels, the pressure level is quite stable over the entire course of the curve, while at a FVF of 0.50, a slight drop in the curve can be observed towards the end. The injection phase itself is barely noticeable and shows a minimal effect on the progression of the curve.

An overview of the median values obtained for each measurement series for $p_{max,dry}$, $p_{end,dry}$ and $p_{end,saturated}$ is provided in Table 7. In addition, the pressure drop between the dry and saturated levels, sorted by material, FVF and number of layers is presented.

Table 7: Overview of the results of the main test series

Material	Layers [-]	FVF [-]	$p_{max,dry}$ [kPa]	$p_{end,dry}$ [kPa]	$p_{end,saturated}$ [kPa]	p_{drop} [%]
NCF	3	0.45	23.5	9.6	8.5	11.4
		0.50	150.3	40.4	33.3	17.5
		0.55	443.4	103.0	80.5	21.8
	5	0.45	18.8	8.0	6.2	22.3
		0.50	122.5	39.4	33.1	16.0
		0.55	368.0	102.2	80.1	21.6
WF	3	0.45	44.7	37.8	22.5	40.5
		0.50	114.9	77.9	48.6	37.6
		0.55	252.3	181.3	99.5	45.1
	5	0.45	52.5	39.9	22.8	42.9
		0.50	130.2	98.6	52.6	46.7
		0.55	285.2	192.5	103.7	46.2
	14	0.45	54.3	45.9	24.1	47.6
		0.50	140.2	110.5	58.2	47.3
		0.55	304.1	230.4	126.1	45.3
Veil	3	0.35	678.7	360.5	312.6	13.3
		0.40	1520.0	784.4	679.0	13.4
	5	0.35	619.4	332.8	275.9	17.1
		0.40	1657.5	945.7	809.3	14.4
		0.45	2126.5	1188.5	965.8	18.7
Knit	5	0.40	847.2	547.9	514.9	6.0
		0.45	1605.7	942.2	875.3	7.1
		0.50	2778.9	1503.9	1408.3	6.4

4.5 Comparisons of the main test series

Figures 56 and 57 show the normalized pressure-time plots for the 3- and 5-layer specimen of NCF and WF at a FVF of 0.55.

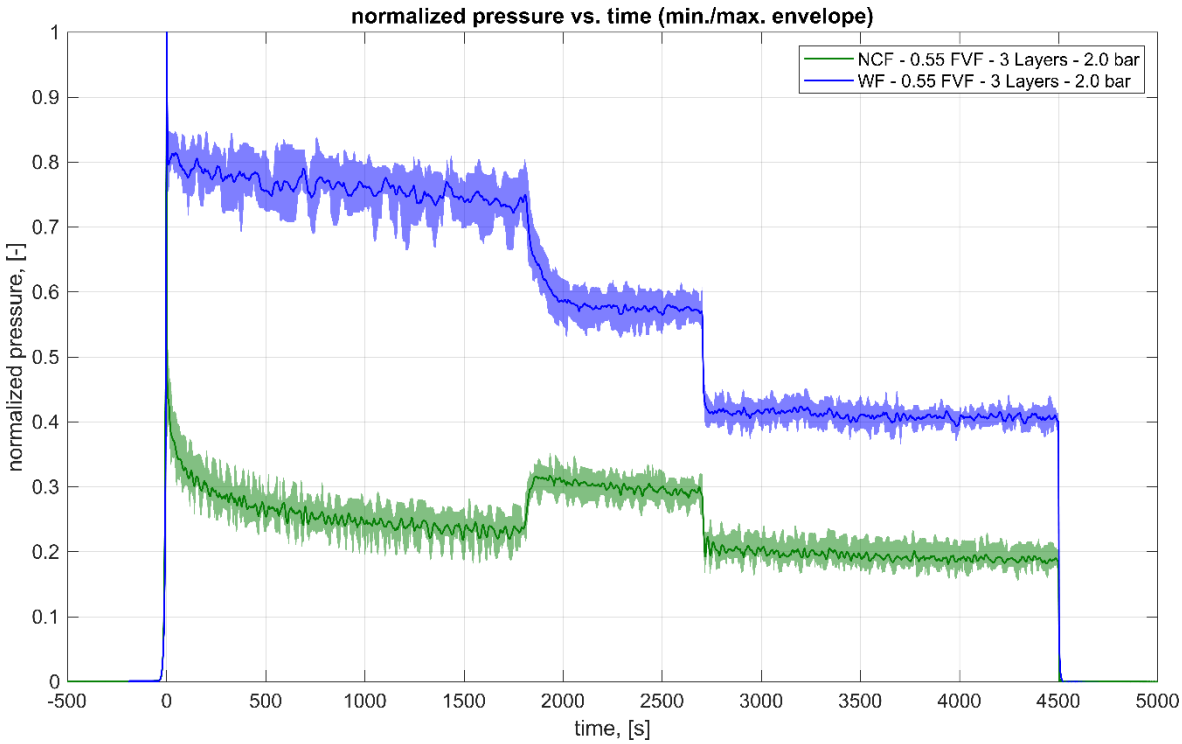

Figure 56: Normalized pressure vs. time (min./max. envelope) – 0.55 FVF – 3 Layers

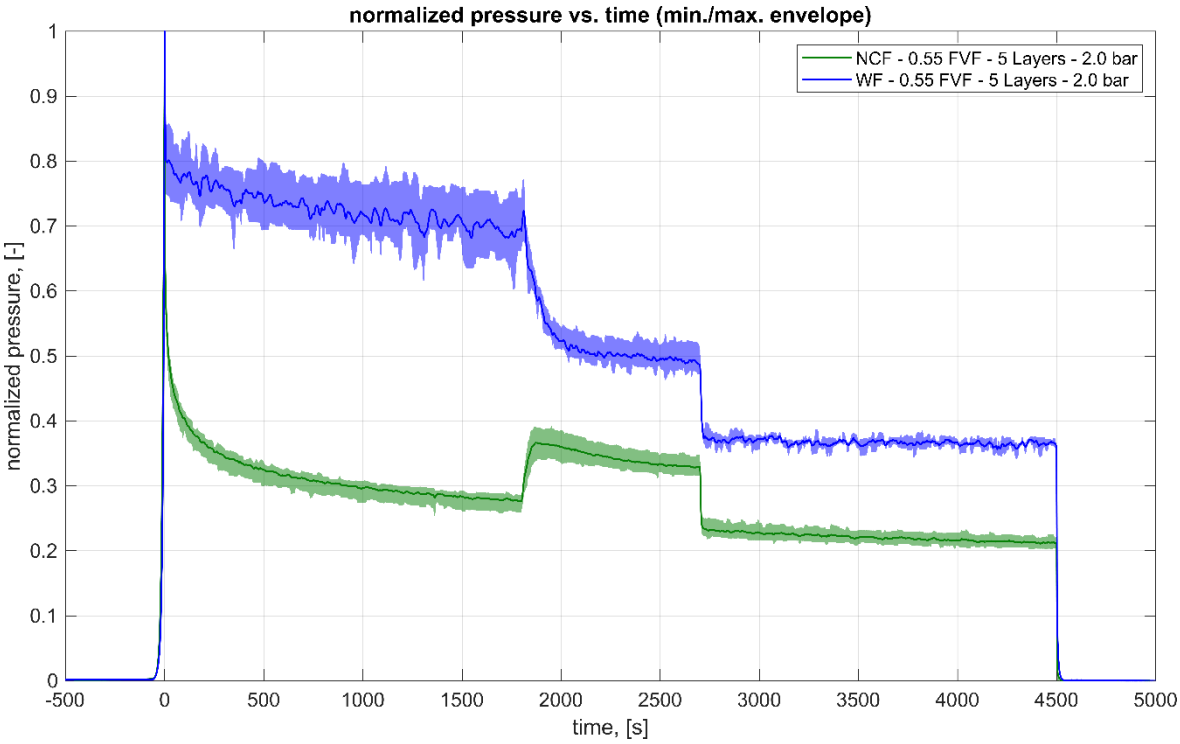

Figure 57: Normalized pressure vs. time (min./max. envelope) – 0.55 FVF – 5 Layers

Starting at the highest compaction levels, a similar trend emerges for 3 as well as for 5 layers of the NCF and WF. The WF shows a strong decreasing trend of total pressure during the fluid injection phase. Thus, the lubrication effect in the WF dominates over the contribution of the fluid pressure. By contrast, the NCF shows a significant increase of the total pressure during the fluid injection phase. This indicates the fluid pressure dominating over the lubrication effect in the NCF. Above all, this becomes obvious when comparing $p_{end,dry}$ and $p_{end,saturated}$: The drop is significant for the WF, but marginal for the NCF.

In the following, Figures 58 and 59 show the plot at a FVF of 0.50, again separated by the number of layers.

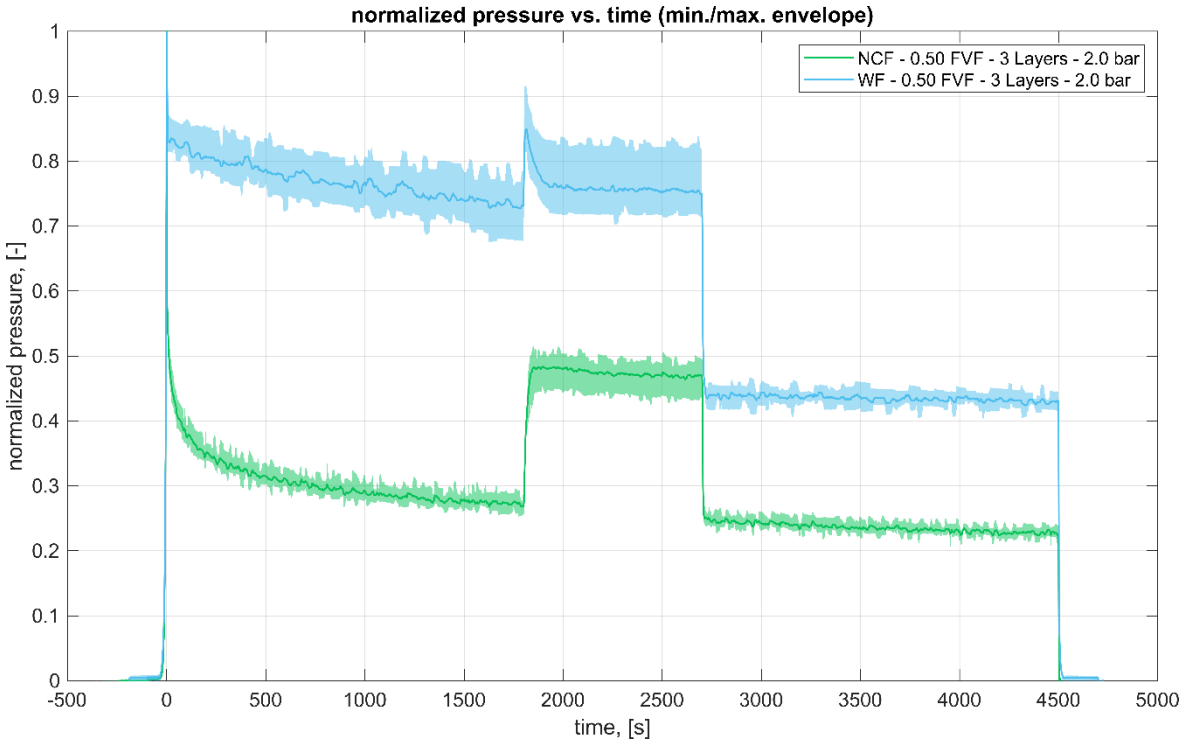

Figure 58: Normalized pressure vs. time (min./max. envelope) – 0.50 FVF – 3 Layers

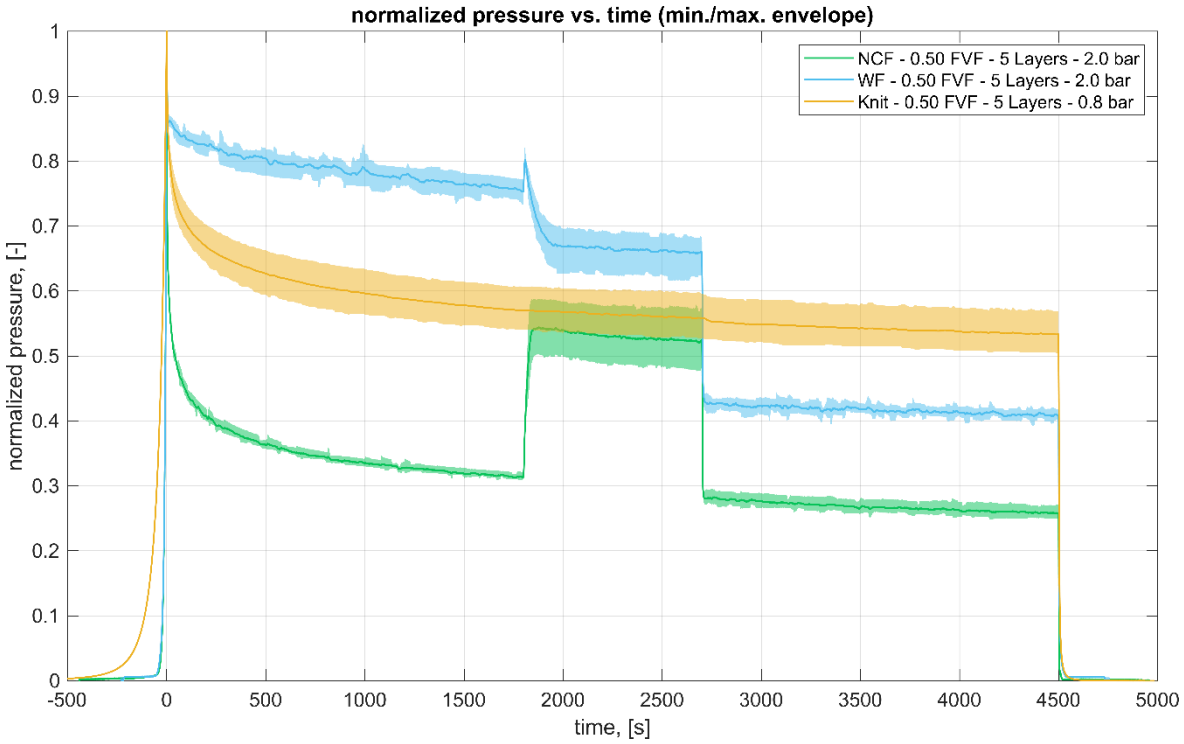

Figure 59: Normalized pressure vs. time (min./max. envelope) – 0.50 FVF – 5 Layers

Here, the increasing influence of the fluid pressure during the injection phase is noticeable. As a result, the relaxation curves during this stage are noticeably

shifted to higher pressure levels. For the Knit, the already known course can be described. Here, one can see that the final pressure level in the saturated area reaches about half of the measured maximum pressure.

Furthermore, Figures 60 and 61 provide similar plots for a FVF of 0.45, starting with 3 layers and followed by the 5 layer-specimen configurations.

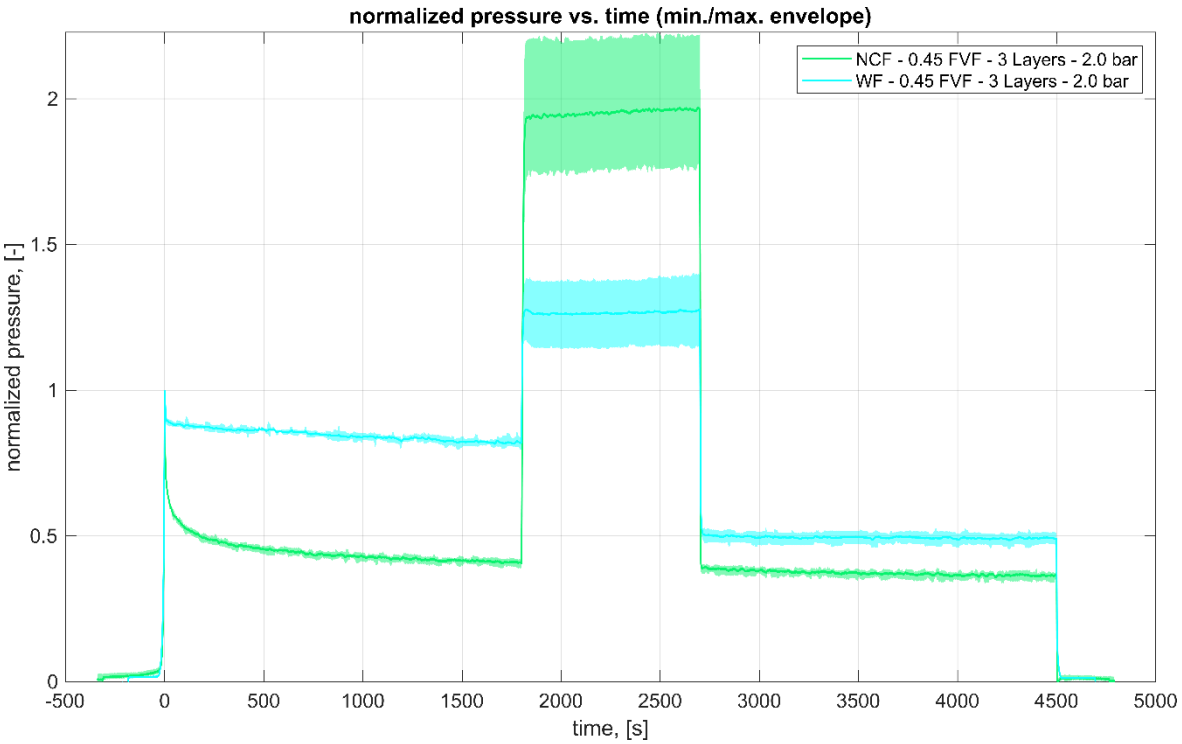

Figure 60: Normalized pressure vs. time (min./max. envelope) – 0.45 FVF – 3 Layers

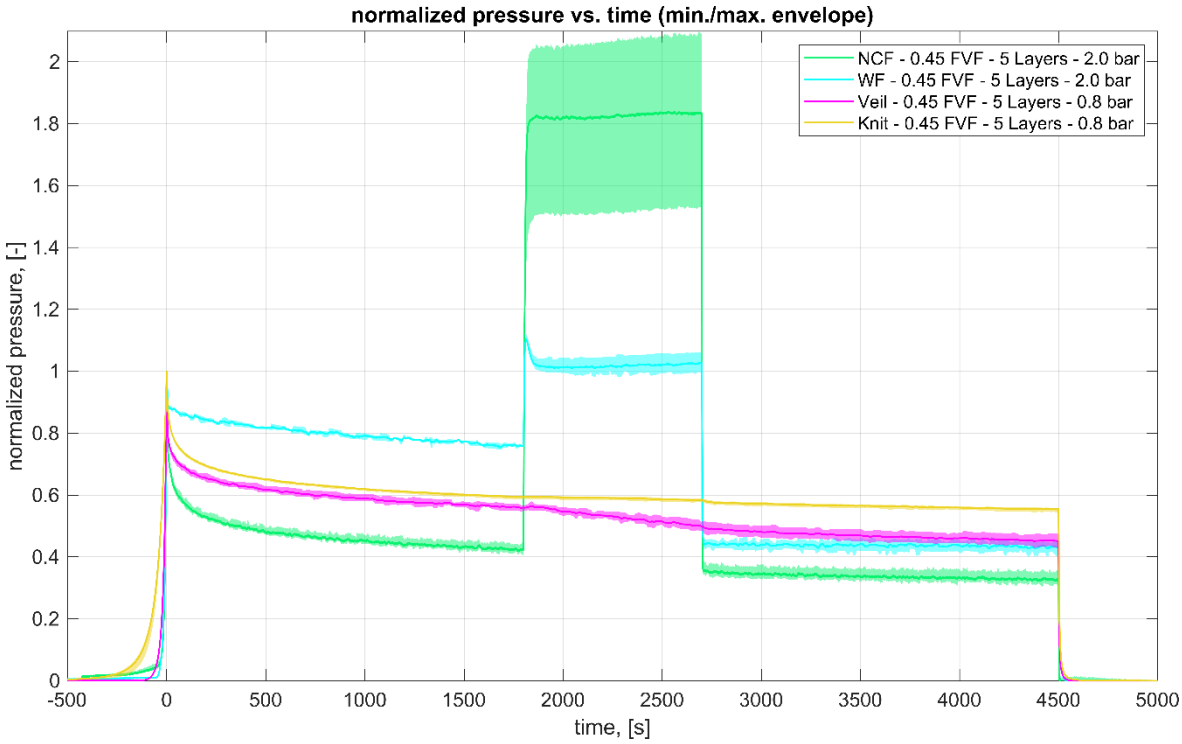

Figure 61: Normalized pressure vs. time (min./max. envelope) – 0.45 FVF – 5 Layers

For the WF and NCF, the fluid injection pressure component is pronounced, such that the combination with compaction pressure exceeds the measured maximum compaction pressure in the initial compaction phase. In direct comparison with the Knit, the Veil shows a stronger response to the presence of the fluid during the injection and thus shows a significant progression to lower pressure levels in the saturated phase. Finally, Figure 62 shows a comparison between Veil and Knit at a FVF of 0.40 and 5 layers.

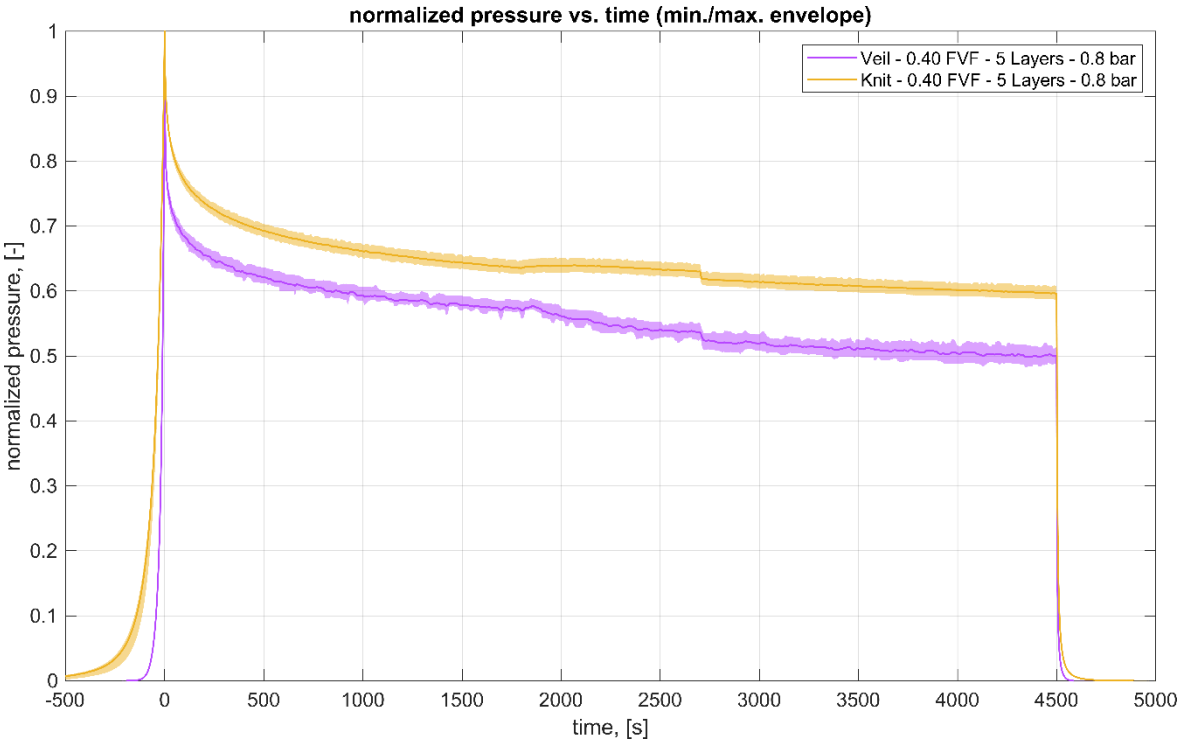

Figure 62: Normalized pressure vs. time (min./max. envelope) – 0.40 FVF – 5 Layers

Here, the increase in the load path is much steeper for the Veil compared to the Knit. This is due to the textile architecture, where the entanglement of the knitted fabric allows for a certain degree of flexibility, which is practically non-existent in the comparatively thin fibre bundles that are bound in the Veil.

Further, the Veil and the Knit show a noticeable response to the presence of the fluid. The proportion of the fluid injection pressure as a share of the total pressure is visible in both trends. A clear difference can be seen in the pressure range at the end of the saturated phase. The pressure level of the Knit is about 60 % and that of the Veil is about 50 % of the maximum pressure.

5 Conclusion

The textile reinforcement architectures investigated in this thesis show different characteristic responses when subjected to transversal compaction. Differences are recognizable, especially in the dry and saturated relaxation stages and during the in-situ impregnation with the test fluid. Already in the initial phase of the experiment, a different compaction profile can be observed. The resulting behaviour is particularly dependent on the number of layers used and the set FVF. The observed relaxation curve is essentially different for each textile reinforcement architecture until a new energy state is established that can be considered ideal for the layered structure in the given constraint. The following section of this thesis discusses the specifics observed during the experiments. Taking into account the already presented observations, further comparisons between the textile reinforcement architectures are made in the following. Finally, the observations are summarized and evaluated accordingly.

5.1 Specifics of the experiments

5.1.1 Oscillations

Particularly noticeable in the range of low numbers of layers is the measurement of strong oscillations in the pressure-time trend. This is most pronounced in textile reinforcement structures specifically designed for high-rigid applications. Starting with the NCF, these strong fluctuations in the curves can be observed best. This is most evident in a range of a low number of layers and at a high FVF, as already shown in the individual characteristics in Figure 41 in the results section. The same behaviour can be observed for the WF, in the pressure-time trend in Figure 45.

To explain this effect, it is helpful to investigate the recorded LVDT and path data of the UTM crosshead first. Therefore, Figure 63 shows a representative example of the corresponding data from a single measurement of the NCF with 3 layers

and a FVF of 0.55. Figure 64 shows the total pressure trend, a combination of the exercised compaction pressure and the applied fluid injection pressure with a set value of 2.0 bar, against the UTM crosshead position.

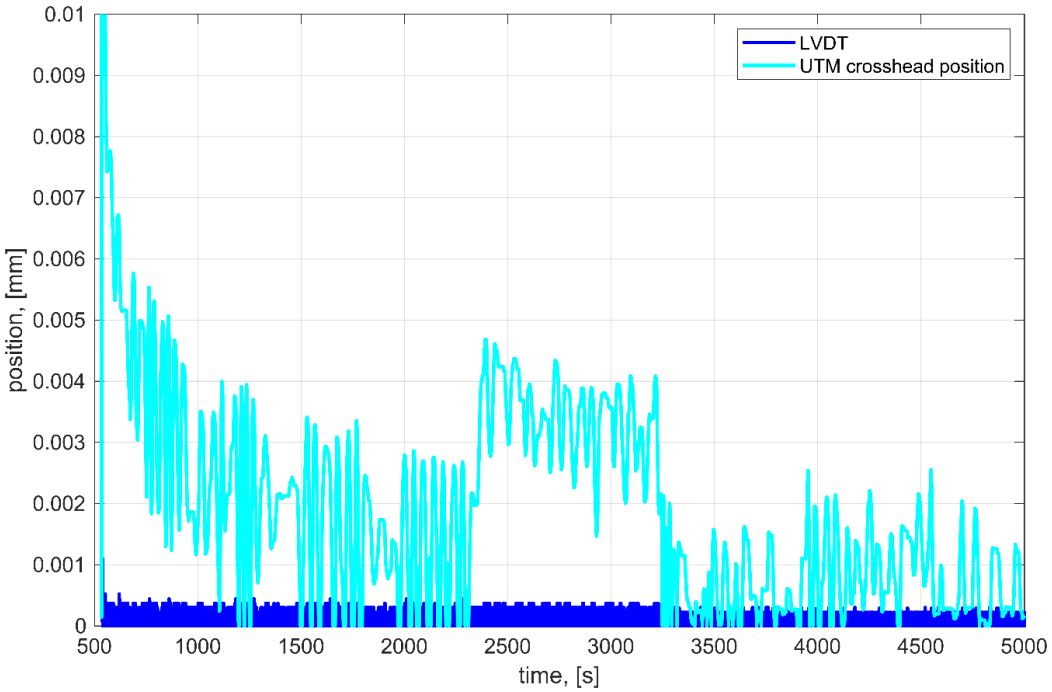

Figure 63: LVDT and UTM crosshead position over experimental time

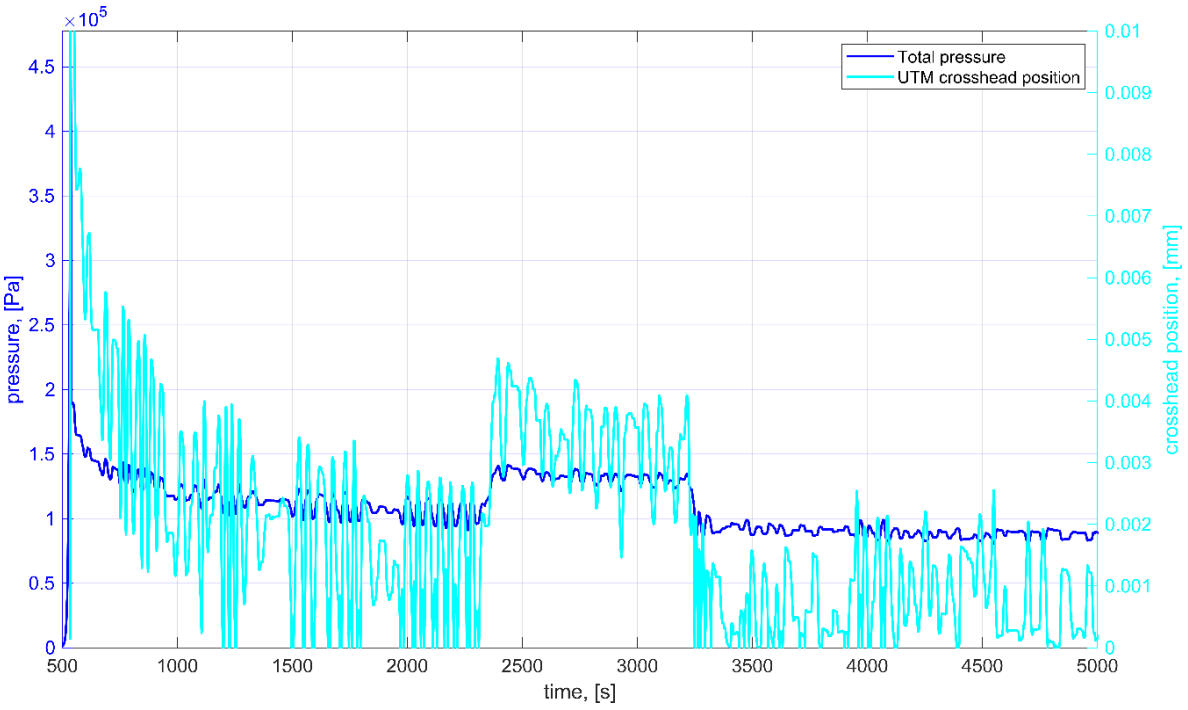

Figure 64: Total pressure and UTM crosshead position over experimental time

On the one hand, the first plot shows that the force-related control of the LVDT remains very constant without any significant fluctuations, and thus no readjustment takes place in this case. However, the UTM-related path data can be perceived as highly oscillating. In the latter plot, on the other hand, it can be seen that the UTM crosshead position correlates strongly with the recorded total pressure profile of the specimen under transversal compaction over the entire measurement period. This indicates that the position of the UTM crosshead adjusts itself during the experiment, causing these oscillatory fluctuations in the observed trend. These minimal path changes of up to 10 µm and predominantly in a range of 3 µm are sufficient enough to cause noticeable variations in the load cell readings.

The observed effects can therefore be completely attributed to the UTM and do not represent any material-related peculiarity. Moreover, this effect becomes less pronounced when increasing the number of layers and is hardly observed in the experiments with the Veil or Knit. To some extent, one reason for this may lie in the composition of the structure itself. But here the recorded pressure level, especially of the Veil, is much higher and therefore the proportional influence of the readjustment of the crosshead position is less pronounced. The same is true when using an increased number of layers. In this case, the oscillations can ultimately be distributed over more inter-layer interfaces. Nevertheless, this is recognizable for the NCF as well as the WF, especially at the high compaction levels with an FVF of 0.55 for the specimen configurations of 5 layers.

5.1.2 Areal weight

Some measurement results, especially those of the Veil, show a rather large scatter. One reason for this is to be found in the textile architecture of the materials. For this purpose, it is first helpful to consider Table 8, which shows the minimum and maximum coefficient of variation c_V for each measurement series. This coefficient, also known as relative standard deviation and often expressed as a percentage, is defined as the ratio of the standard deviation σ to the mean μ, as shown by the following equation [59]:

$$c_V = \frac{\sigma}{\mu} \tag{18}$$

Here, the values presented in the table refer to the real areal weight of a specimen, which is determined by its weight, area and number of layers of the prepared textile stack. Prior to each experiment, the corresponding weight of each specimen was measured using a laboratory balance.

Table 8: Coefficient of variation for the real areal weight according to specimen configuration (min./max.)

Material	Nom. areal weight [g/m²]	Layers [-]	Real areal weight [g/m²]	c_V [%]
NCF	620 ± 19	3	615 .. 619	0.24
		5	615 .. 619	0.20
WF	300	3	289 .. 295	0.89
		5	285 .. 297	0.96
		14	286 .. 295	0.83
Veil	300 ± 15	3	277 .. 331	4.96
		5	285 .. 323	3.26
Knit	450	5	429 .. 495	3.93

As a general rule, it can first be stated that the more layers there are for each specimen configuration, the stronger the homogenization effects and the lower the scatter to be expected [60]. Starting with the NCF, a very small coefficient of variation of only 0.20 % and 0.24 % is shown across all layers. In particular, this material is characterized by very good handling, since the specimen remains extremely dimensionally stable when cut. The rovings are regularly arranged next to each other and there are hardly any processing variations within the textile architecture. The WF, on the other hand, shows slightly increased values in the range of 0.83 % to 0.96 %. Due to the statistically larger range, this variation tend to decrease with an increase in the number of layers for the minimum values. The

maximum values, on the other hand, show clearer inconsistency. However, if one considers the median over all three configurations, values between 291 g/m² and 293 g/m² result for the areal weight. This suggests that the sample configuration was quite uniform and homogenization over the number of layers is of much less importance in this case. The larger range of variation compared to the NCF can be attributed to the significantly more difficult handling. Particularly, when preparing the specimens, specifically when cutting the layers, individual fibre bundles are easily detached. This consequently reduces the areal weight and explains the present coefficient of variation. A similar scatter could be observed in the benchmark exercise [1] already mentioned. Here, the deviations are in the same order of magnitude of 1 % for the same WF material. In addition, due to the architecture of the WF, the handling of this material, reportedly caused difficulties during specimen preparation, resulting in a higher degree of fraying and deformation. As a result, this consequently affected the coefficient of variation during the measurements.

The Veil shows a coefficient of variation of 3.26 % and 4.96 % for 3 and 5 layers respectively. This value is also noticeably higher for the Knit with 3.93 %. The Veil in particular retains its shape very well and is quite easy to handle. Here, individual disordered fibres do come off the specimen, as compared to the NCF, but not enough to explain the high scatter range. In any case, one reason for this lies in the manufacturing of this textile reinforcement architecture. Due to the irregular deposition of the individual fibres on the production line, it is considerably more difficult to specifically set the desired areal weight [2]. Here, due to homogenization effects, the range of the spread decreases with an increase in the number of layers. In the case of the Knit, the deviation can be explained on the one hand by the manufacturing technique and by the type of fibre used. Here, the manufacturing of fibres from natural raw materials usually leads to an increase in deviation [2], [25].

5.2 Summary of observations

In general, the behaviour of the various textile reinforcement architectures, described in detail in the literature, can be observed in the present thesis. The results obtained during compaction from compression-relaxation experiments confirm the complex mixture of basic effects occurring, namely yarn-cross section and bending deformation, yarn flattening, void/gap condensation as well as nesting, especially for the WF. Thereby, the influence of the number of layers on the transverse compaction behaviour of the textile reinforcements using a novel test configuration that involved in-situ impregnation of the specimen, revealing the influence on the textile architecture. [1], [8]–[10], [18], [19], [35], [37]–[40], [52]

For this purpose, Figure 65 shows the results of the compression-relaxation experiments in compact form. Thereby, the corresponding values for the three evaluated measuring points concerning the compaction pressure, previously defined in Figure 18, are shown separately according to the number of layers and FVF.

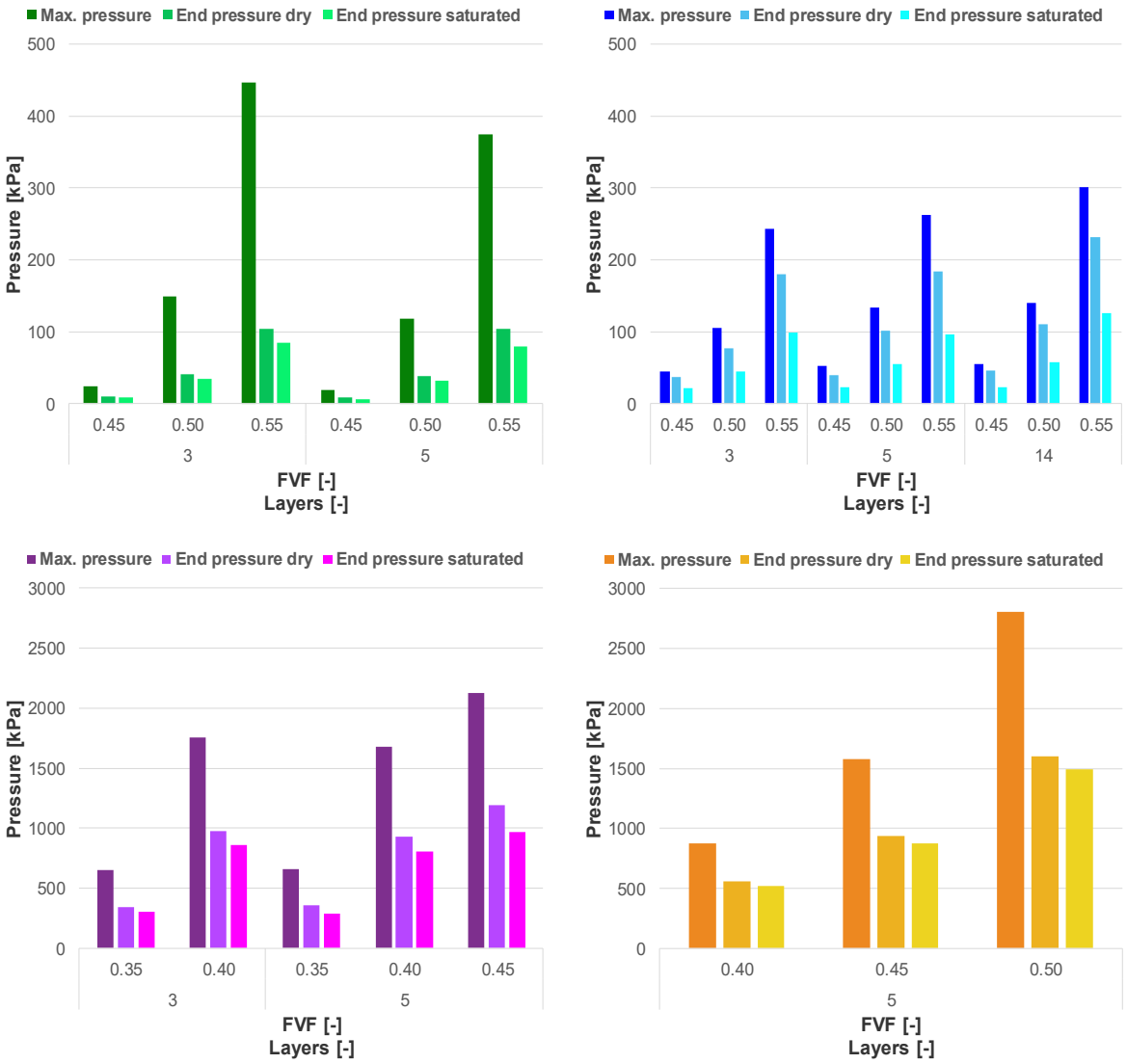

Figure 65: Comparisons of maximum pressure to final pressure levels in the dry and saturated areas for the materials: NCF (top left) and WF (top right) up to 500 kPa, and Veil (bottom left) and Knit (bottom right) up to 3000 kPa

Starting at the top left, the data for the NCF shows, that the maximum pressure values significantly exceed those of the WF, especially at a FVF of 0.55. It can also be seen that higher values are achieved with the NCF in the range of 3 layers than with 5 layers. Comparatively, this textile reinforcement architecture relaxes noticeably more within the first 30 min in the dry phase and even undercuts those pressure values in the same phase of the WF. The same trend continues for the measured values in the saturated stage. In general, the WF shows the opposite trend compared, compared with the NCF. Here, the obtained pressure values increase with the number of layers. In the saturated phase, however, the

differences become noticeably more relative and the obtained data are within a similar range. Particularly concerning the relatively high number of fabric layers used in the 14-layer configuration of the WF, it should be noted that the accurate lay-up and alignment of the plies can be challenging. Different configurations of nesting between the layers can cause a larger scatter in results for a lower number of layers, while convergence, hence a smaller scatter, can be expected for a large number of layers [1]. This can also be applied between the configurations with 3 and 5 layers but will be correspondingly less significant.

Further, it is important to consider that the NCF shows twice the areal weight compared to the WF and the Veil. Accordingly, the measured results are relativized, especially when compared with the WF, but also in direct comparison with the Veil and Knit. Nevertheless, the differences between the dry and saturated phases within the same textile reinforcement can be seen in the diagrams. For the WF, it is clear that the onset of the lubricant effect significantly facilitates the slipping of the fibres, which in turn can be traced back to the fundamental differences in the textile architecture and consequently to the compaction properties. Since the fibre bundles of NCF are not ondulated, the highest achievable theoretical packing fraction can be expected here, compared to all other reinforcement materials used in this thesis. This results in a highly rigid reinforcement structure with the characteristic compaction properties described. Therefore, the effects of nesting tend to be insignificant for NCF, while they tend to be significant for WF specimen configurations. In addition, the maximum achieved compaction pressure tends to be lower for saturated fabrics than for dry fabrics, which is related to the lubrication of the fibres. The effect of specimen wetting is less significant for NCF than for WF, as the fibre fixation is usually stronger and thus less rearrangement of the fibres takes place [1]. In general, the observed material behaviour, due to these lubricant effects occurring between the fibre bundles, can be explained by the presence of the fluid. This mainly explains why lubricated fabric stacks are easier to compact than dry ones. Consequently, the interfibre friction force reduces and the distance between neighbouring filaments in the bundle narrows. Thereby, the number of contact points between adjacent filaments may increase as well and relatively small-scale elastic deformations of

the lubricated fibres may become important during consolidation. [1], [29], [34], [61], [62]

Concerning the results for the Veil and Knit, it should first be noted that the range for the pressure axis in the plot is higher by a factor of 6, compared to the plots for NCF and WF. In any case, significantly higher pressure values were recorded, already close to the permitted measuring range of the load cell. Consequently, this also led to a non-measurable test configuration for the Veil with a FVF of 0.45 at 3 layers. For the Veil itself, a trend more similar to the NCF emerges, in which those configurations with a lower number of layers achieve higher maximum pressure values. The pressure values of the Veil are higher than those of the Knit for the comparable configuration with a FVF of 0.40 as well as 0.45 for 5 layers each. Especially in the final pressure range of the saturated phase, these results increasingly resemble each other and the difference is no longer as clear as in the range of the maximum pressure reached. Due to the random arrangement of the fibres of order in the Veil, the influence of an exact arrangement of the individual layers is further reduced as well as that of the occurring compaction effects. Since predominantly similar results with hardly any variation were measured with different configurations, it can be concluded that the influence of the number of layers on the textile architecture of the Veil is insignificant.

Fluid absorption in plant fibres leads to a softening of the fibres and thus to a reduction in the compaction pressure. As a result, stress relaxation is higher for these preforms in the impregnated state. This observation can also be applied to the present Knit, consisting of viscose. In this case, the fibres are also softened, but no major realignment occurs. Glass fibre mats, such as the Veil, show an opposite trend. As the lubrication effect increases, the tow realignment and reorientation of the fibres, as well as the interactions between successive layers during the compaction stage increase. [23], [25], [47]

5.3 Comparison to a benchmark exercise

The Processing of Composites Group participated in an International Benchmark Exercise (IBE) [1] in 2020 with a NCF specimen consisting of 10 layers and a WF specimen consisting of 14 layers, with the same WF material, as investigated in this thesis. Both specimens were cut to a square dimension with an edge length of 60 mm and were prepared with a homogenous placement of the layers. The stamp itself had a circular shape with a diameter of 50 mm. These dimensions correspond exactly to half of those, presented in this thesis. In the measurement series, the maximum FVF was 0.58 for the NCF as well as 0.54 for the WF. The participants were required to perform compression-relaxation tests over a total of 30 min, on both fabrics under two different conditions, one wet and one dry, each with a minimum number of 5 repeated tests. The impregnation of the specimens with a test fluid was not performed in-situ during the measurement, but the specimens were dripped in a bath of test fluid for a total of 15 min, beforehand.

To show the differences between the tests performed in this thesis and those performed in the benchmark exercise, Table 9 shows the relevant parameters as well as the values measured in the dry test phases. One major difference is, on the one hand, that the FVF was set in the thesis, resulting in the necessary calculated compaction height. In the IBE, on the other hand, the target height was set at 3 mm, which resulted in the FVF shown.

Table 9: Comparison of the IBE and the Master Thesis

	Specimen size Stamp diameter	**h [mm]**	**FVF [-]**	**$p_{max,dry}$ [kPa]**	**$p_{end,dry}$ [kPa]**	**Δ [%]**
IBE	60 mm x 60 mm Ø 50 mm	3.00	0.54	224.0	182.0	18.8
Master Thesis	120 mm x 120 mm Ø 100 mm	2.95	0.55	301.0	231.0	23.3
		3.00 (calculated)	0.54 (calculated)	223.0	-	-

Since the measurement configurations differ, the initial maximum pressure occurring during compaction in the dry area can only be determined for the compaction height of 3 mm by evaluating the recorded measurement data. Thus, there are no values in the final range after a measuring time of 30 min. However, it can be seen that the evaluated range of maximum pressure is in the same range and differs by only 1 kPa. This allows the conclusion that the size of the specimen, with the same ratio as the size of the stamp, has no effect on the results. The difference resulting from the material relaxation in the end zone can be completely attributed to the higher compaction level.

To evaluate the compaction behaviour independently from each participant, a curve fit to the raw data was applied for the specimen thickness t as a function of the compaction pressure p, acquired during the compression phase of the tests. Thereby, the following power-law function as proposed by Robitaille et al. [8] was used:

$$t = A\ {p_n}^B \tag{19}$$

A specimen thickness at $p_n = 1$ in mm

B exponent to describe the shape of the curve

Here, the dimensionless compaction pressure p_n at a compaction pressure of 1 kPa is obtained as follows:

$$p_n = \frac{p}{1\ kPa} \tag{20}$$

As shown in Table 10, the results for the WF, using both equations, in this thesis are the same as in the benchmark exercise.

Table 10: Results from the benchmark exercise and this thesis for A and B

	dry		**wet**	
	A [mm]	**B**	**A [mm]**	**B**
Benchmark	4.96	- 0.10	4.70	- 0.10
Thesis	4.96	- 0.10	4.70	- 0.10

Thus, this test series, like the benchmark exercise, yields a correlation coefficient between the measured data and fitted curves of smaller than 0.995. Nevertheless, an exact agreement is shown even with the doubled specimen size and with in-situ impregnation instead of impregnation of the specimen before measurements with the test fluid. Moreover, for pre-wetted specimens, the compaction pressure is not only related to the properties of the reinforcement itself, but also to the flow of the test fluid that is squeezed out of the reinforcement as the specimen thickness decreases [63], [64].

Consequently, from this relationship between compaction pressure and fluid flow, the measured compaction pressure may depend on the compaction speed, the permeability of the reinforcement and also on the specimen size, which affects the length of the fluid flow paths. In this case, the permeability decreases as the degree of compaction increases, which means that the fluid pressure increases during a compression test [1]. Since the tests performed with in-situ impregnation and at twice the specimen size, lead to the same results, it can be assumed, that the relationship between compaction pressure and fluid flow depends only on the permeability of the textile reinforcement.

Therefore, the permeability of a textile architecture is not only pressure dependent, but also during compaction there is a heterogenization of the FVF distribution. Both effects, compaction and heterogenization, cause a reduction in permeability, leading to a stagnation of the flow rate with an increase in the pressure drop. [14], [31], [32]

5.4 Concluding remarks

In the present thesis, after the detailed study of the transversal compaction behaviour, the influence of four different textile architectures was investigated. For this purpose, extensive series of experiments were carried out by varying the FVF, the number of layers and the fluid injection pressure level.

The major findings are listed below:

- The general trends for the different textile reinforcement architectures during transversal compaction with in-situ impregnation could be shown by means of a novel test configuration. The differences between the dry and saturated relaxation stages are presented.
- Sources of error regarding the measurement were pointed out and addressed accordingly. In particular, the influence of the areal weight and the importance of the handling of the individual textile architectures were highlighted. Furthermore, the influence of the test rig used could be shown.
- Especially for measurements that result in a high FVF and a low number of layers, the corresponding textile reinforcement architectures must be taken into account. For example, the measured pressure values for random fibre arrangements are multiple times higher than those obtained with non-crimp or woven fabrics.
- The choice of the fluid injection pressure level has to be considered according to the given textile architecture. This is particularly relevant for textile reinforcement structures with high permeability to limit fluid consumption accordingly.
- The investigated textile reinforcements show a different strong response to the in-situ impregnation with the test fluid, significantly depending on the selected pressure level. In this phase of the test, the total pressure is composed of a combination of the exhibited compaction pressure and the applied fluid injection pressure.
- In general, the relaxation response under transverse compaction differs significantly between the textile architectures. Here, the NCF and WF as well as the Veil and Knit, each form a group with comparable behaviour.

6 Symbols and abbreviations

6.1 Symbols

Symbol	Description	Unit
V_f	Fibre volume fraction	[-]
V_{fa}	Available fibre volume fraction	[-]
V_{f0}	Initial fibre volume fraction	[-]
E_f	Flexural modulus of the fibre	[Pa]
β	Ratio of arc length and arc height	[-]
R	Relaxation factor	[-]
h	Initial height of the specimen	[mm]
t	Thickness of the specimen in compaction	[mm]
E_d	Volumetric dissipation energy	[J]
m	Stiffening index	[-]
p	Compaction pressure	[Pa]
p_0	Initial compaction pressure	[Pa]
α	Relaxation index	[-]
k_{eq}	Spring constant	[N/m]
n	Number of layers	[-]
γ	Nesting coefficient	[-]
v	Average velocity of the fluid	[m/s]
η	Viscosity of the fluid	[Pa s]
m_A	Areal weight of the fabric	[kg/m²]
ρ_f	Density of the fibre	[kg/m³]

ρ	Density of the fluid	[kg/m³]
λ	Flow coefficient	[-]
$\bar{v}$	Mean flow velocity	[m/s]

6.2 Abbreviations

Abbreviation	**Description**
FVF	Fibre volume fraction
RTM	Resin Transfer Moulding
UTM	Universal testing machine
LCM	Liquid Composite Moulding
VARI	Vacuum-Assisted Resin Infusion
VARTM	Vacuum-Assisted Resin Transfer Moulding
CFRP	Carbon fibre-reinforced plastics
WF	Woven fabric
NCF	Non-crimp fabric
LVDT	Linear Variable Differential Transducer
IBE	International Benchmark Exercise

7 List of Figures

8 List of Tables

9 References

[1] Yong, A., Aktas, A., May, D., Endruweit, A., Lomov, S., Advani, S., Hubert, P., Abaimov, S., Abliz, D., Akhatov, I., Ali, M., Allaoui, S., Allen, T., Berg, D., Bickerton, S., Caglar, B., Causse, P., Chiminelli, A., Comas-Cardona, S., Danzi, M., Dittmann, J., Dransfeld, C., Ermanni, P., Fauster, E., George, A., Gillibert, J., Govignon, Q., Graupner, R., Grishaev, V., Guilloux, A., Kabachi, M., Keller, A., Kind, K., Large, D., Laspalas, M., Lebedev, O., Lizaranzu, M., Long, A., López, C., Masania, K., Michaud, V., Middendorf, P., Mitschang, P., van Oosterom, S., Schubnel, R., Sharp, N., Sousa, P., Trochu, F., Umer, R., Valette, J. and Wang, J.: Experimental characterisation of textile compaction response: A benchmark exercise, Composites Part A: Applied Science and Manufacturing, 142 2021.

[2] M. Neitzel, P. Mitschang, and U.P. Breuer, Eds.: Handbuch Verbundwerkstoffe: Werkstoffe, Verarbeitung, Anwendung, 2. Aufl., Hanser, München 2014.

[3] Schürmann, H.: Konstruieren mit Faser-Kunststoff-Verbunden: Mit 39 Tabellen, 2. Aufl., Springer, Berlin, Heidelberg, 2007.

[4] K.-T. Hsiao and S.G. Advani, Eds.: Manufacturing techniques for polymer matrix composites (PMCs), Woodhead Pub, Philadelphia, Pa 2012.

[5] Lässig, R., Eisenhut, M., Mathias, A., Schulte, R.T., Peters, F., Kühmann, T., Waldmann, T. and Begemann, W.: Serienproduktion von hochfesten Faserverbundbauteilen 2012.

[6] Campbell, F.: Manufacturing technology for aerospace structural materials, 1. Aufl., Elsevier, Amsterdam, Kidlington, 2006.

[7] P. Boisse, Ed.: Advances in composites manufacturing and process design, Woodhead Publishing, Cambridge, UK 2015.

[8] Robitaille, F. and Gauvin, R.: Compaction of textile reinforcements for composites manufacturing. I: Review of experimental results, Polym. Compos., 19 1998, 198–216.

[9] Robitaille, F. and Gauvin, R.: Compaction of textile reinforcements for composites manufacturing. II: Compaction and relaxation of dry and H2O-saturated woven reinforcements 1998.

[10] Robitaille, F. and Gauvin, R.: Compaction of textile reinforcements for composites manufacturing. III: Reorganization of the fiber network 1998.

[11] Fauster, E., Thirunavukkarasu, J., Hergan, P. and Schledjewski, R.: Experimental process pressure analysis for model-based manufacturing of composites by resin transfer moulding, IOP Conf. Ser.: Mater. Sci. Eng., 406 2018, 12060.

[12] Hautefeuille, A., Comas-Cardona, S. and Binetruy, C.: Consolidation and compression of deformable impregnated fibrous reinforcements: Experimental study and modeling of flow-induced deformations, Composites Part A: Applied Science and Manufacturing, 131 2020, 105768.

[13] Pearce, N. and Summerscales, J.: The compressibility of a reinforcement fabric, Composites Manufacturing, 6 1995, 15–21.

[14] Becker, D. and Mitschang, P.: Influence of process parameters on the efficiency of transverse impregnation of textiles 2015.

[15] Sousa, P., Lomov, S.V. and Ivens, J.: Methodology of dry and wet compressibility measurement, Composites Part A: Applied Science and Manufacturing, 128 2020, 105672.

[16] Gutowski, T.G., Cai, Z., Bauer, S., Boucher, D., Kingery, J. and Wineman, S.: Consolidation Experiments for Laminate Composites, Journal of Composite Materials, 21 1987, 650–669.

[17] Gutwoski, T.G. and Dillon, G.: The Elastic Deformation of Lubricated Carbon Fiber Bundles: Comparison of Theory and Experiments 1992.

[18] Bickerton, S., Buntain, M.J. and Somashekar, A.A.: The viscoelastic compression behavior of liquid composite molding preforms, Composites Part A: Applied Science and Manufacturing, 34 2003, 431–444.

[19] Grieser, T. and Mitschang, P.: Investigation of the compaction behavior of carbon fiber NCF for continuous preforming processes, Polym. Compos., 38 2017, 2609–2625.

[20] Luo, Y. and Verpoest, I.: Compressibility and relaxation of a new sandwich textile preform for liquid composite molding, Polym. Compos., 20 1999, 179–191.

[21] Kruckenberg, T., Ye, L. and Paton, R.: Static and vibration compaction and microstructure analysis on plain-woven textile fabrics, Composites Part A: Applied Science and Manufacturing, 39 2008, 488–502.

[22] Lengsfeld, H., Mainka, H. and Altstädt, V.: Carbonfasern: Herstellung, Anwendung, Verarbeitung, Hanser, München, 2019.

[23] W. Burchard, Ed.: Polysaccharide: Eigenschaften und Nutzung Eine Einführung, Springer Berlin Heidelberg, Berlin, Heidelberg 1985.

[24] Rouette, H.-K.: Handbuch Textilveredlung: Technologie, Verfahren und Maschinen, 14. Aufl., Dt. Fachverl., Frankfurt am Main, 2003.

[25] Koslowski, H. J.: Chemiefaser-Lexikon: Begriffe, Zahlen, Handelsnamen, 12. Aufl., Dt. Fachverl., Frankfurt am Main, 2008.

[26] Wikimedia Commons: Multiaxial Fabric, URL: https://commons.wikimedia.org/wiki/File:Multiaxial_Fabrics.svg.

[27] G. Kellie, Ed.: Advances in technical nonwovens, Woodhead Publishing is an imprint of Elsevier, Duxford, UK 2016.

[28] Aranda, S., Klunker, F. and Ziegmann, G.: Compaction response of fibre reinforcements depending on processing temperature 2009.

[29] Li, L., Zhao, Y., Yang, J., Zhang, J. and Duan, Y.: An experimental investigation of compaction behavior of carbon non-crimp fabrics for liquid composite molding, J Mater Sci, 50 2015, 2960–2972.

[30] Chen, B., Cheng, A.-D. and Chou, T.-W.: A nonlinear compaction model for fibrous preforms, Composites Part A: Applied Science and Manufacturing, 32 2001, 701–707.

[31] Potluri, P. and Sager, T.V.: Compaction modelling of textile preforms for composite structures 2008.

[32] Becker, D., Brzeski, M., Linster, D. and Mitschang, P.: Perform compaction and deformation during through the thickness impregnation 2019.

[33] Somashekar, A.A., Bickerton, S. and Bhattacharyya, D.: An experimental investigation of non-elastic deformation of fibrous reinforcements in composites manufacturing, Composites Part A: Applied Science and Manufacturing, 37 2006, 858–867.

[34] Kruckenberg, T. and Paton, R.: Compaction of Dry and Lubricated Reinforcements 2006.

[35] Chen, B. and Chou, T.-W.: Compaction of woven-fabric preforms in liquid composite molding processes: single-layer deformation, Composites Science and Technology, 59 1999, 1519–1526.

[36] Maschinenbau-Wissen: Federmodell, URL: https://www.maschinenbau-wissen.de/.

[37] Chen, B. and Chou, T.-W.: Compaction of woven-fabric preforms: nesting and multi-layer deformation, Composites Science and Technology, 60 2000, 2223–2231.

[38] Yang, X., Wang, Y., Mo, F., Wei, K. and Duan, S.: Characterization of nesting effects on compression processes for plain woven fabrics in composites manufacturing, Journal of Reinforced Plastics and Composites, 36 2017, 1503–1513.

[39] Chen, B., Lang, E.J. and Chou, T.-W.: Experimental and theoretical studies of fabric compaction behavior in resin transfer molding, Materials Science and Engineering: A, 317 2001, 188–196.

[40] Yousaf, Z., Potluri, P. and Withers, P.J.: Influence of Tow Architecture on Compaction and Nesting in Textile Preforms, Appl Compos Mater, 24 2017, 337–350.

[41] Ivanov, D.S. and Lomov, S.V.: Compaction behaviour of dense sheared woven preforms: Experimental observations and analytical predictions, Composites Part A: Applied Science and Manufacturing, 64 2014, 167–176.

[42] Lomov, S.V., Verpoest, I., Peeters, T., Roose, D. and Zako, M.: Nesting in textile laminates: geometrical modelling of the laminate, Composites Science and Technology, 63 2003, 993–1007.

[43] Nguyen, Q.T., Vidal-Sallé, E., Boisse, P., Park, C.H., Saouab, A., Bréard, J. and Hivet, G.: Mesoscopic scale analyses of textile composite reinforcement compaction, Composites Part B: Engineering, 44 2013, 231–241.

[44] Grimsley, B., Hubert, P., Song, X., Cano, R., Loos, A. and Pipes, R.: Flow and Compaction During the Vacuum Assisted Resin Transfer Molding Process 2001.

[45] Saunders, R.A., Lekakou, C. and Bader, M.G.: Compression and microstructure of fibre plain woven cloths in the processing of polymer composites, Composites Part A: Applied Science and Manufacturing, 29 1998, 443–454.

[46] Hammami, A.: Effect of reinforcement structure on compaction behavior in the vacuum infusion process, Polym. Compos., 22 2001, 337–348.

[47] Francucci, G., Vázquez, A. and Rodríguez, E.S.: Key differences on the compaction response of natural and glass fiber preforms in liquid composite molding, Textile Research Journal, 82 2012, 1774–1785.

[48] Stöven, T.: Beitrag zur Ermittlung der Permeabilität von flächigen Faserhalbzeugen, Zugl.: Kaiserslautern, Techn. Univ., Diss., 2004, Inst. für Verbundwerkstoffe, Kaiserslautern, 2004.

[49] Weitzenböck, J.R., Shenoi, R.A. and Wilson, P.A.: Radial flow permeability measurement. Part A: Theory, Composites Part A: Applied Science and Manufacturing, 30 1999, 781–796.

[50] Grössing, H., Fauster, E. and Schledjewski, R.: Accurate 2D permeability measurement: Optical permeability characterization, 2013.

[51] Nedanov, P.B. and Advani, S.G.: A Method to Determine 3D Permeability of Fibrous Reinforcements, Journal of Composite Materials, 36 2002, 241–254.

[52] Adams, K.L. and Rebenfeld, L.: Permeability characteristics of multilayer fiber reinforcements. Part I: Experimental observations, Polym. Compos., 12 1991, 179–185.

[53] Weitzenböck, J.R., Shenoi, R.A. and Wilson, P.A.: Measurement of three-dimensional permeability, Composites Part A: Applied Science and Manufacturing, 29 1998, 159–169.

[54] Becker, D., Broser, J. and Mitschang, P.: An experimental study of the influence of process parameters on the textile reaction to transverse impregnation, Polym. Compos., 37 2016, 2820–2831.

[55] Han, K., Trevino, L., Lee, L.J. and Liou, M.: Fiber mat deformation in liquid composite molding. I: Experimental analysis, Polym. Compos., 14 1993, 144–150.

[56] Sigloch, H.: Technische Fluidmechanik, Springer Berlin Heidelberg, Berlin, Heidelberg, 2012.

[57] DeNevers, N.: Fluid mechanics, Addison-Wesley, Reading, Mass., 1977.

[58] Howell, G. W., Weathers, T. M. and TRW SYSTEMS GROUP REDONDO BEACH CA.: Aerospace Fluid Component Designers' Handbook. Volume I, Revision D, Defense Technical Information Center, 1970.

[59] Everitt, B.: The Cambridge dictionary of statistics, 1. Aufl., Cambridge Univ. Press, Cambridge, 1998.

[60] Bleymüller, J., Gehlert, G. and Gülicher, H.: Statistik für Wirtschaftswissenschaftler. 14., überarb. Aufl, Vahlen, München, 2004.

[61] Rosa, L.G., Colella, A. and Anjinho, C.A.: Effect of Paraffin Oil Used as a Lubricant in Tensile Tests of Carbon Fibre Bundles, MSF, 514-516 2006, 672–676.

[62] Cai, Z. and Gutowski, T.: The 3-D Deformation Behavior of a Lubricated Fiber Bundle, Journal of Composite Materials, 26 1992, 1207–1237.

[63] Buntain, M.J. and Bickerton, S.: Compression flow permeability measurement: a continuous technique, Composites Part A: Applied Science and Manufacturing, 34 2003, 445–457.

[64] Comas-Cardona, S., Binetruy, C. and Krawczak, P.: Unidirectional compression of fibre reinforcements. Part 2: A continuous permeability tensor measurement, Composites Science and Technology, 67 2007, 638–645.